

KU Leuven
Groep Biomedische Wetenschappen
Faculteit Bewegings- en Revalidatiewetenschappen
Departement Bewegingswetenschappen



REAL-TIME ANALYSE VAN HOGE- DENSITEIT EEG SIGNALLEN VOOR CLOSED-LOOP TOEPASSINGEN

Roberto GUARNIERI

Promotor: Prof. Dante Mantini

Proefschrift voorgedragen
tot het behalen van de
graad van Doctor in de
Biomedische
Wetenschappen

Juni 2021

REAL-TIME ANALYSIS OF HIGH-DENSITY EEG SIGNALS FOR CLOSED-LOOP APPLICATIONS

Roberto GUARNIERI

Jury:

Promoter: Prof. Dante Mantini
Chair: Prof. Werner Helsen
Jury members: Prof. Genevieve Albouy
Prof. Kaat Alaerts
Prof. Marc Van Hulle
External Jury: Prof. Camillo Porcaro

Dissertation presented in partial fulfilment of the requirements for the degree of Doctor in Biomedical Sciences

June 2021

Table of Contents

<i>Frequently used abbreviations</i>	<i>III</i>
<i>Samenvatting</i>	<i>IV</i>
<i>Summary</i>	<i>VII</i>
1 General introduction	1
1.1 Neural plasticity	1
1.1.1 The neuron and its functioning	1
1.1.2 Brain stimulation methods.....	3
1.2 Techniques for non-invasive recording of neural activity	6
1.2.1 Electroencephalography	6
1.3 Estimating neural activity from noninvasive electrophysiological recordings	8
1.3.1 EEG pre-processing.....	8
1.3.2 EEG source reconstruction.....	12
1.3.3 Analysis of task-related neural responses.....	14
1.4 Decoding and modulating neural activity in real-time	16
1.4.1 Neurofeedback.....	16
1.4.2 Closed-loop neuromodulation	18
1.5 Thesis aims and outline	21
2 Online EEG artifact removal for BCI applications by adaptive spatial filtering	22
Abstract	22
2.1 Introduction	22
2.2 Methods	25
2.2.1 Description of the method.....	25
2.2.2 Validation of the method.....	27
2.3 Results	30
2.3.1 Definition of BSS-REG standard settings.....	30
2.3.2 Analysis of BSS-REG performance on simulated EEG data.....	32
2.3.3 Analysis of BSS-REG performance on real EEG data	33
2.4 Discussion	35
2.4.1 Primary features of the BSS-REG method.....	36
2.4.2 Analysis of the method performance	36
2.4.3 Potential application in the field of BCI	37
2.4.4 Limitations and future work.....	38
2.5 Conclusions	38
3 A computationally efficient method for the attenuation of alternating current stimulation artifacts in electroencephalographic recordings	39
Abstract	39
3.1 Introduction	40
3.2 Methods	41
3.2.1 Description of the method.....	41
3.2.2 Validation of the method.....	42
3.3 Results	47
3.4 Discussion	54

3.4.1	Primary features of AC-REG	54
3.4.2	Analysis of method performance	54
3.4.3	Limitations and future work.....	55
3.5	Conclusions	56
4	<i>RT-NET: real-time source reconstruction of neural activity using high-density EEG</i>	57
	Abstract	57
4.1	Introduction	57
4.2	Methods.....	58
4.2.1	Toolbox description.....	59
4.2.2	Validation of RT-NET.....	66
4.3	Results.....	68
4.3.1	Computation time for RT-NET analysis.....	68
4.3.2	Accuracy of RT-NET analysis.....	68
4.4	Discussion.....	74
4.4.1	Primary features of RT-NET and comparison with alternative solutions	74
4.4.2	Validation of real-time neural activity reconstruction by RT-NET	76
4.4.3	Limitations and possible caveats.....	77
4.5	Conclusions	78
5	<i>General discussion</i>	79
5.1	Summary of main findings.....	79
5.1.1	Real-time biological artifact removal.....	80
5.1.2	Real-time stimulation artifact removal.....	80
5.1.3	Real-time source localization	81
5.2	Clinical impact	81
5.3	Future directions	82
5.3.1	Source-based neurofeedback	82
5.3.2	Closed-loop neuromodulation	82
	References	84
	Appositions.....	107
	Acknowledgments.....	107
	Scientific acknowledgments	108
	Personal Contribution.....	109
	Conflict of Interests Statement.....	109
	About the author.....	109
	List of publications.....	109
	Publications in peer-reviewed journals.....	109
	Conference Abstracts.....	110

Frequently used abbreviations

EEG	Electroencephalography
hdEEG	High-density EEG
REG	Regression
BSS	Blind source separation
EOG	Electrooculography
EMG	Electromyography
IC	Independent component
ICA	IC analysis
MR	Magnetic resonance
MRI	MR image
BEM	Boundary element method
BCI	Brain-computer interface
fMRI	Functional MR imaging
ERP	Event-related potentials
tACS	Transcranial alternating current stimulation
RT-NET	Real-time noninvasive electrophysiology toolbox
PCA	Principal component analysis
ERS	Event-related synchronization
ERD	Event-related desynchronization
AC-REG	Alternating current regression
SupMA	Superimposition of moving averages
M1	Primary motor cortex
SMA	Supplementary motor area
VPMC	Ventral premotor cortex
STG	Superior temporal gyrus
ROI	Region of interest

Samenvatting

Het brein is het meest complexe en mysterieuze orgaan van het menselijk lichaam. Een groot deel van het neurologische wetenschappelijk onderzoek gaat over het achterhalen van de werking van het brein alsook de invloed van stoornissen geassocieerd met neurologische problemen. Nog maar enkele decennia geleden nam de wetenschap aan dat het brein relatief onveranderd bleef na de kindertijd. Daarnaast veronderstelde men dat als delen van het brein beschadigingen opliepen, de aangetaste functies bestuurd door deze gebieden voor altijd verloren zouden zijn. Het feit dat personen die een beroerte of een traumatische breinbeschadiging opliepen spontaan herstellen, spreekt de voorgaande theorie tegen. Elk deel van het brein is continu aan het aanpassen en evolueren in reactie tot wat wij denken, zien en doen. Indien het brein forceert om nieuwe neurologische connecties aan te maken, zal het dit ook doen tijdens elk moment van zijn bestaan. Omdat het brein emotionele gezondheid, psychologische gezondheid en alle lichaamssystemen controleert, zullen er substantiele effecten optreden bij het gedrag indien het brein beter leert werken. Dit kan met doen met technologische oplossingen zoals “neurofeedback” en “closed-loop neuromodulatie” gebaseert op transcraniële wisselstroom simulatie (tACS). Deze oplossingen zijn beperkt in termen van data analyse. Ten eerste, meerdere kanalen dataverwerking, zoals in het geval van EEG, is computationeel zeer intensief. Dit leidt typisch tot de prestatie van EEG analyses op het niveau van de sensor i.p.v. aan de bron. Daarbij komt ook nog dat oog, musculaire en cardiale artifacten aanwezig zijn in EEG opnames. Daarnaast kan men een prominent artifact geïnduceerd door tACS vinden in EEG data door closed-loop neuromodulatie experimenten.

Met name hiervoor beschikken wetenschappers over verschillende empirische methodes om breinfuncties te onderzoeken. Hierbij is het van belang om te vertrouwen op niet-invasieve methodes om hersenactiviteit te onderzoeken bij gezonde mensen en patiënten. Een opkomende techniek voor beeldvorming van de hersenen is “hoge-densiteit elektro-encefalografie” (hdEEG), waarbij men elektrische potentialen van de hoofdhuid meet. De variaties in potentiaal zijn daarbij direct gerelateerd aan de neurologische activiteit in de grijze materie. HdEEG-systemen maken gebruik van meer dan 100 elektroden geplaatst op de hoofdhuid. De bekomen hdEEG-data, gecombineerd met precieze informatie over de anatomie van het brein en uitgebreide algoritmes voor bronlokalisatie, laten toe om neurale activiteit van de hersenen te reconstrueren. Er zijn echter verschillende stappen nodig om te gaan van EEG opnames naar driedimensionale afbeeldingen van neurale activiteit. Tegenwoordig gebeuren hdEEG analyses offline, want om real-time hdEEG-analyses uit te voeren is het nodig om nog verschillende technische obstakels aan te pakken.

Het doel van deze doctoraatsthesis is om een complete workflow-analyse te ontwikkelen voor eenvoudige real time analyse van hdEEG-data op bronniveau om te kunnen gebruiken in de context van neurofeedback en closed-loop neuromodulatie experimenten. Om betrouwbare real-time bron activiteit te verzekeren bij het gebruik van EEG, streven we ernaar om computationeel-efficiënte artifact verwijderingstechnieken en efficiënte bronlokalisatie te ontwikkelen. Dit hebben we opgelost door een

nieuwe online EEG artifact verwijderings methode te ontwikkelen. Hierbij hebben we offline verwerkings gereedschap, die ontwikkeld zijn voor hdEEG, geïmplementeerd als ruimtelijke filters. Onze aanpak toont de noodzaak van een calibratieve opnamemethode voor de initialisatie van de ruimtelijke filter. Deze vernieuwende methode overtrof alternatieve methodes in termen van artifact verwijderings accuraatheid en computationele efficiëntie. In het bijzonder verzwakte het verschillende soorten artefacten met een precisie die vergelijkbaar is met die van een offline methode, terwijl de echte neurale activiteit behouden bleef.

De sterke artefacten die worden geïnduceerd door gelijktijdige tACS zijn erg groot, en dit is tot dusver een sterke hindernis geweest voor de studie van neurale dynamica tijdens stimulatie. De meeste EEG-tACS-onderzoeken zijn tot dusverre uitgevoerd waarbij men de EEG-data verzameld in de periode zonder stimulatie zijn geanalyseerd. Om closed-loop neuromodulatie toepassingen mogelijk te maken, hebben we een nieuwe online techniek voor het verwijderen van tACS-artefacten met lage rekencomplexiteit geïntroduceerd. Dit was nodig om verzwakking van het stimulatieartefact in real-time mogelijk te maken. Onze technologische oplossing bleek beter te presteren dan andere methoden in termen van nauwkeurigheid bij het verwijderen van artefacten en rekentijd, met behoud van echte neurale activiteit.

Ten slotte zijn montages met hoge dichtheid vereist om bronlokalisaties uit te voeren met behulp van EEG-data. Toegewijde tools om real-time reconstructie van neurale activiteit uit te voeren, ontbreken momenteel. Dit lossen we op door een real-time niet-invasieve elektrofysiologische toolbox te ontwikkelen, die via een speciale grafische gebruikersinterface online artefactverwijdering en bronlokalisatie mogelijk maakt. Hiervan evalueren we de effectiviteit en validiteit door te vergelijken met echte hdEEG-data. We hebben met name de neurale activiteit die is gereconstrueerd in een online modaliteit vergeleken met die verkregen met behulp van een offline analyse-workflow. Over het algemeen maakte onze software het mogelijk om real-time neurale activiteit te schatten met een nauwkeurigheid die vergelijkbaar is met offline methoden. Daarnaast hebben we een gebruikersinterface ontwikkeld die real-time 2D- en 3D-visualisatie van sensor- en brongegevens mogelijk maakt. Onze software kan het werk vergemakkelijken van onderzoekers die niet vertrouwd zijn met complexe analyse workflow en software, dankzij de grafische gebruikersinterface.

Over het algemeen suggereren onze resultaten dat het mogelijk is om hdEEG te gebruiken als een niet-invasieve techniek voor real-time schatting van neuronale activiteit. Wij zijn van mening dat de analysetools die we hebben ontwikkeld voor real-time hdEEG-data-analyse verschillende nieuwe toepassingen kunnen vinden, specifiek voor hersenverbetering en voor de behandeling ervan. In de context van prestatieverbetering kan bron-gebaseerde neurofeedback erg belangrijk zijn voor topsporters, en in het bijzonder voor profvoetballers en andere topsporters. Neurofeedback biedt in dit geval de mogelijkheid voor een gerichte training van motorische, perceptuele en cognitieve functies die cruciaal zijn voor sportprestaties, wat nauwelijks bereikt kan worden door alleen fysieke training. Daarentegen kan men door euromodulatie met gesloten lus ziekten te behandelen door het perifere

zenuwstelsel elektrisch te stimuleren als reactie op fysiologische veranderingen. Er is aanzienlijk experimenteel en computationeel bewijs dat closed-loop-systemen gebaseerde op tACS effectief kunnen meesleuren, wat leidt tot veranderingen in zicht, beweging en auditie. Met name closed-loop neuromodulatie kan men gebruiken voor een verscheidenheid aan klinische doeleinden, waaronder de behandeling van farmaco-resistente epilepsie, bewegingsstoornissen en mogelijk psychiatrische stoornissen, waaronder depressie en drugsverslaving.

Summary

The brain is the most complex organ of our body, and a large bulk of research is conducted to understand its basic mechanisms and its impairments associated with neurological deficits. Just a few decades ago, it was widely assumed that the brain remained relatively unchanged after childhood. And it was presumed that if parts of the brain were damaged, the functions governed by those areas would be lost forever. The fact that people who have had a stroke or a traumatic brain injury recover spontaneously, for example, contradicts this theory. Every part of the brain is continually evolving and adapting in reaction to what we think, see, and do. If the brain is asked to do so, it may form new neuronal connections at any time during its existence. Since the brain controls emotional health, psychological health, and all of the body's systems, teaching it to work better can have substantial effects at the behavioral level. This can be done using technological solutions such as neurofeedback and closed-loop neuromodulation based on transcranial alternating current stimulation (tACS). These solutions have however still some limitations in terms of data analysis. First of all, processing of multi-channel data, as in the case of EEG, is computationally intensive. This typically leads to the performance of EEG data analyses at the level of the sensors, instead of the sources. Also, ocular, muscular and cardiac artifacts are typically present in the EEG recordings. In addition, a prominent artifact induced by tACS can be found in EEG data from closed-loop neuromodulation experiments.

Notably, there are a variety of empirical methods that allow scientists to examine brain functioning. In particular, it is necessary to rely on non-invasive techniques to study brain activity in healthy people and patients. An emerging technique for brain imaging is the high-density electroencephalography (hdEEG), which records the changes in electrical potential on the scalp. These variations are directly related to neuronal activity in the gray matter. HdEEG systems have more than 100 electrodes placed over the scalp. HdEEG data, if combined with precise information of the head anatomy and sophisticated source localization algorithms, permit the reconstruction of neural activity in the brain. However, several processing steps are needed to move from EEG recordings to 3-dimensional images of neuronal activity. Nowadays, hdEEG analyses have been conducted in an offline manner. Important technical issues need to be addressed for real-time hdEEG analyses.

The purpose of this PhD thesis is to develop a complete analysis workflow for real-time analysis of source-level hdEEG data, to be used in the context of neurofeedback and closed-loop neuromodulation experiments. The effectiveness of neurofeedback applications based on EEG data strongly depends on the effective attenuation of artifacts that are mixed in the recordings. To address this problem, we develop a novel online EEG artifact removal method. This was done by adapting offline processing tools that we developed for hdEEG and re-implementing them as spatial filters. Importantly, our approach necessitates the use of a calibration recording for the initialization of the spatial filter. Our approach outperformed alternative methods in terms of artifact removal accuracy and computational efficiency. Specifically, it attenuated various types of artifacts with precision comparable to that of an offline method while maintaining true neural activity.

The strong artifacts induced by simultaneous tACS are very large, and this has so far been a strong hurdle for the study of neural dynamics during stimulation. Indeed, most EEG-tACS studies have been so far conducted analyzing the EEG data collected in the off-stimulation period. To enable closed-loop neuromodulation applications, we introduced a novel online tACS artifact removal technique with low computational complexity. This was necessary to enable attenuation of the stimulation artifact in real-time. Our technological solution was found to outperform other methods in terms of artifact removal accuracy and computational time, while preserving true neural activity.

Finally, high-density montages are required to perform source localizations using EEG data. Dedicated tools to perform real-time reconstruction of neural activity are currently lacking. We fill this gap by developing a real-time noninvasive electrophysiology toolbox, which -through a dedicated graphical user interface- enables online artifact removal and source localization of hdEEG data. We evaluate its effectiveness and validity on real hdEEG data. Notably, we compared the neural activity reconstructed in an online modality to that obtained using an offline analysis workflow. Overall, our software permitted to estimate real-time neural activity with accuracy comparable to offline methods. We developed a user interface that allows for real-time 2D and 3D visualization of sensor and source data. Our software may facilitate the work of researchers who are unfamiliar with complex analysis workflows and software, thanks to its graphical user interface.

Overall, the results of the PhD thesis work suggest that it is possible to use hdEEG as a non-invasive technique for real-time estimation of neuronal activity. We believe that the analysis tools we developed for real-time hdEEG data analysis can find several new applications, specifically for brain enhancement and for the treatment of neurological diseases. In the context of performance enhancement, source-based neurofeedback can be very important for high-level sportsmen, and in particular for professional football players and other top-level athletes. In this case, neurofeedback offers the possibility of a targeted training of motor, perceptual and cognitive functions that are crucial for sport performance, which can be very hardly achieved by physical training only. Closed-loop neuromodulation, on the other hand, attempts to treat disease by electrically stimulating the peripheral nervous system in response to physiological changes. There is considerable experimental and computational evidence that closed-loop systems based on tACS can effectively entrain brain oscillations, leading to changes in vision, movement and audition. Notably, closed-loop neuromodulation is used for a variety of clinical purposes, including the treatment of pharmaco-resistant epilepsy, movement disorders, and possibly psychiatric disorders including depression and drug addiction.

1 General introduction

1.1 Neural plasticity

The brain is the most complex organ of the human body, with approximately 86 billion neuronal cells or neurons being largely interconnected with each other (Azevedo et al. 2009). Notably, connections between neurons can change through experience (Andrade-Talavera et al. 2016). The nervous system's ability to change its function and structure in response to both intrinsic and extrinsic stimuli is called neuroplasticity (Mateos-Aparicio and Rodríguez-Moreno 2019; von Bernhardi et al. 2017). In healthy individuals, neuroplasticity represents the basis of brain development, learning, and memory (Kolb and Whishaw 1998), whereas in patients this term relates to molecular, synaptic, cellular events in the brain after degeneration or injury (Prosperini et al. 2015). Different forms of neural plasticity have been identified. A primary distinction needs to be made between transmission efficacy plasticity and structural plasticity (Fauth and Tetzlaff 2016). The former is linked to structural changes of neuronal connections. By contrast, synaptic plasticity is referred to as changes in the circuit connectivity involving modification of synapses (Fauth and Tetzlaff 2016).

1.1.1 The neuron and its functioning

As already mentioned, neurons are the fundamental elements of the nervous system. They carry electrical signals produced by the movement of ions through its membrane. Each neuron is connected with 5.000-200.000 other neurons and the network complexity escalates with brain maturation.

The neurons can be classified into three classes depending on their function: sensory, motor, and interneurons (figure 1.1). Sensory neurons transform stimuli from the environment into internal electrical impulses. Then, motor neurons transfer information and commands to muscle and organs, after getting signals from other neurons. Lastly, the interneurons, the central nodes of the neural circuits, connect one neuron to another. A neuron is made up of axon, dendrites and the so-called, soma, which is the cell body. Dendrites, meant as the projections of a neuron, can be connected to both axons or other dendrites, and can receive electric signals from other nervous cells. The synapses are contact sites which transmit the signal between neurons, therefore they are elements of connection between the nerve cells. The information flow is mostly unidirectional along the fibers and synapses.

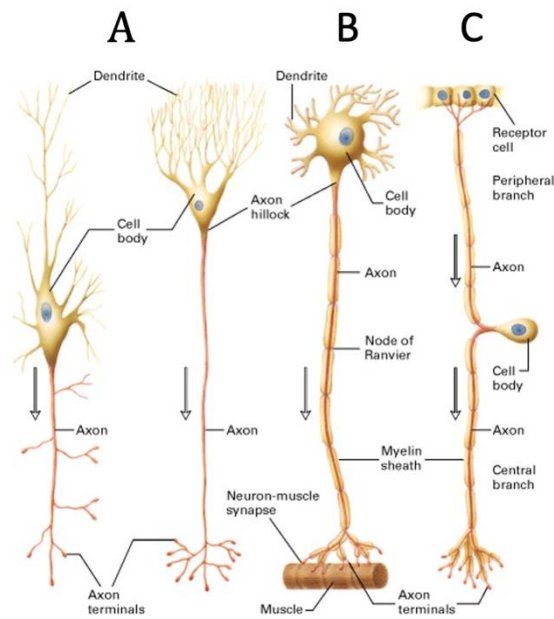


Figure 1.1. Different types of neurons and their structure. A) Interneurons empower sensory or motor neurons to communicate with the central nervous system; B) motor neurons convey signals to muscle cells to control their functional output; C) sensory neurons receive information via their receptors and convert this information into electrical impulses. This figure is adapted from Lodish et al. (2000), with permission.

At the functional level, the neuron is a cell that can be excited or activated. The activation process corresponds to the modification of the electrochemical activity of the nervous cell (figure 1.1). This activity produces a change in the difference of potential across the cell membrane. Therefore, when the cell is at rest, the membrane has a natural polarization, with a transmembrane potential typically between -50mV and -100mV . As a result of an excitation, a depolarization is determined, the duration of which varies greatly depending on the type of excitable cell involved. For a neuron this duration is of the order of ms. Under the cell membrane, a negative potential ($60\text{-}70\text{ mV}$), which varies with the synaptic activity, may be recorded.

Cortical pyramidal neurons become electrical dipoles due to their peculiar anatomical configuration with a long apical dendrite perpendicular to the cortical surface and equal capacitive currents caused by electrotonic spread of postsynaptic potentials along the apical dendrites (Kirschstein and Köhling 2009). An excitatory postsynaptic potential (EPSP) is a shift in membrane voltage of a postsynaptic cell caused by the influx of positively charged ions into the cell (typically Na^+) as a result of the activation of ligand-sensitive channels (Harvey and Dickenson 2010). With more action potentials (APs) in the same fiber, the EPSP will be summed, and a new AP will be generated in the postsynaptic neuron (Shepherd 2004). Inhibitory postsynaptic potentials (IPSPs) are caused by the influx of negative ions (e.g., Cl^-) into the postsynaptic cell or the efflux of positive ions (e.g., K^+) out of the cell. As a consequence, cell hyperpolarization occurs, reducing the probability of AP propagation, and inhibitory synapses are formed. Both forms of postsynaptic potentials are graded, resulting in an excitatory or inhibitory effect when added together (Harvey and Dickenson 2010). As soon as the summation of excitatory events

exceeds the threshold, an AP is generated and transits along the nerve (figure 1.2). In both cases, a dipole is created with separation of charge oriented vertically in the cortex, with extracellular negativity in more superficial laminae surface, and extracellular positivity in deeper laminae (Holmes and Khazipov 2007).

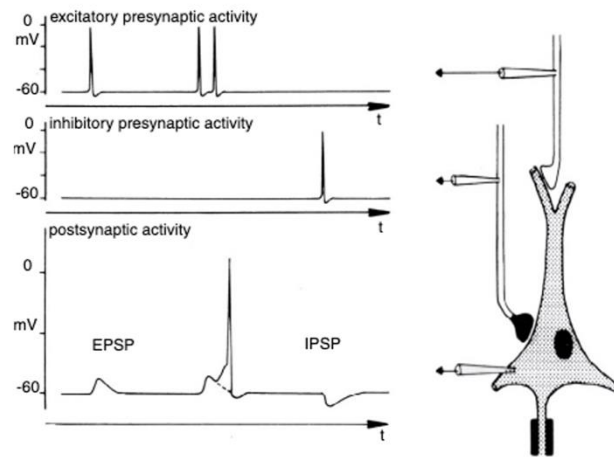


Figure 1.2. Measurements of excitatory and inhibitory post synaptic potentials in various parts of the neuron. On the left topside of the picture, excitatory APs are shown. In the middle graph, there is an example of inhibitory AP. All the incoming potentials are processed by the neuron. Finally, in the left-bottom graph of the figure, it is shown that the neuron fires when, in a short amount of time, two excitatory post synaptic potentials occur. In case there is no second excitatory AP, there is an EPSP (dotted line). If at the end of the fiber an inhibitory synapse occurs, then there will be a hyperpolarization (marked as IPSP). This figure is adapted from Niedermeyer and da Silva (2005), with permission.

The definite spikes timing influences plasticity amplitude and polarity (Shouval et al. 2010). Spike-timing-dependent plasticity (STDP) governs the strength of connections between neurons (Bi and Poo 1998; Markram et al. 1997; Shouval et al. 2010), which is crucial for synaptic plasticity in adults (Andrade-Talavera et al. 2016). STPDs can change the strength of neural connections by timing the output and input APs of neurons. Timing-dependent long-term potentiation (t-LTP) is a synaptic reinforcement caused by repeated stimulation of a presynaptic cell until spikes in a postsynaptic cell over tens of milliseconds. On the other hand, timing-dependent long-term depression is the opposite mechanism (t-LTD). The STDP mechanism, with special attention to t-LTP and t-LTD, elucidates the activity-dependent evolution of the nervous system in part.

1.1.2 Brain stimulation methods

In parallel with synaptic plasticity, neuromodulation can be also considered to facilitate adaptation to environmental demands. Neuromodulation is the active stimulation of the brain, spinal cord or peripheral nerves electrically (neurostimulation) or by administering drugs. Through the release of neurotransmitters, neuromodulation achieves transitional changes in the functional properties of neurons and synapses, as well as adapting neural circuits for immediate behavioral requirements.

Several neurostimulation methods are currently available. Invasive neurostimulation techniques need surgical interventions to implant electrodes and an implantable pulse generator (IPG). One suggestive and impressive example of modern invasive neurostimulation modality is the deep brain stimulation (DBS). DBS is usually placed subdermally below the clavicle. A battery and electronic components compose this unit, which provides electrical stimulation. Moreover, both patients or clinicians may externally monitor the DBS. To achieve optimum effectiveness, stimulation parameters such as frequency, pulse duration, and voltage must be modified (Pycroft et al. 2018). Several application exemplars of the use of DBS can be mentioned. For example, movement problems such as Parkinson's disease, critical tremor, and dystonia may all be treated with DBS (Perlmutter and Mink 2006) or refractory pain (Keifer Jr et al. 2014). In addition, DBS techniques is influenced by several factors, such as the location of the stimulating electrode and the stimulation frequency. The first has an impact on the pain-relieving process, while the latter indicates that DBS controls certain disease-related rhythmic or oscillatory processes within definite neural circuits (Nandi et al. 2003).

Non-invasive neuromodulation techniques, such as transcranial Electrical Stimulation (tES), have been increasingly used in recent years (Woods et al. 2016). Using rubber electrodes in saline-soaked sponges, small quantities of current are propagated through the scalp during tES (Morales-Quezada et al. 2014). Transcranial Direct Current Stimulation (tDCS), which uses a constant current, transcranial Alternating Current Stimulation (tACS), which uses sinusoidal oscillating currents, and transcranial Random Noise Stimulation (tRNS), which uses randomly generated currents, are all examples of stimulation (figure 1.3). Furthermore, tES techniques are characterized by electrode size, shape, amount, montage, duration, number, and interval of stimulation sessions, stimulating current modality, amplitude, polarity (for tDCS), and phase (for tACS) (Yavari et al. 2017).

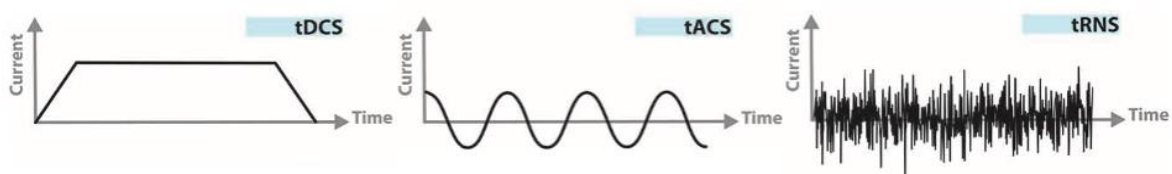


Figure 1.3. Different examples of applied currents in tES. tDCS applies a direct current, tACS an alternating current and tRNS a random current. In relation to neuronal activity, the current form, length, frequency, and phase may be adjusted. This figure is adapted from Yavari et al. (2017), with permission.

With tACS, sinusoidal currents are typically injected using two electrodes over the scalp, to directly interfere with brain native oscillatory patterns (figure 1.4) (Antal et al. 2008). During one half cycle of a tACS oscillation, one electrode will serve as anode and the other one as cathode and current strength will increase and decrease following a half sine wave (Antal and Herrmann 2016; James Dowsett and Herrmann 2016).

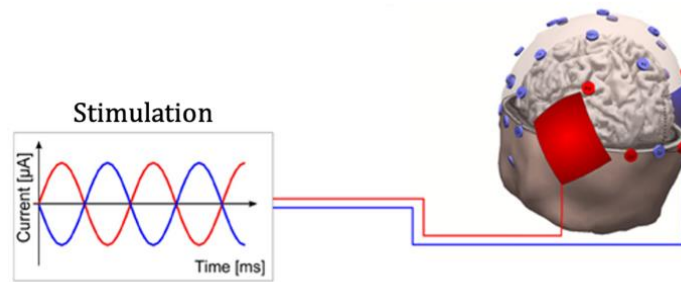


Figure 1.4. Illustration of a typical tACS electrode montage together with EEG electrodes. The current, which is applied sinusoidally, changes direction by 180° every half-wave. The anode is represented by the red stimulation electrode during the positive half-wave. The current direction is 180° inverted during the negative half-wave. The current direction remains constant throughout each half-wave, but the intensity varies. The tACS sponge electrodes were located bilaterally over the parietal–occipital cortex at electrode locations P7-P07 (red left hemisphere) and P8-P08 (blue right hemisphere). This figure is adapted from Strüber et al. (2014), with permission.

Stimulating electrodes with size of 5 cm x 7 cm are commonly used. However, smaller electrodes and more than two stimulation electrodes have proven to substantially increase spatial specificity in tACS (Fröhlich et al. 2015). Precise electrode positioning is extremely difficult and demanding. This uncertainty may result in an unbalanced electrical current distribution across the scalp (Heise et al. 2016). A circular ring electrode covering the central electrode overlaying the target area (figure 1.5) has been introduced to address this problem and provide more focal stimulation (Heise et al. 2016). Furthermore, using frequency-based interference techniques (Grossman et al. 2017) and multi-channel montages (Alekseichuk et al. 2019) of various electrode sizes (Nitsche et al. 2007), shapes (Datta et al. 2008), and number of electrodes (Faria et al. 2009), the spatial specificity problem may be effectively addressed.



Figure 1.5. Montage with a circular return electrode surrounding the target electrode. This figure is adapted from Heise et al. (2016), with permission.

The magnitude of tACS-induced physiological effects varies with the intensity of the induced area, and the effectiveness of the stimulation, and its implications on neuronal function are dependent on a number of experimental variables. The most suitable modality to study the tACS effects and efficacy is to study it during the stimulation. However, the presence of the massive electrical artifact limits the

possibility of analyzing the tACS efficacy in an online manner (Voskuhl et al. 2018). Therefore, in many experimental researches, only the difference between pre- and post-stimulation neural measurements is taken into account (Pikovsky et al. 2003; Thut et al. 2011).

tACS has been shown in both experimental (Herrmann et al. 2013; Marshall et al. 2011) and computational (Ali et al. 2013; Merlet et al. 2013) studies to entrain brain oscillations. Moreover, alpha and gamma tACS can be used for investigating endogenous and exogenous attention (Hopfinger et al. 2017). In addition, tACS has been successfully applied to modulate audition (Riecke 2016; Riecke et al. 2015), motion perception (Helfrich, Knepper, et al. 2014), mental rotation (Kasten and Herrmann 2017), visuo-motor coordination (Santaracchi et al. 2017) and movement (Feurra et al. 2011). Finally, functional magnetic resonance imaging (fMRI) showed that tACS can induce short-term neuroplastic effects over relatively specific cortical regions (Bächinger et al. 2017; Cabral-Calderin et al. 2016)

1.2 Techniques for non-invasive recording of neural activity

1.2.1 Electroencephalography

Electroencephalography (EEG), which is one of the oldest techniques to non-invasively measure underlying human brain activity, measures the large-scale synchronization of neural network (Cacioppo et al. 2016; Michel and Brunet 2019). The first human EEG measurement was recorded in 1924 by the psychologist psychiatrist Hans Berger (1873–1941) using two platinum needle electrodes at the frontal and occipital poles of the head. Nowadays, EEG is widely used for clinical diagnosis, neuroscience, psychology and medical research. Due to the technological development, much progress has been made in the last years, both on the acquisition and the processing of the recorded signal.

In other words, EEG measures the difference in voltage between two electrodes placed at distinct scalp locations (Olejniczak 2006). When a large number of brain cells (neurons) are activated, the postsynaptic potentials (0.1-10 mV and last 10-20ms) are produced and summed across the neighboring neurons. This synaptic current generates an electrical field over the scalp, which can be measured using EEG electrodes attached on the scalp.

Neural oscillations are described by their frequency, amplitude and phase. The amplitude is modulated by the intensity of neuronal firing and neural synchrony (Musall et al. 2012). The EEG frequency depends on the level of activation of the cerebral cortex. The different levels of cortical activation are linked to several psychological and behavioral states (figure 1.6) (Bennett et al. 2009). Notably, the frequency of EEG recordings ranges from ~0.05 to 600 Hz and the intensity goes from -50 to 50 μ V. Delta (1-4Hz), theta (4-8Hz), alpha (8-13Hz), beta (13-30Hz), and gamma (30-100Hz) are the four basic EEG frequency patterns. Behavioral (e.g., sleep, and wakefulness) and pathological (e.g., coma, stroke) states are connected by oscillations or EEG rhythms. Low frequency and large amplitude rhythms are associated with states of rest or sleep; high frequency and low amplitude rhythms are associated with states of alertness and cognitive engagement (Brown et al. 2012).

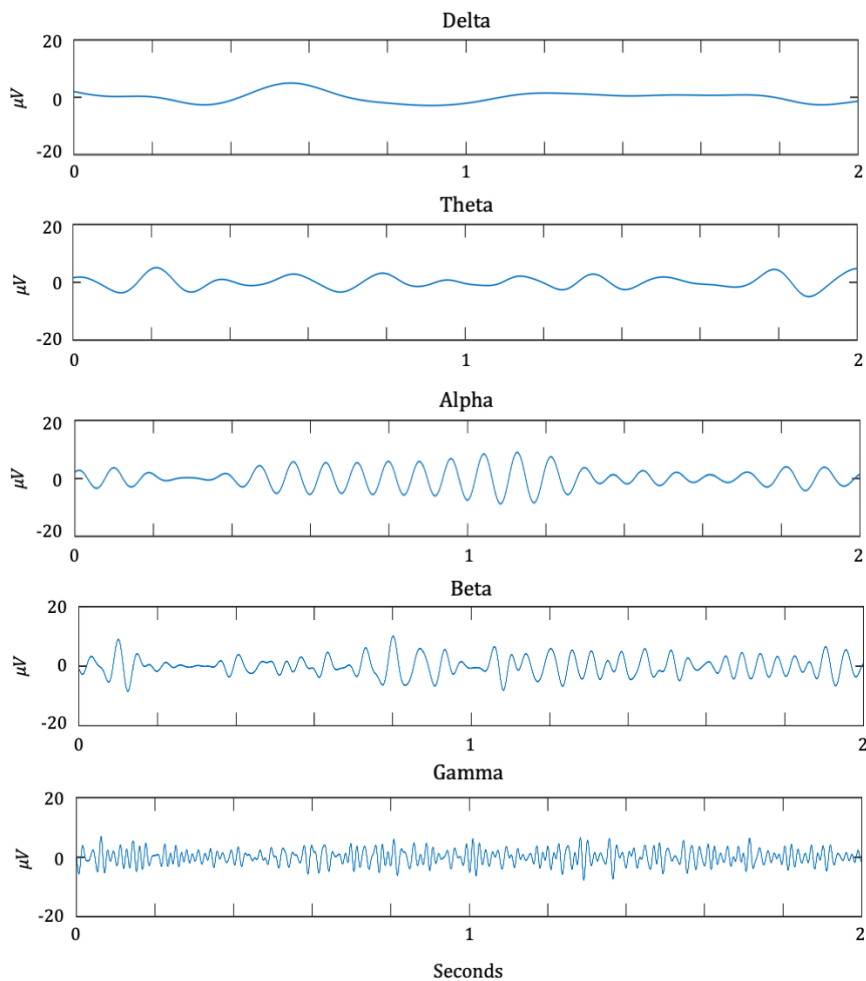


Figure 1.6. Brain waves with dominant frequencies. As mentioned, specific brain waves correspond to different mental states. High frequency and low amplitude rhythms are associated with states of alertness and cognitive engagement, whereas brain rhythms with low frequency and large amplitude are associated with rest or sleep.

Notably, the EEG is measured between an active and a reference electrode (Kondraske 1986). Thus, EEG signal collected from a given electrode will be in fact the difference between the potential at electrode itself and the potential of the reference channel. Ideally, a channel with neutral signal should be chosen. Nonetheless, it does not exist. Notably, the most widely used physical reference is the channel at vertex (Mulert et al. 2008). Moreover, in some cases, also the mastoid or the earlobe references are used (Flanigan et al. 1995). The choice of the reference channel is very important, as it affects all the EEG data set (Liu et al. 2015). Therefore, the effect of residual neuronal activity in the physical reference should be attenuated by re-referencing the data. This can be done by estimating the signal at a virtual neutral location, and subtracting it from each EEG signal (Kayser and Tenke 2010).

Essentially, it is possible to acquire simultaneously multiple EEG signals if a multi-channel system, with electrodes placed inside an EEG cap, is used. To ensure consistent reproducibility within and between subjects, the position of electrodes in EEG caps have been standardized (Klem et al. 1999). Precision landmarks such as the nasion, preauricular points, and inion are used to segment the head

into proportional distances. These landmarks cover all regions of the brain effectively. Therefore, the low-density ‘10-20’ (figure 1.7A) and ‘10-10’ montages have been widely used.

In recent years, technical progress has led to the development of high-density EEG (hdEEG) systems, with more than hundred electrodes (figure 1.7B). They allowed the reconstructed neural activity to have a higher spatial resolution (B. He et al. 2011; Michel and Murray 2012).

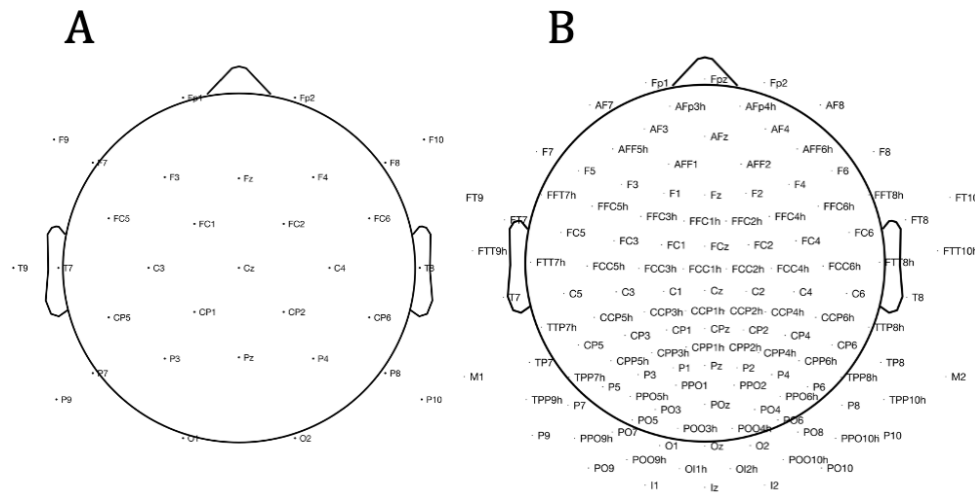


Figure 1.7. Conventional electrode positions for: A) a 32-channel EEG system; B) a 128-channel system.

By exploiting source localization algorithms and head anatomy information, hdEEG systems can be used as a neuroimaging technique (Michel and Brunet 2019). The high spatial sampling for the scalp potential distribution offers new opportunities for achieving substantially higher spatial accuracy in the estimation of neural sources (B. He et al. 2011; Michel and Murray 2012). Notably, the current flow from sources to sensors is attenuated by the skull and other head tissues. To uncover the correct potential underlying each scalp electrode generated by a source in the brain, the attenuation needs to be accurately mapped.

However, hdEEG systems present also some disadvantages, especially for use in clinical practice. First of all, the time that needs to be dedicated to the preparation of the participant before starting an experimental session is a limiting factor. Specifically, an electro-conductive gel is typically applied under the electrodes to reduce contact impedance. This can be very time consuming for high-density EEG montages. Moreover, there is the risk of bridging between EEG sensors over the scalp. If the electrodes are enclosed in saline soaked sponges, there is no need of applying an electro-conductive gel, but the evaporation of the solution over time may lead to conductivity issues.

1.3 Estimating neural activity from noninvasive electrophysiological recordings

1.3.1 EEG pre-processing

Any EEG dataset is affected by the problem of the reference electrode and may be contaminated by biological artifacts, hardware noise, power line interference (i.e. 50/60 Hz) and channels with higher

impedance and lower signal-to-noise ratio (SNR), referred to as 'bad channels'. In the following sections, we will introduce all the pre-processing steps: bad channel correction, filtering, artifact removal, re-referencing.

Bad channel correction

In EEG acquisitions, there is the possibility that some sensors may register more environmental or biological noise than brain activity. For those channels, there is the need to attenuate the noise using specific signal processing techniques or even eliminate those electrodes from the analysis. The related channels need to be defined as 'bad'. It is critical to detect low-signal-quality sensors early in the pre-processing phase because the efficiency of subsequent artifact removal is dependent on it. They can be manually detected, although this procedure may be subject to errors made by the operator. Alternatively, there are different criteria to automatically detect bad channels. The most widely used technique is to define the bad channels with zero variance, or very high variance as compared to others. Another approach is based on cross-channel correlation or covariance and the assumption that signals recorded from the bad channels have rare similarity with all the other scalp channels.

After the bad channels are detected, there are two strategies to attenuate their effects: 1) excluding the bad channels; 2) repairing the bad channels using neighboring channels. In the latter case, linear or non-linear interpolation based on the surrounding good channels is typically used in EEG analysis (Oostenveld et al. 2011).

Filtering

Digital filtering is a common pre-processing step when analyzing EEG data for removing noise mixed in the recordings (Correa 2011). Usually, in EEG signal processing, a high-pass filter, with 0.1 Hz or even often 1 Hz cutoff frequency, is applied to remove the slow voltage drift due to sweating or heating up device. Moreover, a low-pass filter is usually applied to filter out frequencies above the highest frequency of interest (Bronzino 1999). Notably, they prevent the signal distortion due to the aliasing. Lastly, power line noise (usually at 50Hz or 60Hz, depending on the country) can be largely suppressed by digital notch filtering.

There are two categories of digital filters: Finite Impulse Response (FIR) and Infinite Impulse Response (IIR). The length of an impulse response is used to classify each type of filter. The output of a FIR filter has an impulse response for a finite time before going to zero and producing equivalent delays at all frequencies. IIR filters, on the other hand, have an infinite impulse response and use a portion of the filter's output as feedback. This results in unequal delays at various frequencies. This suggests that the output signal is delayed in comparison to the input signal, with certain frequency components being delayed rather than others. Butterworth, Chebyshev (I or II type), and Elliptic filters are the most popular IIR filters (Bhogeshwar et al. 2014). Another aspect to take into consideration is the direction of the input signal. Causal filters rely only on past and present information, whereas noncausal filters

depend on the past and future input. The main difference between causal and non-causal filters depends on whether the response is after (causal filters) or before the onset (non-causal filters) (Rousselet 2012).

There are few parameters to choose while using a digital filter, such as cutoff frequency, filter order, roll-off, phase delay (zero-phase, linear-phase, non-linear phase). Roll-off is the rate at which attenuation increases beyond the cut-off frequency. It is important to consider that phase distortions and delays may be added to the signal, depending on the response of the filter.

Finally, it is crucial the parameters choice to have an optimal filtering of EEG data.

Artifact removal

When working with EEG data, one of the most important aspect is that we need to maintain uncorrupted clean signals with a high SNR. Generally, artifacts are undesired components of the EEG signal not directly generated by brain activity (figure 1.8) (Urigüen and Garcia-Zapirain 2015). The artifacts need to be filtered from the EEG to keep the neural information and we need to ensure that true neural activity is not distorted (Guarnieri et al. 2018).

Importantly, EEG artifacts that are physiological (ocular, muscle, or cardiac activity, perspiration, and respiration) can be distinguished from those that are non-physiological (electrode pop, cable movement, incorrect reference placement, electromagnetic interferences, and body movements) (Sörnmo and Laguna 2005; Urigüen and Garcia-Zapirain 2015).

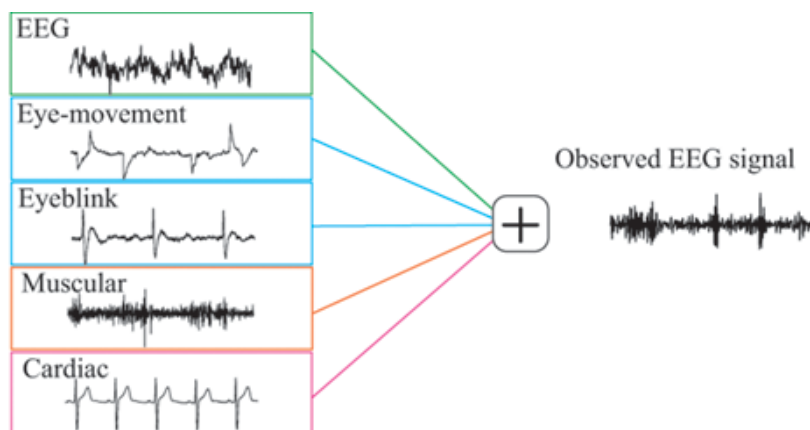


Figure 1.8. Example of four types of non-neuronal and neuronal signals recorded during an EEG acquisition: pure EEG, eye movement, eyeblink, muscular and cardiac artifacts. Their frequencies overlap with the frequency of EEG signals. This figure is adapted from Kanoga (2017), with permission.

It is worth noting that artifacts have a frequency spectrum overlapping with that of EEG signals. Indeed, they cannot be removed with digital filtering. Furthermore, in relation to the neural activity of interest, artifacts have conflicting frequencies. As a result, temporal filtering is unlikely to be a viable EEG artifact removal method (Muthukumaraswamy 2013).

Regression techniques (REG) (P. He et al. 2004; Schlogl et al. 2007) and blind source separation (BSS) techniques are the two key solutions currently in use for artifact removal (Choi et al. 2005).

The weighted subtraction of electrical signals reflecting artefactual origins, such as electrooculography (EOG) and electromyography (EMG) signals, is the basis for REG. The regression approach for removing artefactual behaviors is based on the premise that there is no association between true neuronal activity and EOG/EMG signals (Jervis et al. 1988; Sadasivan and Dutt 1996). Furthermore, regression estimation of proper weights is accurate when EOG/EMG signals have very close waveforms to the individual artifacts in the EEG data. This expectation is not always met, since the artefactual source's relative location to the EEG and EOG/EMG signals does not always fit (Guarnieri et al. 2018).

BSS is used in a further category of artifact removal techniques. Signals originating from various elements, which are mixed in recordings, can be separated using BSS methods (A Delorme et al. 2012; Zeng et al. 2013). The most well-known approach in this category is independent component analysis (ICA) (Turnip 2014). ICA has been proven to be an effective technique for removing EEG artifacts in the last decade, capable of separating non-neural and neural signals mixed in EEG data (Jung, Makeig, Humphries, et al. 2000; Makeig et al. 1996). The classification of neural independent components (ICs) and artefactual ICs is a crucial step in ICA-based artifact removal. The EEG dataset is first decomposed into many ICs. The remaining (neural) ICs are then projected back to the sensors after artefactual ICs are detected. Therefore, EEG signals that are free of artifacts are reconstructed in this way. The classification of ICs can be done in two ways: manually or automatically. The former needs a visual inspection of each signal's time course, as well as a scalp map and power spectrum. Several automated approaches for IC classification, on the other hand, have been suggested (Li et al. 2006; Vorobyov and Cichocki 2002). BSS solutions have the possible drawback of assuming source stationarity, which means that the weights associated with the components are set over the entire EEG recording (Marino, Liu, Del Castello, et al. 2018; Winkler et al. 2011).

Re-referencing

It is important to consider that the EEG signals are recorded measuring the electrical activity at one electrode relative to another (reference) location. The reference has two effects on the amplitude of each EEG channel and time point: it determines the degree of zero voltage, and it is used to measure the amplitude of all other channels. Several physiological complex processes are involved in all physical electrode locations. Because a non-constant temporal dimension is introduced, they would undoubtedly change the temporal dynamic and spectral EEG analysis (Liu et al. 2015). The voltage at the EEG scalp channels can be expressed in terms of another, new reference using a signal processing technique called re-referencing. During re-referencing, the signal of the new reference is subtracted from each EEG channel. There are different re-referencing methods, such as average re-referencing (Offner 1950) which assumes that the average signal measured across channels is always null, infinity re-referencing

technique (also called reference standardization technique) which is very sensitive to the head model used (Yao 2001) and the method of linked-mastoid re-referencing, which is based on a linear combination of potentials calculated at mastoid sites (Nunez et al. 1997).

1.3.2 EEG source reconstruction

Notably, since EEG is characterized by a poor spatial resolution, it is challenging to recover the electrical activity at the level of the sources by using the neuronal activity measured on the scalp. In recent years, hdEEG systems have become available, permitting to increase the spatial resolution of the reconstructed neural activity (B. He et al. 2011). These developments, combined with advanced source localization techniques and precise information of the head anatomy, have opened up the doors to the use of hdEEG as an offline brain imaging tool (Michel and Murray 2012). Furthermore, due to the high computational cost, EEG source analysis combining pre-processing and source localization is usually solved offline (Pion-Tonachini et al. 2015). Notably, additional steps are needed, such as the solution of the forward and the inverse problems. The first one is referred to the assessment of EEG recordings from brain sources whereas the latter is referred to estimation of brain sources from EEG recordings (Ganzetti and Mantini 2013; Pfurtscheller and Lopes Da Silva 1999).

Forward problem

EEG forward modeling predicts the electromagnetic fields and potentials produced by any arbitrary source model for any possible position, orientation, and amplitude parameter value (Baillet 2013). The estimation of the forward solution requires a realistic head-volume conductor model to be generated from an individual's MRI (which needs to be segmented), and the correct electrode locations to be defined with respect to the conductor model. Currently, realistic and individualized head models are generated based on the structural MRI of the subject's head. The workflow for the creation of a realistic head model is illustrated in figure 1.9.

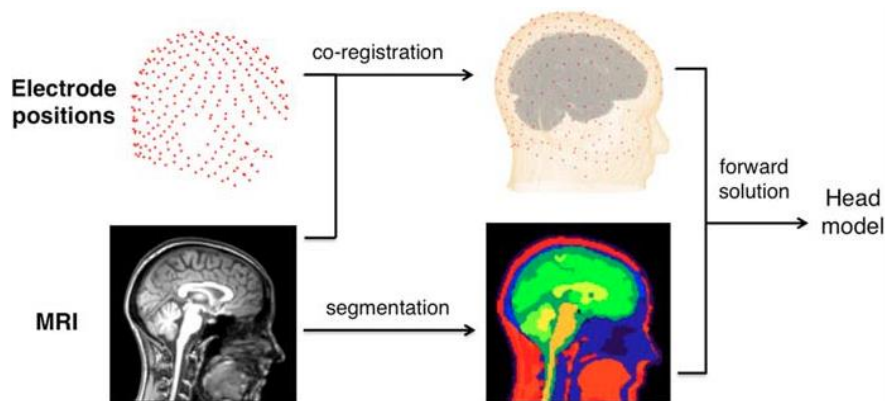


Figure 1.9. Pipeline for the solution of the forward problem. Specifically, the structural image of the head needs to be segmented into different brain tissues, each one characterized by a specific conductivity value. Then, the recorded electrode positions have to be spatially co-registered to the head image. Finally, the forward solution is calculated, leading to the creation of the leadfield matrix. This figure is adapted from Q. Liu et al. (2017), with permission.

In EEG analysis, solving the forward problem means being able to predict the electrical potentials measurable on the scalp for each given source distribution in the brain. At a given time, one dipole source at location can be considered a vector representing the current flowing in the three Cartesian directions. Sources are modeled as single current dipoles. The leadfield matrix, which relates a specific source to the scalp map, is the forward problem solution. In addition, the leadfield matrix defines the current flow through each dipole location for a given electrode (Pascual-Marqui 1999). Calculating the leadfield matrix necessitates the construction of a head model. The surface potentials given by current sources in a piecewise homogeneous volume conductor are measured using boundary element methods (BEMs) (figure 1.10) (Hallez et al. 2007).

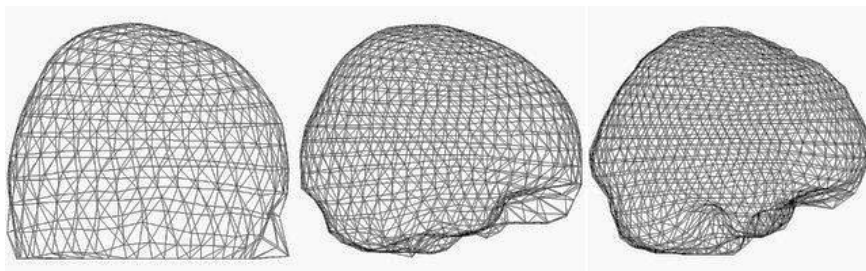


Figure 1.10. Example of triangulated mesh of the human head used in BEM. The various interfaces of the human head are depicted in this diagram: air-scalp, scalp-skull, and skull-brain are all terms used to describe the relationship between the air and the scalp. This figure is adapted from Zaytsev et al. (2015), with permission.

Due to their low computational requirements, BEMs are commonly used to solve volume problems by extracting potential values at the volume's interfaces and boundaries caused by a given dipole. The interfaces separate the conducting volume from non-conducting air, while the boundary is the outer surface that separates the conducting volume from non-conducting air. A tissue-based BEM head model is composed of various surfaces (for example three surfaces, such as brain-skull, skull-scalp and exterior surfaces). Importantly, each tissue must be encapsulated by each surface. The conductivity of the regions between the interfaces is considered to be homogeneous and isotropic. For the purpose of calculating a solution, each interface is tessellated with small boundary elements. When the distance between the source and one of the surfaces is equal to the size of the triangles in the mesh, BEM has the drawback of decreasing precision (Hallez et al. 2007). Other methods for estimating the leadfield matrix, which includes neuronal current propagation in the head, include finite element methods (FEMs) and finite difference methods (FDMs). By indicating the scalp distribution of voltage produced by each dipole in gray matter, these methods are used to solve the forward problem and numerically generate the leadfield matrix.

Inverse problem

The estimation of brain sources from EEG recordings is typically referred to as the inverse problem (Pfurtscheller and Lopes Da Silva 1999). The solution of the EEG inverse problem is not unique because of all the admissible output voltages.

Several solutions for solving the EEG inverse problem have been proposed. For instance, the linearly constrained minimum variance beamformer (LCMV) estimates the behavior of a source at a specific position while removing all other sources and noise captured in the data covariance matrix (Van Veen et al. 1997). Multiple-signal Classification (MUSIC) is a signal processing-based algorithm for finding multiple asynchronous dipolar sources in EEG and magnetoencephalography (MEG) data (Mosher et al. 1992). Minimum norm estimates (MNE), its weighted variant wMNE, low resolution electromagnetic tomography (LORETA), uniform LORETA (sLORETA), and exact LORETA (eLORETA) are other commonly used approaches. LORETA incorporates lead-field normalization with the Laplacian operator based on the solution's maximal smoothness and is based on neuroanatomical and electrophysiological constraints (Pascual-Marqui et al. 2002). sLORETA (Pascual-Marqui 2002) and eLORETA (Pascual-Marqui et al. 2011) are modified versions of LORETA, showing superior performance under specific conditions. Under ideal (no-noise) conditions, eLORETA performs source localization with zero error (Pascual-Marqui et al. 2011).

1.3.3 Analysis of task-related neural responses

Depending on the experimental paradigm, EEG may be used to evaluate event-related potentials (ERP) and event-related desynchronization/synchronization (ERD/ERS) as well as measure neuronal activity (Pfurtscheller and Lopes Da Silva 1999). In the first case, the ERP is phase-locked to the event, whereas ERD/ERS is not.

ERPs are voltage fluctuations reported on the scalp that represent a time-locked brain response to repeated stimulus presentation. ERP refers to a brain mechanism that involves thousands of simultaneous visual processing, attentional selection, awareness, and sensory-motor coupling (Al-Ezzi et al. 2020). For detecting ERPs, averaging techniques, with the goal of enhancing the SNR, are commonly used. Continuous EEG activity is referred to as additive noise because it has a fixed time delay in relation to the stimulus. This basic and commonly used model, on the other hand, is just a rough approximation of the actual situation. Therefore, evoked potentials (EPs) are assumed to be the product of reorganizing the phases of ongoing EEG signals. The ERP is notable for being a wave with both positive and negative peaks. Their polarity determines how they are labeled (P for positive and N for negative). In addition, the wave's latency in milliseconds is noted, as well as its polarity (with P100, is the positive peak around 100 ms after the onset of the stimulus is intended). Particularly, negative waves are associated with activation, while positive waves are associated with inhibition (figure 1.11). The P100, N100, and P200 components, for example, are all connected to simple, low-level perception and are completely

automatic. As a result, they appear following each perceptual stimulus. Finally, later components (after 250 ms) reflect conscious cognitive processing and can be elicited under some conditions (Beres 2017).

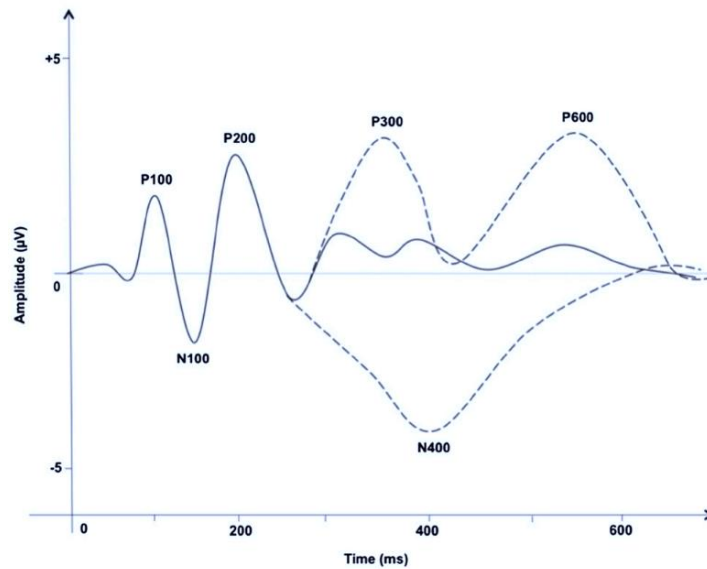


Figure 1.11. Example of the most common ERP components. The ERP is distinguished by the presence of both positive (P) and negative (N) peaks. The wave's latency in milliseconds is also noted. P100, for example, is the positive peak that appears about 100 milliseconds after the stimulus begins. Positive waves are linked to activation, while negative waves are linked to inhibition. This figure is adapted from Beres (2017), with permission.

ERD/ERS, on the other hand, which must be detected by investigating the frequency bands, consist decreases or increases in power, respectively. Therefore, they address frequency direct changes in the ongoing EEG activity. The underlying neuronal populations' synchrony decreases or increases as a result of these processes. Since ERD/ERS has a high temporal resolution, it can be used to research complex, time-related cognitive processes (Krause et al. 2008). The frequency of brain oscillations is generally inversely proportional to their amplitude, as mentioned in the previous chapter. Moreover, ERD/ERS are defined as the percentage of power decrease or increase, respectively. Notably, due to the slowness of event-related adjustments in ongoing EEG, the time between two consecutive events should last at least a few seconds (Pfurtscheller and Lopes Da Silva 1999). While ERD/ERS are activated by changes in one or more parameters that regulate oscillations in neuronal networks, ERPs are a series of transient post-synaptic responses of pyramidal neurons in response to a specific stimulus. Furthermore, ERD/ERS reflect changes in the behavior of local interactions between main neurons and interneurons, whereas ERPs influence the behavior of cortical neurons' responses (Pfurtscheller and Lopes Da Silva 1999). The most significant distinction between the two phenomena is that ERD/ERS occurs in different frequency bands, with ERD and ERS occurring at the same or different locations on the scalp.

1.4 Decoding and modulating neural activity in real-time

EEG has often been used as a diagnostic and investigational technique. EEG analysis has progressed from a simplistic visual inspection of amplitude and frequency patterns over time to a detailed review of the observed signals' temporal and spatial characteristics, thanks to technological advancements (Michel and Brunet 2019). EEG is now widely used for studying brain function and behavior in the sub-second range, as well as measuring neuronal processes (Michel et al. 2004; Michel and Brunet 2019). Real-time EEG applications are also becoming more popular, thanks to faster processors and algorithmic advances. For instance, the use of EEG permits the development of neurofeedback and closed-loop neuromodulation applications (Müller-Putz et al. 2005).

To date, several software solutions have been made available to the neuroscientific community for offline analysis of EEG recordings, including EEGLab (Arnaud Delorme and Makeig 2004), Fieldtrip (Oostenveld et al. 2011), Brainstorm (Tadel et al. 2011), SPM (Litvak et al. 2011) and MNE (Gramfort et al. 2014). Moreover, our research group proposed an offline analysis workflow specifically suited for hdEEG data, which integrates several tools from existing software with original solutions for data preprocessing, realistic head model generation and source localization. So far, our analysis workflow for hdEEG has been used to reconstruct large-scale brain networks (Liu et al. 2017, 2018) and to examine functional connectivity between network nodes (Samogin et al. 2019). Such an application does not require online data processing, which is instead needed for neurofeedback and closed-loop neuromodulation studies.

On the other hand, MNE Scan (<https://www.mne-cpp.org/index.php/category/development/mne-scan>) and NeuroPype (<https://www.neuropype.io>) have been recently introduced as new software packages for online analysis of EEG data. They offer several tools for real-time EEG data processing and feature extraction, and also incorporate source localization tools. They are not optimized for hdEEG systems as they rely on a template head model that does not consider electrode positions collected during the same experimental session (Van Hoey et al. 2000).

1.4.1 Neurofeedback

Neurofeedback is a self-regulation technique which is used to train brain activity (Thibault et al. 2016). This strategy is viably used for rehabilitation and enhancement. Thoughts, sensations, actions, and emotions are produced by contact between groups of cells in the brain, and these are decoded as thoughts, sensations, actions, and emotions. Brain activity is measured in real time during a neurofeedback session (figure 1.12), and the subject receives auditory or visual feedback when the brain increases or decreases its activity to achieve a pre-set goal level (Hsueh et al. 2016; Thibault et al. 2016).

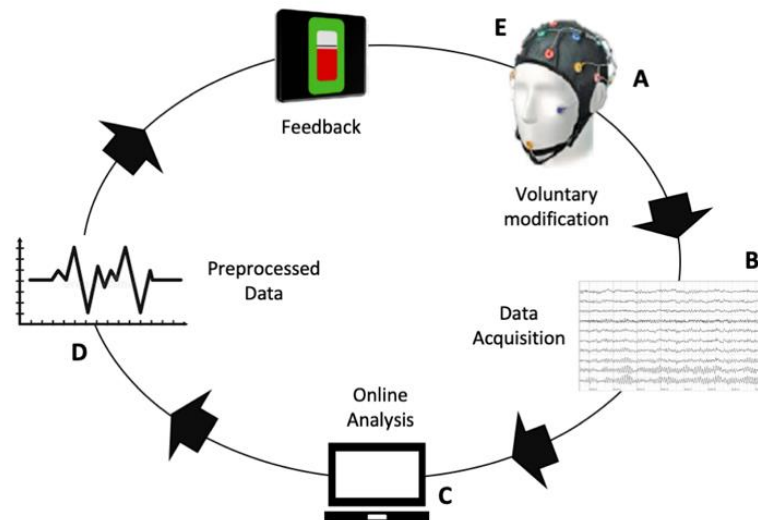


Figure 1.12. Neurofeedback experimental loop. A) The acquisition device receives scalp signals. B) which are recorded and stored on a local computer; C) another computer reads the data and performs online analysis.; D) processed data is presented to the participant in form of a visual object or a sound, moving or changing frequency, respectively, according to the recorded activity; E) via subjective experience, the participant influences his brain activity and thus controls the graphical object.

Neurofeedback allows a person to learn how to control their brain activity (Huster et al. 2014). For example, neurofeedback provides real-time input to a user about their own brain activity (e.g., in the visual domain, as a varying bar graph) (Pereira et al. 2019). During this process, the individual becomes aware of the improvements that have occurred during training and is able to evaluate their progress in order to reach optimum results (Marzbani et al. 2016). Moreover, the neurofeedback training is positively correlated with the numbers of the sessions and the precision of feedback (Thibault et al. 2016).

Different acquisition methods may be used to deliver neurofeedback and it can be divided into various groups based on the study's aim or acquisition technique (Huster et al. 2014). One of the most popular neurofeedback strategies for treating attention deficit hyperactivity disorder (ADHD), anxiety, and insomnia is frequency/power neurofeedback, which uses EEG as a recording method (Blaskovits et al. 2017; Enriquez-Geppert et al. 2019; Schabus et al. 2017). Then, epilepsy and migraine are treated with slow cortical potential neurofeedback (SCP-NF), which is again based on EEG (Gevensleben et al. 2014). Furthermore, a low-energy neurofeedback device (LENS) alters patients' brain waves by delivering a weak electromagnetic stimulus when they are motionless with their eyes closed (Ochs 2013), while Z-score neurofeedback could treat insomnia (Hammer et al. 2011).

Source-based neurofeedback is a relatively new approach (Boe et al. 2014; van Lutterveld et al. 2017). It may have a number of significant advantages over conventional sensor-based neurofeedback, including the ability to target the desired physiological signal in a more functionally and spatially specific manner. Neurofeedback derived from real-time source level analysis of MEG data has previously been shown to effectively modulate behavior in particular brain regions (Boe et al. 2014; Florin et al. 2014) and to provide a scalable approach to assist individuals in identifying and encouraging specific

cognitive states associated with meditation practice (van Lutterveld et al. 2017). Furthermore, the connectivity between cortical regions has been enhanced using fMRI (Pereira et al. 2019), suggesting that it may be used as a therapeutic tool in diseases like stroke that include impaired interhemispheric connectivity (Boe et al. 2014; Liew et al. 2016; Pereira et al. 2019). Notably, source-based EEG neurofeedback is an effective tool for modifying connectivity between various brain regions. Since fMRI has temporal resolution of the order of seconds and its signal is delayed by about 5 seconds with respect to neural events, fMRI neurofeedback cannot be used to measure connectivity on short time scales. To date, no research group has been able to implement connectivity-based EEG neurofeedback, as estimating connectivity changes over time requires real-time reconstruction of neural activity, which is methodologically very challenging.

In this regard, there are several technological limitations that have prevented the development of source-based neurofeedback applications. An important impediment for a reliable use of this technique is the presence of artifacts, which may be observed in the EEG data but are not related to neural activity (Guarnieri et al. 2018). It is essential that EEG data are cleaned before their use in the neurofeedback paradigm while preserving true neural activity, with high accuracy and algorithmic efficiency, necessary for real-time applications. As stated before, there are two main solutions that are currently in use: linear regression (REG) and blind source separation (BSS). In particular, the latter is in general computationally very expensive, and therefore less suited for real-time applications. Moreover, there are a limited number of studies that have attempted to combine REG and BSS techniques, tackling their major drawbacks and combining their positive features (Gao, Yang, et al. 2010; Klados et al. 2011; Kong et al. 2013; Mannan et al. 2016; Siew Cheok and Raveendran 2008; Zhang et al. 2015). In short, these studies proposed: (1) to decompose the EEG data by BSS; (2) select artefactual components; (3) apply regression analysis to remove true artifacts from them while preserving residual neural activity; and finally, (4) back-reconstruct the clean EEG data by recombining the non-artefactual components as well as the residuals of the artefactual components. The combination of regression and BSS techniques may hold strong potential; we identify however three potential issues with the approach described above. First, as in classical regression procedures, the method assumes the similarity between the time courses of non-cerebral electrical signals and those of the components produced by BSS. Second, the regression analysis is applied to selected components only, so it is still possible that residual artefactual contribution is present in the components that are recombined to generate the 'clean' EEG data. Third, the artifact removal is not implemented in the form of a spatial filter, which makes computations particularly intensive in the case of hdEEG data.

1.4.2 Closed-loop neuromodulation

Several neuromodulation systems provide stimulation in an open-loop modality. Specifically, The experimenter predetermines defined stimulus parameters such as phase, frequency, pulse form, and intensity based on prior empirical evidence (Sun and Morrell 2014). Remarkably, these parameters,

while remaining fixed during open-loop neuromodulation, do not automatically relate to changes in the patient's symptoms (Iturrate et al. 2018; Sun and Morrell 2014).

Closed-loop systems can increase the efficacy of stimulation by modulating or adapting therapy in response to physiological changes (Sun and Morrell 2014). The adaptive design of closed-loop neuromodulation naturally decreases intra- and inter-subject variability (Iturrate et al. 2018). In a closed-loop neuromodulation scenario, neural activity is continuously monitored, the huge stimulating artifact on the electrophysiological signal must be attenuated, a biomarker must be extracted in real-time, and magnetic/electrical stimulation must be dynamically modified based on this biomarker (figure 1.13) (Guggenmos et al. 2013; Iturrate et al. 2018; Rebesco et al. 2010). Preliminary results obtained with invasive stimulation protocols have demonstrated that using such closed-loop technology can be beneficial (Little et al. 2013, 2016).

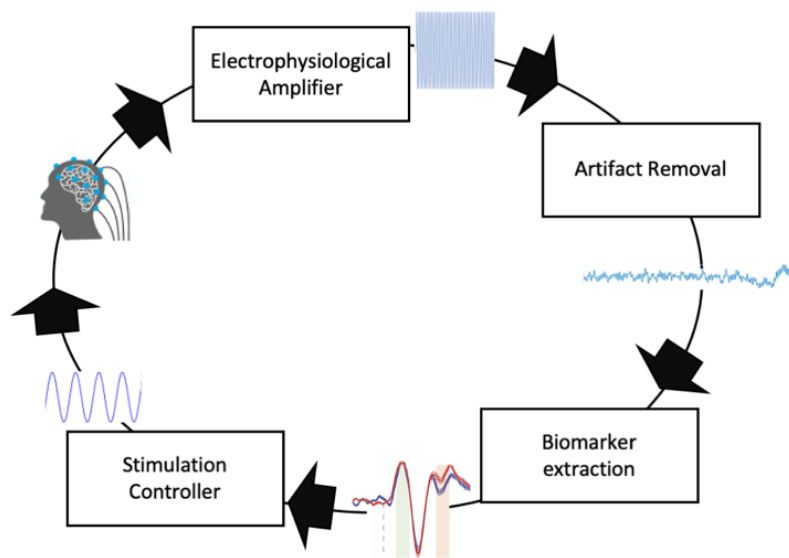


Figure 1.13. Closed-loop neuromodulation scenario. The stimulation parameters are adapted based on the biomarkers. In a closed-loop neuromodulation experiment, there are three main stages to take in consideration: biomarker extraction, stimulation controller, and the stimulation artifact removal.

In general, there are different closed-loop neuromodulation control strategies that can be employed (figure 1.14). These variations depend on the biomarker type and the stimulation parameter to be regulated (Iturrate et al. 2018).

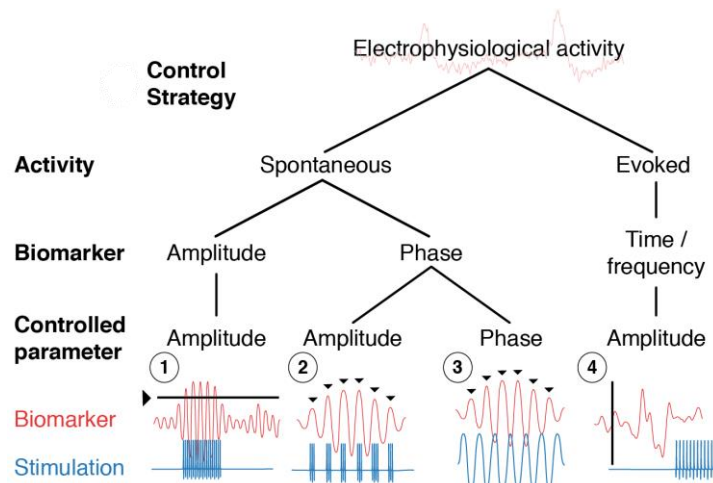


Figure 1.14. Various biomarkers and control approaches. (1) The amplitude of stimulation is determined by an amplitude threshold. (2 and 3) The phase of the oscillatory biomarker is detected (black triangles) and used to either trigger stimulation bursts (2) or lock the stimulation phase (3). (4) When evoked activity is decoded in time or frequency domains, the stimulus amplitude is altered accordingly. This figure is adapted from Iturrate et al. (2018), with permission.

In the biomarker amplitude–stimulation amplitude strategy, the amplitude or strength of the biomarker controls the stimulation intensity (figure 1.14.1) (Little et al. 2013). In the biomarker phase–stimulation amplitude (figure 1.14.2), the stimulation intensity is triggered on the phases of the biomarker (Zrenner et al. 2018). The biomarker phase–stimulation phase (figure 1.14.3) then adjusts the stimulation phase to target the phase of a biomarker (Brittain et al. 2013). Finally, other biomarkers have been investigated and may be superior in some situations. For example, an event-related potential (figure 1.14.4) can be decoded for each single trial (Iturrate et al. 2015) or in the frequency domain (Ezzyat et al. 2018).

Although the closed-loop neuromodulation is an encouraging technique, there are still a few challenges, such as the presence of the stimulation artifact on EEG data (Guarnieri, Brancucci, et al. 2020). Finally, the artifacts can have a number of characteristics depending on the stimulated tissue, the stimulus type, and the recording modality (Iturrate et al. 2015). In particular, the combination of EEG and tACS is technically challenging, because of the massive artifact that is mixed in the EEG data, in the form of a quasi-sinusoidal signal with main harmonic at the stimulation frequency. For this reason, most EEG-tACS studies have been so far conducted using an interleaved stimulation protocol, and in particular analyzing the EEG data collected in the off-stimulation period (Mansouri et al. 2017; Pahor and Jaušovec 2018; Vossen et al. 2015). Currently, few solutions exist to attenuate the tACS artifact from EEG recordings. A first approach that has been proposed is the subtraction of a constant sine wave fitted to the EEG signal. Due to variations in the EEG signal primarily induced by slow changes in electrode conductance and by movements of the participant’s head, this solution often yields unsatisfactory results (Helfrich, Schneider, et al. 2014). Other tACS methods require the whole EEG recording to be available, and are therefore unsuitable for closed-loop neuromodulation studies (Helfrich, Schneider, et al. 2014; Kohli and Casson 2020). For instance, the one proposed by Helfrich and colleagues follows a two-step procedure: an artifact template is first subtracted from the data, and the remaining artifacts are then attenuated using principal component analysis (PCA) (Helfrich, Schneider, et al. 2014). Only

one method, the superimposition of moving averages (SupMA) (Kohli and Casson2015), has been used for real-time removal of tACS artifacts. However, in its current implementation, SupMA can simultaneously process only few EEG signals. Furthermore, it tends to strongly suppress the harmonics associated with the tACS artifact, possibly inducing large distortions in the frequency characteristics of neural signals (Kohli and Casson 2019).

1.5 Thesis aims and outline

The main goal of this thesis is to develop a real-time hdEEG workflow for source-based neurofeedback and neuromodulation. Such a workflow should incorporate reliable real-time EEG source activity reconstruction and EEG source localization using accurate bio-physical models.

In Chapter 2, we tackle a specific issue in real-time EEG processing: biological artifact removal (Guarnieri et al. 2018). The successful attenuation of artifacts that are mixed in the recordings is critical to the success of neurofeedback applications based on EEG data. To address this problem, we introduce a novel online EEG artifact removal method for neurofeedback applications. Notably, we have used both simulated data and real experiment data to assess the performance of our method.

In Chapter 3, we present an approach for stimulation artifact removal in real-time (Guarnieri, Brancucci, et al. 2020). The massive artifact that is mixed in the EEG data is one of the main reasons why there are so few studies examining effects on neural activity during tACS. To enable closed-loop neuromodulation applications, we have developed a novel online tACS artifact removal technique.

In Chapter 4, we present an optimized pipeline for source-based EEG localization in real-time. High-density montages are required to perform source localizations using EEG data. To take advantage of the hdEEG for novel brain computer interface (BCI) applications, dedicated tools are currently lacking. With the goal of enabling neural activity reconstruction, we have developed a real-time noninvasive electrophysiology toolbox (RT-NET) for the online processing of hdEEG data (Guarnieri, Zhao, et al. 2020).

Finally, in Chapter 5, we discuss the novel contributions and limitations in the PhD thesis work, and we suggest future research directions as well.

2 Online EEG artifact removal for BCI applications by adaptive spatial filtering

Guarnieri R, Marino M, Barban F, Ganzetti M, Mantini D. *Online EEG artifact removal for BCI applications by adaptive spatial filtering*. J Neural Eng. 2018 Oct;15(5):056009. doi: 10.1088/1741-2552/aacfd. Epub 2018 Jun 28.

Abstract

Objective. The performance of brain–computer interfaces (BCIs) based on electroencephalography (EEG) data strongly depends on the effective attenuation of artifacts that are mixed in the recordings. To address this problem, we have developed a novel online EEG artifact removal method for BCI applications, which combines blind source separation (BSS) and regression (REG) analysis.

Approach. The BSS-REG method relies on the availability of a calibration dataset of limited duration for the initialization of a spatial filter using BSS. Online artifact removal is implemented by dynamically adjusting the spatial filter in the actual experiment, based on a linear regression technique.

Main results. Our results showed that the BSS-REG method is capable of attenuating different kinds of artifacts, including ocular and muscular, while preserving true neural activity. Thanks to its low computational requirements, BSS-REG can be applied to low-density as well as high-density EEG data.

Significance. We argue that BSS-REG may enable the development of novel BCI applications requiring high-density recordings, such as source-based neurofeedback and closed-loop neuromodulation.

Keywords: electroencephalography, brain–computer interface, blind source separation, independent component analysis, linear regression, online processing

2.1 Introduction

A brain–computer interface (BCI) is a computer-based system that acquires brain signals, analyses them, and eventually translates them into commands for an electronic device to carry out a desired action (Shih et al. 2012). BCIs are often used to assist, restore or augment human sensory-motor or cognitive functions (Krucoff et al. 2016). BCI technology is the focus of big research endeavors involving neuroscientists, engineers and clinicians. The most widely used technique for acquiring brain signals to be used in BCIs is electroencephalography (EEG) (Müller-Putz et al. 2005). EEG measures changes in electrical potentials at different locations on the scalp, which are produced by the synchronized firing of thousands of neurons. It has the advantage of being relatively cheap and portable, and providing millisecond temporal resolution. All these features are particularly important for BCI applications. In recent years, high-density EEG (hdEEG) systems have become available, permitting to increase the spatial resolution of the reconstructed neural activity (B. He et al. 2011). These developments have

opened up the doors to the use of hdEEG as a brain imaging tool (Michel and Murray 2012). Such advances may be particularly relevant also in the context of BCI, as it may be possible to rely on real-time information about brain activity in one brain region, or about connectivity between two brain regions, instead of using sensor-space EEG signals.

An important impediment for a reliable use of EEG for BCI applications is the presence of artifacts, which may be observed in the EEG data but are not related to neural activity. Such artifacts may be produced by power lines, electrical equipment, or be of biological origin. Sources of biological artifacts include eye blinks, cardiac activity, muscle contractions, and head movements (Kong et al. 2013; Winkler et al. 2011). It is essential that EEG data are cleaned before their use in BCI system, to ensure that any control achieved is related to the participant's brain activity. By the same token, it is also important that true neural activity is not distorted. Moreover, online EEG processing is strictly required in the case of BCI applications. As such, an artifact removal solution that combines high accuracy and algorithmic efficiency needs to be sought.

Generally speaking, artifacts have overlapping frequencies with respect to the neural activity of interest. As such, temporal filtering is unlikely to be an effective solution for EEG artifact removal (Muthukumaraswamy 2013). On the other hand, spatial filtering is a computationally efficient approach, which permits to remove artifacts by exploiting information about their spatial distribution over the EEG sensors (Lagerlund et al. 1997). Spatial filters are widely used in the field of BCI (Wu et al. 2017), as they can be applied to each input data sample as it becomes available. To carry out spatial filtering of artefactual signals, EEG data are multiplied by a $[g \times g]$ image operator, where g is the number of recordings. Such image operator can be created following different methodological approaches. There are two main solutions that are currently in use: (i) regression techniques (REG) (P. He et al. 2004; Schlogl et al. 2007) and (ii) blind source separation (BSS) techniques (Choi et al. 2005).

REG are based on the weighted subtraction of electrical signals representing artefactual sources, as for example electrooculography (EOG) and electromyography (EMG) signals. Removal of artefactual activities using regression method is indeed based on an assumption that there is no correlation between the true neuronal activity and EOG/EMG signals (Jervis et al. 1988; Sadasivan and Dutt 1996). As a matter of fact, any activity common to EEG and EOG/EMG signals is attenuated, if not suppressed, by regression. Furthermore, the estimate of proper weights by regression is accurate when EOG/EMG signals have very similar waveforms as compared to the actual artifacts in the EEG data. This assumption is not always met, as the relative position of the artefactual source with respect to EEG and EOG/EMG signals is not matching.

Another group of artifact removal techniques relies on BSS. The most famous method belonging to this group is independent component analysis (ICA) (Nolan et al. 2010; Turnip 2014; Xiaopei and Zhongfu 2005), but there are also other BSS approaches such as principal component analysis (PCA) (Turnip and Junaidi 2014) and canonical correlation analysis (CCA) (Gao, Zheng, et al. 2010). BSS methods are capable of separating signals originating from different sources (i.e. components), which

are mixed in the recordings (A Delorme et al. 2012; Zeng et al. 2013). By means of BSS, it is possible to isolate artefactual components and remove them from the EEG data with proper weights. The main disadvantage of this methodology is that the automated classification of artefactual components is not straightforward (Mahajan and Morshed 2015), and the latter may also contain residual neural activity (Winkler et al. 2014). Another potential limitation of BSS solutions is that they typically assume the stationarity of the sources, i.e. the weights associated with the components are fixed over the whole EEG recording (Marino, Liu, Del Castello, et al. 2018; Winkler et al. 2011). Some BSS approaches do not suffer from this limitation, as they can estimate components on short time windows (Daly et al. 2015). However, they are computationally very expensive, and therefore less suited for BCI applications.

A limited number of studies have attempted to combine regression and BSS techniques, tackling their major drawbacks and combining their positive features (Gao, Yang, et al. 2010; Klados et al. 2011; Kong et al. 2013; Mannan et al. 2016; Siew Cheok and Raveendran 2008; Zhang et al. 2015). In short, these studies proposed: (1) to decompose the EEG data by BSS; (2) select artefactual components; (3) apply regression analysis to remove true artifacts from them while preserving residual neural activity; and finally, (4) back-reconstruct the clean EEG data by recombining the non-artefactual components as well as the residuals of the artefactual components. The combination of regression and BSS techniques may hold strong potential; we identify however three potential issues with the approach described above. First, as in classical regression procedures, the method assumes the similarity between the time courses of non-cerebral electrical signals and those of the components produced by BSS. Second, the regression analysis is applied to selected components only, so it is still possible that residual artefactual contribution is present in the components that are recombined to generate the 'clean' EEG data. Third, the artifact removal is not implemented in the form of a spatial filter, which makes computations particularly heavy for hdEEG data. In this study, we present a novel online EEG artifact removal method for BCI applications, which, by combining BSS and REG in an original way, addresses each of the three problems mentioned above. Our BSS-REG method is primarily intended as an adaptive spatial filter approach. This is meant to be particularly suitable for hdEEG due to its low computational requirements, but can be also applied to low-density EEG. In the first instance, BSS is run on a calibration dataset for the creation of a spatial filter capable of extracting artefactual signals from EEG data. This filter, while being applied to actual EEG data, is fine-tuned in a dynamic manner using regression analysis. This adaptive spatial filtering approach can be applied for the removal of a wide range of biological and non-biological artifacts.

In this study, its performance is assessed by focusing on ocular artifacts, which strongly contaminate almost any EEG recording (Schlogl et al. 2007; Zeng et al. 2013) and have been shown to substantially affect BCI performance (Fatourechi et al. 2007). In this case, simulated data are used to accurately quantify performance in controlled settings. A comparison with alternative methods for the online correction of ocular artifacts is conducted, both in terms of accuracy and computational efficiency. Finally, the validation is extended to real EEG data, which are corrupted by different kinds of artifacts,

such as ocular and muscular artifacts. A comparison is carried out between the results obtained using our online correction method and a previously validated offline artifact removal approach based on BSS.

2.2 Methods

2.2.1 Description of the method

The BSS-REG method relies on the availability of a calibration dataset of limited duration for the initialization of a spatial filter, which is then dynamically adjusted in the actual experiment for online artifact removal.

2.2.1.1 Spatial filter initialization on a calibration dataset

First of all, BSS is applied to an EEG calibration dataset for the decomposition of cerebral and artefactual signals that are present in the recordings. The number of time samples n in this EEG dataset does not need to be fixed a priori. However, this will inherently have an impact on the performance of data decomposition by BSS. The BSS model can be mathematically described as:

$$X(t) = A \cdot S(t) \tag{2.1}$$

where $X(t) = [x_1(t), \dots, x_g(t)]$ is the matrix of g observed signals, $S(t) = [s_1(t), \dots, s_m(t)]$ the matrix of m underlying signals and $A [g \times m]$ denotes the mixing matrix (Stone 2004). It is a generative model, which means that it describes how the observed data are generated by a process of mixing the underlying signals s_i (with $i = 1, \dots, m$), also referred to as sources or components. A solution for the BSS problem is possible if the number of components is at most equal to the number of observed signals ($m \leq g$). In this case, the components can be retrieved by determining a $[m \cdot g]$ matrix W , named unmixing matrix, such as:

$$S(t) = W \cdot X(t) \tag{2.2}$$

Notably, ICA can be used for BSS, when the components can be assumed to be statistically independent (Hyvärinen et al. 2004). On the other hand, PCA and CCA rely on the assumption that these are statistically uncorrelated (less stringent criterion) (Gao, Yang, et al. 2010; Turnip and Junaidi 2014). In the current implementation of BSS-REG, BSS is performed using FastICA (<http://research.ics.aalto.fi/ica/fastica>), an ICA algorithm which has shown to have fast convergence and yield accurate data decomposition (Hyvärinen et al. 2004; Nolan et al. 2010). However, other BSS algorithms, such as Infomax (Bell and Sejnowski 1995) and JADE (Rutledge and Jouan-Rimbaud Bouveresse 2013), PCA (Shlens 2014; Turnip and Junaidi 2014; Wold et al. 1987) and CCA (Hotelling 1936), could also be alternatively used. Though, it is worth noting that the specific BSS approach to be

used should be chosen depending on the specific characteristics of the artifacts to be removed (Halder et al. 2007).

After BSS has been applied to the EEG calibration dataset, the underlying signals that are associated with the artifacts need to be identified. To this end, different selection criteria can be used, depending on the specific artifact. In BSS-REG, for the identification of artifactual independent components (ICs), we use the same parameters as in (Liu et al. 2017): (1) correlation between the power of the IC with the vertical EOG (vEOG), horizontal EOG (hEOG) and EMG; (2) the coefficient of determination obtained by fitting the IC power spectrum with a $1/f$ function; (3) the kurtosis of the IC. The components with at least one of the three parameters outside the normal range, as defined in (Liu et al. 2017), are classified as artefactual. The unmixing matrix W_A for the artefactual components $S_A(t)$ is obtained by selecting the corresponding rows of the matrix W . This matrix W_A is essentially a spatial filter, which permits to obtain an estimate of (uncorrelated or independent) artefactual components $S_A(t)$, according to:

$$S_A(t) = W_A \cdot X(t) \quad (2.3)$$

2.2.1.2 Adaptive spatial filtering for online artifact removal

During the real experiment requiring online artifact removal, EEG signals are read and stored in a buffer of k samples. The spatial filter W_A calculated on a calibration dataset is applied, for each given instant, to the EEG data $X(\tau)$ in the buffer, such that an estimate of the artefactual signals $S_A(\tau)$ can be obtained:

$$S_A(\tau) = W_A \cdot X(\tau) \quad (2.4)$$

At this stage, regression analysis is used to dynamically estimate the weights B_A to be used for artifact removal. This permits to account for the non-stationarity of the artefactual contribution in the EEG signals. Different approaches can be used for estimating the weights B_A to be associated with the artefactual components (Croft and Barry 2000; Gomez-Herrero et al. 2006; Jung, Makeig, Westerfield, et al. 2000), to satisfy the following equation:

$$X(\tau) = B_A \cdot S_A(\tau) + \varepsilon(\tau) \quad (2.5)$$

where $\varepsilon(\tau)$ is the residual of $X(\tau)$ that cannot be explained by a linear combination of $S_A(\tau)$. In BSS-REG, we employ the ordinary least squares (OLS) regression method (Moretti et al. 2003) due to its low computational complexity and numerical efficiency. Accordingly, the weights B_A are obtained as:

$$B_A = X_A(\tau) \cdot S_A^T(\tau) \cdot \left(S_A(\tau) \cdot S_A^T(\tau) \right)^{-1} \approx X(\tau) \cdot S_A^T(\tau) \cdot \left(S_A(\tau) \cdot S_A^T(\tau) \right)^{-1} \quad (2.6)$$

This permits us to build an adaptive spatial filter $F(\tau)$ to dynamically obtain artifact-free signals $X_c(\tau)$, such as:

$$X_c(\tau) = F(\tau) \cdot X(\tau) \quad (2.7)$$

Specifically, $F(\tau)$ is defined as follows:

$$F(\tau) = I - X(\tau) \cdot S_A^T(\tau) \cdot \left(S_A(\tau) \cdot S_A^T(\tau) \right)^{-1} \cdot W_A \quad (2.8)$$

where I is an identity matrix with dimension $[g \cdot g]$.

2.2.2 Validation of the method

The performance of the BSS-REG method was assessed on both simulated and real EEG data, with special focus on ocular artifact removal. In this case, it is indeed possible to use a wide range of alternative methods as benchmark. Since BSS-REG can be used also for other kinds of artifacts in EEG recordings, we extended the validation to real datasets. The accuracy in terms of artifact removal achieved by BSS-REG was compared against that of an offline artifact removal method based on ICA (Liu et al. 2017).

2.2.2.1 Real and simulated EEG data

Data used in this study were obtained from hdEEG recordings collected in 17 healthy right-handed participants (4 males and 13 females, with age ranging from 21 to 43 years). These recordings were used in our previous studies (Liu et al. 2015, 2017). All participants reported normal or corrected-to-normal vision, had no psychiatric or neurological history, were free of psychotropic or vasoactive medication. Before undergoing the examination, they gave written informed consent to the experimental procedures, which were approved by the Institutional Ethics Committee of ETH Zurich. hdEEG signals were recorded at 1000 Hz using a 256-channel system from Electrical Geodesics (Eugene, US). The electrode at vertex (labeled as Cz in the 10/20 international system) was used as physical reference. In addition to hdEEG, we also recorded horizontal and vertical EOG (hEOG/vEOG), as well as EMG for masseter and platysma muscles, to detect head movement and swallowing, respectively.

For each participant, we recorded hdEEG signals during resting state (for 4 min) and during visual oddball tasks (for 3 min). In the resting state condition, each participant fixated a cross in the center of a screen. The visual oddball task consisted of a presentation of 80% of frequent stimuli and 20% of rare stimuli respectively (Mantini et al. 2009). The stimuli included purple circles of 3.2° and 1.6° of visual angle for frequent and rare events respectively. They were presented on a black background for 7 ms. The task consisted of pressing a button as soon as possible after the rare event (target) appeared. The

interval between stimuli was 2 s, for a total number of 90 trials (Murphy et al. 2014; O’Connell et al. 2012).

The collected hdEEG data were preprocessed using EEGLAB (<https://sccn.ucsd.edu/eeglab/index.php>) and built-in MATLAB functions. The preprocessing steps included: bad-channel detection and interpolation, digital filtering in the band 1–80 Hz, resampling to 200 Hz and average re-referencing. In addition, off-line artifact removal was performed by means of ICA, using the same criteria used in BSS-REG, and previously described in (Liu et al. 2017). The artifact-cleaned dataset obtained with ICA was used as a reference to evaluate the performance of the online artifact removal by BSS-REG. In addition, the same dataset was used for the generation of a new dataset, in which simulated ocular artifacts were added (figure 2.1).

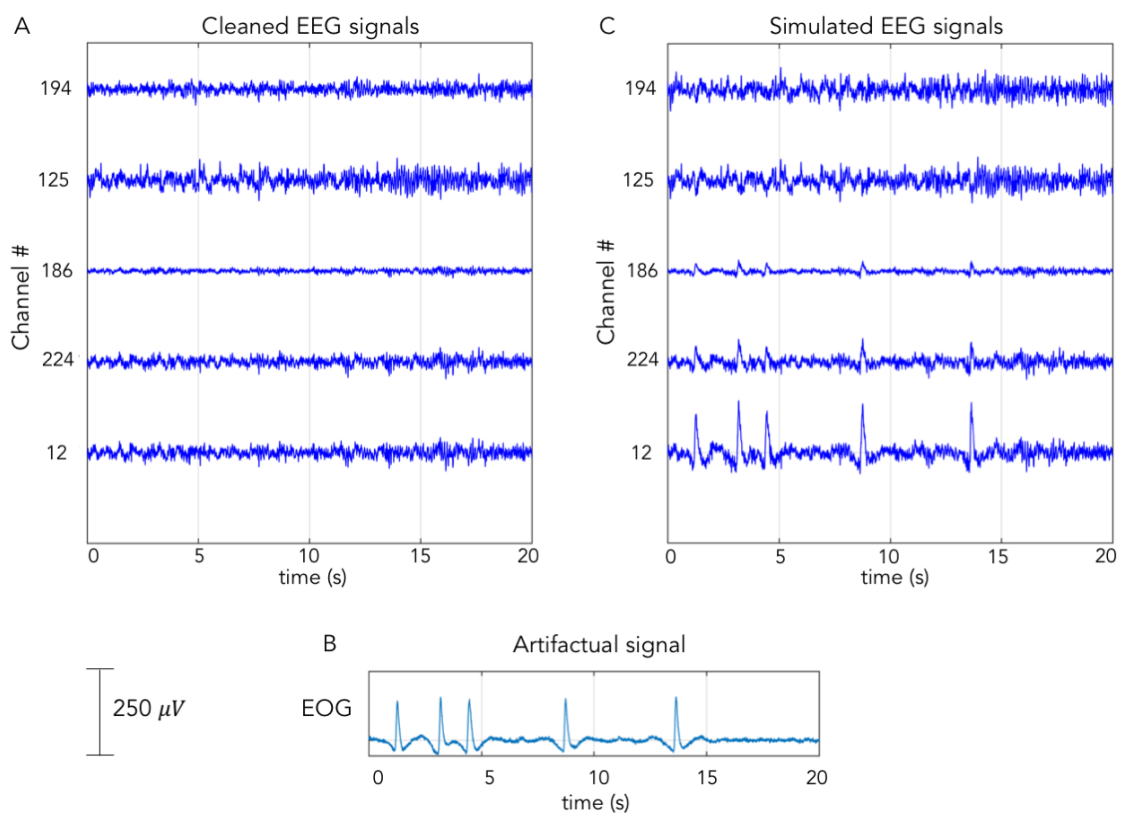


Figure 2.1. Illustrative example of 20 s of (A) cleaned EEG signals in five representative channels; (B) simulated ocular artifact; and (C) simulated EEG signals, obtained adding the ocular artifact to the cleaned EEG signals. (A) and (B) are extracted from different subjects.

These ocular artifacts were obtained from signals reconstructed by superimposing the contribution of IC associated with EOG collected in another participant to the hdEEG recordings of the initial dataset (Romero et al. 2008). For the definition of BSS-REG standard settings we selected seven datasets, and we then validated them using the remaining ten datasets. Both in the case of simulated and real hdEEG data, a pseudo-online test was performed by using a moving window approach, to generate a ‘virtual’ buffer of data to be given as input to BSS-REG and other online artifact removal algorithms.

2.2.2.2 Analysis of BSS-REG performance

We first performed an optimization of the BSS-REG parameters and settings using the first seven datasets. Since BSS-REG relies on the creation of an initial spatial filter by performing BSS on a calibration dataset, we first compared different BSS solutions on the simulated resting-state EEG data. Specifically, we assessed the ability of the BSS-derived spatial filter to reconstruct the ocular signal that was superimposed over the EEG signals. By using resting-state EEG data, we compared the results obtained using the FastICA algorithm (our default solution) against other ICA algorithms, such as Infomax, JADE, PCA and CCA. Reconstruction performance, which was quantified in terms of temporal correlation between simulated and reconstructed ocular signals, was examined for different durations of the calibration recording (ranging between 30 s and 4 min). By using a pseudo-online test, we also assessed what size of the data buffer can lead to the best combination of artifact attenuation accuracy and computation speed required for online processing. Accuracy was quantified by means of the cosine similarity measure (CSM) (Eldeen et al. 2017; Niknazar et al. 2018), defined as follows:

$$CSM = \frac{\langle X_b(t), X_c(t) \rangle}{\|X_b(t)\| \cdot \|X_c(t)\|} \quad (2.9)$$

where $X_b(t)$ is the simulated EEG dataset before artefactual contamination and $X_c(t)$ is the reconstructed EEG dataset after artifact removal. CSM ranges between 0 and 1, and values close to 1 are associated with good reconstruction performance. Computational time was quantified using MATLAB (release 2016b) running under MacOS (with 2.5 GHz Intel Core i7 processor and 16 GB RAM). Both accuracy and computation time were evaluated using the visual oddball paradigm data for different length of the buffer size (ranging between 100 and 2000 ms).

After defining the BSS method to be used and the method settings, we compared the performance of BSS-REG with respect to other methods using 10 additional datasets. The utility of the two-step approach implemented in BSS-REG was assessed by comparing its performance with that of BSS spatial filtering (Jung, Makeig, Humphries, et al. 2000) and OLS regression (Moretti et al. 2003), separately. Furthermore, we employed a number of commonly used approaches for online ocular artifact removal as benchmark for our method. Specifically, we used adaptive filtering (AF) (P. He et al. 2004), least mean squares (LMS) (Haykin 1996), conventional recursive least squares (CRLS) (P. He et al. 2004) and an adaptive algorithm based on time varying H^∞ (HINFTV) (Puthusserypady and Ratnarajah 2005). The first of those methods is implemented in BCILAB (<https://scn.ucsd.edu/wiki/BCILAB>), whereas the other ones are part of the Automatic Artifact Removal toolbox (http://germangh.github.io/eeglab_plugin_aar) (Gomez-Herrero et al. 2006). A repeated-measures one-way ANOVA and post-hoc paired t-tests were carried out to assess significant differences across and between methods with regard to accuracy and computational efficiency.

Finally, after conducting an assessment of the performance on ocular artifact removal, we extended our investigation to other kinds of artifacts, such as muscular and movement artifacts, that are present

in the EEG data. Accordingly, we used the resting state dataset for the initialization of the BSS-REG spatial filter, and applied the adaptive spatial filtering of BSS-REG to the visual oddball dataset. The reconstruction performance was assessed against that obtained on the same dataset using offline ICA processing. Both in the case of online BSS-REG and offline ICA processing, we evaluated event-related potentials (ERPs) for rare events (100 ms pre-stimulus and 600 ms post-stimulus time) only, as these are the ones supposedly showing the P300 response (Liu et al. 2015; Mantini et al. 2009; Picton 1992). We specifically quantified pre-stimulus noise level as the root mean square (RMS) in the pre-stimulus interval (Mantini et al. 2009) and inter-trial variability defined the mean of across-trial standard deviation (Marino, Liu, Koudelka, et al. 2018; Vanderperren et al. 2010). Improvement following artifact removal was assessed by calculating the ratio between each index before and after artifact removal respectively. A paired t-test was used to evaluate whether there are significant differences between online BSS-REG and offline ICA processing in terms of pre-stimulus noise level and inter-trial variability, respectively.

2.3 Results

2.3.1 Definition of BSS-REG standard settings

The performance of the BSS-REG approach relies in the first instance on the BSS algorithm used and on the amount of data available for the initialization of the spatial filter. Accordingly, we analyzed the accuracy and stability of different BSS approaches for the reconstruction of the ocular artifact. As expected, the correlation between the simulated ocular signal and the reconstructed one generally increased for any BSS method under investigation (figure 2.2).

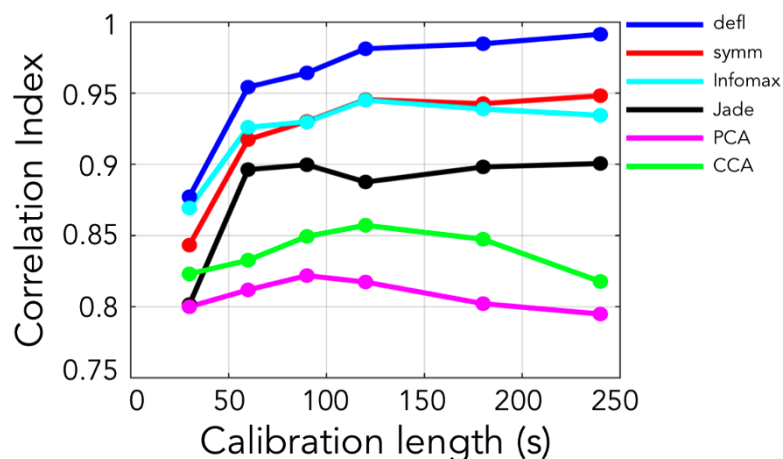


Figure 2.2. Quantitative comparison of different BSS method under investigation. Comparison is performed by correlating ocular signal and reconstructed one for any BSS method across all the subjects. For each subject, the FastICA (deflation approach) method outperforms all the other methods in terms of ocular signal reconstruction as shown by the consistently higher correlation, regardless of the calibration length. Moreover, the performances of any method generally improve depending on the amount of data.

Overall, the FastICA and Infomax algorithms showed superior performance than JADE, PCA and CCA. FastICA required more input data than Infomax to achieve a good data decomposition, and hence ocular signal reconstruction. However, when using a calibration dataset of 4 min, FastICA yielded the best reconstruction of the ocular artifact, which is likely to be acceptable in a wide range of applications. We therefore relied on this solution for adaptive spatial filtering by BSS-REG.

We then moved to the analysis of the BSS-REG performance in a pseudo-online test. As such, we examined to what extent and how the size of the data buffer influences the reconstruction of the ocular artifact. We observed that both accuracy (figure 2.3A) and computational time (figure 2.3B) increased with a longer data buffer. However, we found that a buffer of 1000 ms or more yielded a computation time above 5 ms. Since the EEG signal was sampled at 200 Hz, 5 ms is the maximum delay that could be accepted in online EEG processing. Based on these considerations, we selected 500 ms as the standard buffer size for BSS-REG. This choice yielded a CSM equal to 0.957, and a computation time equal to 2.1 ms (see figure 2.3).

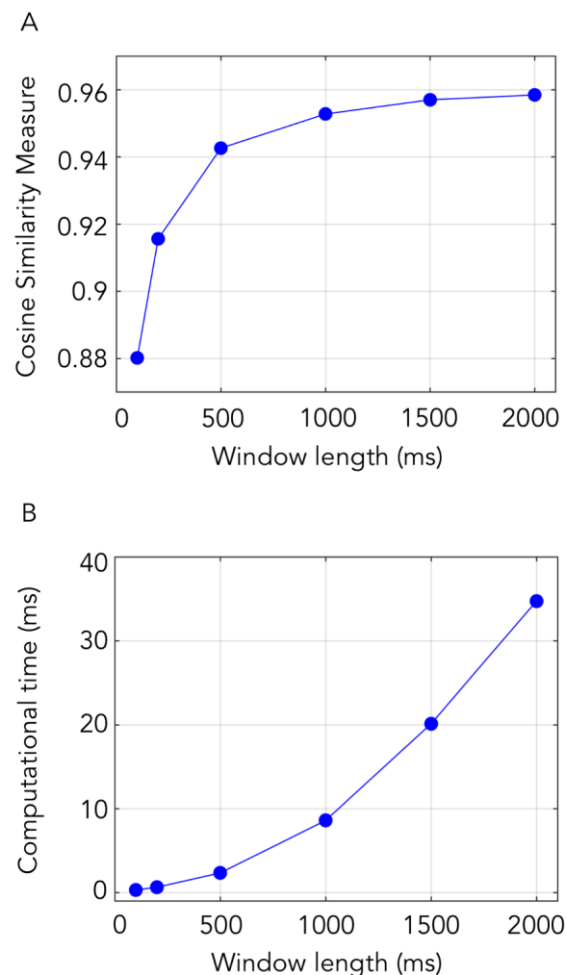


Figure 2.3. BSS-REG performance in a pseudo-online test. The size of the data buffer influences the reconstruction of the ocular artifact. With a longer data buffer, (A) CSM and (B) computational time both increase.

2.3.2 Analysis of BSS-REG performance on simulated EEG data

By using simulated EEG data, we could also quantify the performance of BSS-REG with respect to alternative approaches. First, we examined whether our method, in its standard settings, performs better than when using BSS and linear regression separately. As for BSS, we calculated a spatial filter on resting state EEG data by using ICA and applied it directly to the oddball paradigm EEG data. Linear regression was implemented through OLS, using the recorded EOG signals as reference signals for online artifact removal. A repeated measures one-way ANOVA revealed significant differences among BSS-REG, ICA and OLS methods ($p < 0.0001$) (figure 2.4).

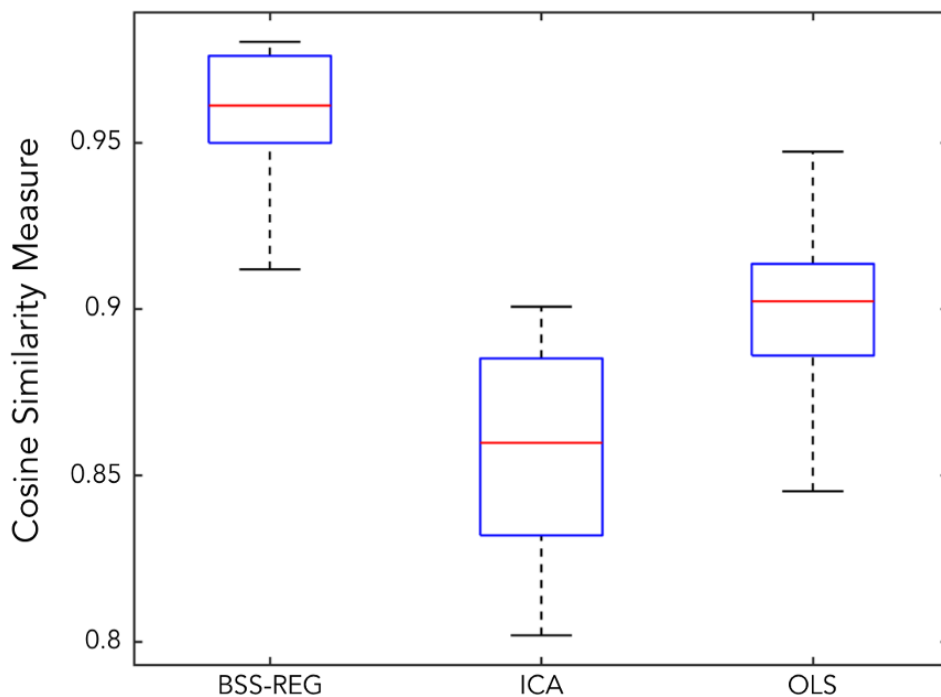


Figure 2.4. Quantitative assessment of EOG artifact attenuation across methods. Comparison is performed by examining the CSM and box plots are provided. BSS-REG, ICA and OLS methods were applied for removing the EOG artifact from the EEG recordings. For each subject, the BSS-REG method outperforms the other methods in term of EOG artifact attenuation.

Significant differences were found between BSS-REG and ICA ($p < 0.0001$) and between BSS-REG and OLS ($p = 0.0004$). This finding confirmed that the use of an adaptive spatial filter obtained by combining BSS and linear regression is beneficial to achieve a more accurate online artifact removal. Furthermore, the use of BSS-REG can lead to a more effective removal of ocular artifacts in comparison to AF, LMS, CRLS and HINFTV both in terms of accuracy (figure 2.5A) and computational time (figure 2.5B). A repeated measures one-way ANOVA confirmed that there were significant differences among BSS-REG, AF, LMS, CRLS and HINFTV methods, both for accuracy and computational time ($p < 0.0001$). In terms of accuracy, paired t-tests denoted significant differences between BSS-REG and AF, CRLS and HINFTV ($p = 0.0042$, $p < 0.0001$ and $p < 0.0001$, respectively), and no significant difference between BSS-REG and LMS ($p = 0.415$). With regard to computational efficiency, paired t-tests revealed significant differences between BSS-REG and all other methods ($p < 0.0001$).

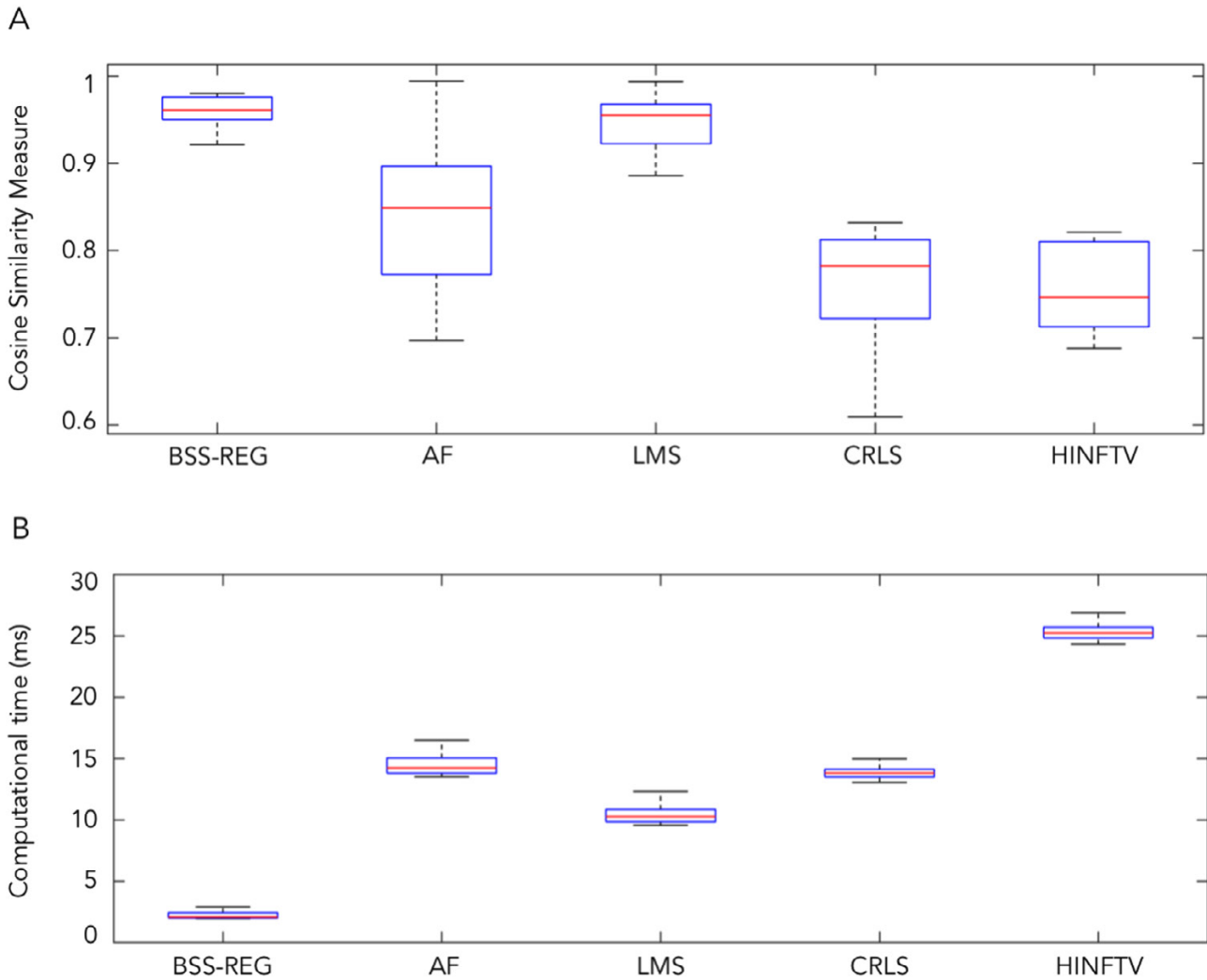


Figure 2.5. Quantitative assessment of EOG artifact attenuation across methods: (A) BSS-REG, AF, LMS, CRLS and HINFTV methods were applied for removing the EOG artifact from the EEG recordings. A comparison is performed by examining the CSM and box plots are provided. For each subject, the BSS-REG method outperforms the other methods in term of EOG artifact attenuation; (B) boxplots showing the computational time for each method for a single data buffer of 500 ms. The runtimes are measured over a total of 360 ‘virtual’ data buffers for each subject. The use of BSS-REG can lead to a more effective removal of ocular artifacts in comparison to the other methods, both in terms of accuracy and computational time.

2.3.3 Analysis of BSS-REG performance on real EEG data

We finally evaluated whether BSS-REG can be used for the removal not only of ocular artifacts, but also muscular artifacts. To this end, we used real EEG data collected during a visual oddball paradigm (figure 2.6).

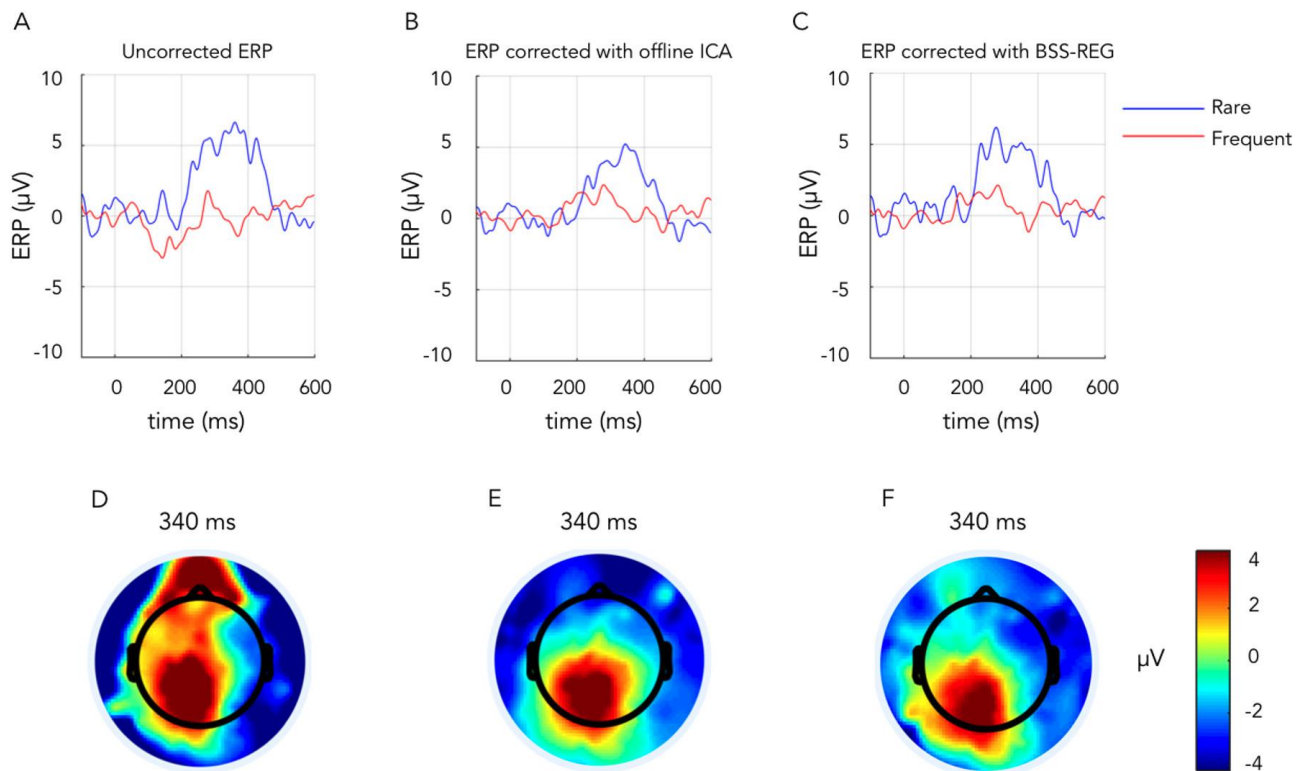


Figure 2.6. Single-subject ERP analysis of EEG signals at the electrode Pz for rare and frequent events: (A) uncorrected; (B) corrected with offline ICA; and (C) corrected with BSS-REG. Scalp topography of ERPs associated with P300 response at 340 ms: (D) uncorrected; (E) corrected with offline ICA; and (F) corrected with BSS-REG.

These data were also processed by using a standard artifact removal approach based on ICA, which served as benchmark. Our ERP results showed that BSS-REG yielded a reduction of 21.04% and 26.5% in noise and inter-trial variability, respectively, with respect to unprocessed EEG data. Conversely, although there was 7.73% more noise and 10.06% more inter-trial variability with BSS-REG than offline ICA, differences between online and offline methods were on the border of significance for inter-trial variability ($p = 0.0526$) and pre-stimulus noise ($p = 0.0689$), respectively (figure 2.7).

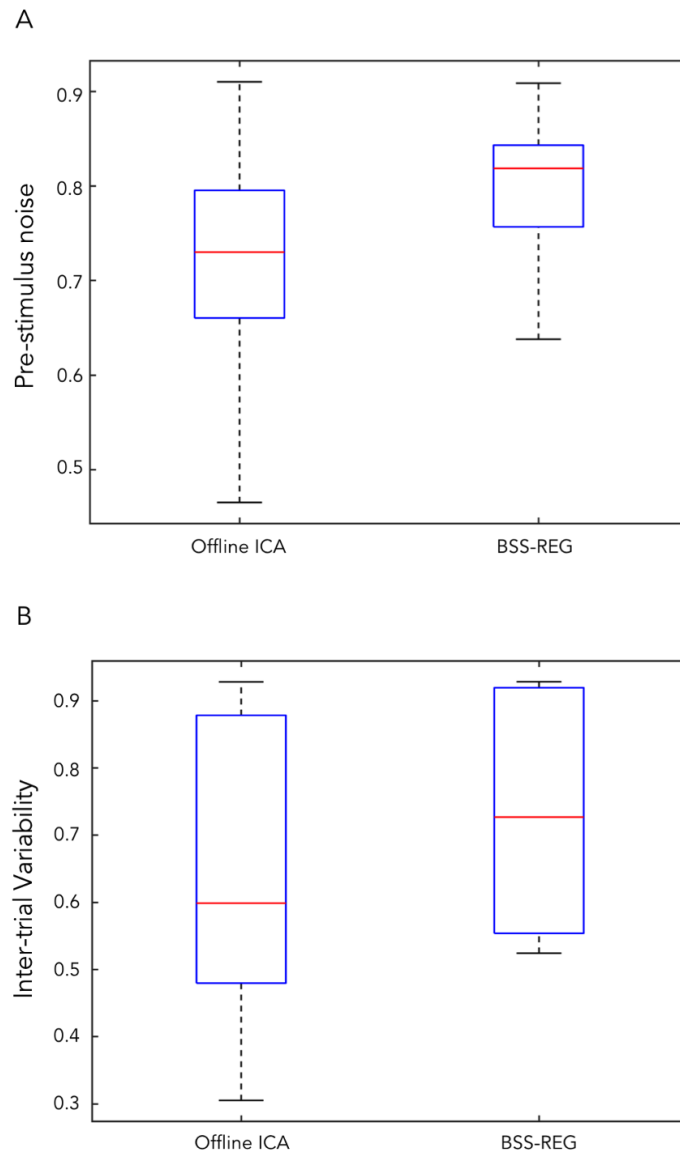


Figure 2.7. Quantitative assessment of ERP analysis across ICA offline and BSS-REG. A comparison is performed by examining (A) pre-stimulus noise and (B) inter-trial variability. Inter-trial variability and pre-stimulus noise are relatively larger for BSSREG, but there are no significant differences between methods ($p > 0.05$).

The topology of the scalp map at the latency of the maximum peak (between 320 and 470 ms across subjects) was largely similar (spatial and temporal correlation equal to 0.744 ± 0.1475 and 0.7978 ± 0.1447 , respectively).

2.4 Discussion

The BSS-REG method has been developed for online artifact removal from EEG signals, which is a very important requirement for BCI application. Our method has shown to perform better than several alternative methods for the removal of ocular artifacts. No extensive validation has been conducted on simulated data for other types of artifacts, as no specific gold-standard exists. However, we have successfully applied BSS-REG on real EEG data containing multiple artefactual sources, and have shown that the performance is comparable to those of a standard offline artifact removal approach based on

ICA. What is particularly remarkable is the low computation time, which makes the BSS-REG method suitable for use not only with low-density but also high-density EEG recordings. Importantly, this feature may enable the development of more advanced BCI applications in the future.

2.4.1 Primary features of the BSS-REG method

The method has been specifically developed to operate in an online mode during EEG acquisitions. Like other methods (Croft and Barry 1998; Schlogl et al. 2007; Zhang et al. 2015), it relies on a calibration dataset for feature extraction. In BSS-REG, this is particularly important, as it ensures that a low computation time is required during the actual EEG experiment. Since BSS is used for the initialization of the spatial filter, the spatial stationarity of the artefactual sources between the calibration and the experimental phase is assumed. In other words, the demixing matrix obtained in the calibration phase is assumed to approximate the one that would be obtained by using BSS on the EEG data collected during the experiment. Our results show that this may be the case, at least for EEG data collected in the same experimental session. Furthermore, we observed that the demixing matrix that specifically relates to artefactual sources is not strongly affected by the specific task performed by the participant. A possible caveat of our approach is that the calibration dataset should contain a sufficient number of artifactual occurrences (for instance, explaining at least 1% of the total variance) for an effective initialization of the spatial filter. In this regard, it may be helpful to ask the participant to intentionally generate such artifacts (Zhang et al. 2015).

Importantly, other studies proposed the use of ICA for online artifact removal (Halder et al. 2007; Radüntz et al. 2015), and some of them in combination with REG (Klados et al. 2011; Mannan et al. 2016; Siew Cheok and Raveendran 2008). Since we conducted our testing on hdEEG data, all the techniques using ICA based on a moving window approach could not be used due to very high computation times. Indeed, the computational complexity of ICA scales at least quadratically with the number of input channels (Hyvärinen et al. 2004). Furthermore, the number of samples required for an effective ICA decomposition is also related to the number of recordings, and this constrains its application in an online modality. One study specifically proposed the combination of ICA and REG for online removal of the ocular artifact (Mannan et al. 2016). That approach may appear very similar to BSS-REG, but this is really not the case. Indeed, ICA is performed in an online modality, linear regression is applied to each component using EOG signals, and the cleaned components are then back-projected over the recordings. Besides the considerations on computational complexity already made, we argue that this specific implementation may have low performance when the waveforms of EOG signals do not well match that of the ocular artifact in the EEG data.

2.4.2 Analysis of the method performance

To assess the performance of the BSS-REG, we first relied on a simulated dataset consisting of neural signals contaminated only by ocular artifacts. With known ground truth, we could effectively compare

the mean CSM and computation time of BSS-REG with those of alternative approaches, such as AF, LMS, CRLS and HINFTV (figure 2.5). We also examined the performance of ICA and OLS, which allowed us to appreciate the potential advantages of using the combined (twostep) approach implemented in BSS-REG (figure 2.4). With the exclusion of LMS, BSS-REG outperformed all other methods in terms of artifact removal accuracy. Also, it was by large the fastest method, with a delay below 5 ms even with high-density (256-channel) EEG data (figure 2.3B).

The BSS-REG method was also assessed using actual EEG signals collected in participants during visual oddball paradigm. Through the analysis of ERP data, we could quantitatively evaluate the effectiveness in the removal of different artifacts (figure 2.7). The noise level and the inter-trial variability can be used to evaluate the effectiveness of artifact attenuation. On the other hand, signal preservation could be assessed by examining the main peak intensity in the ERP (figure 2.6). In addition to these measures, we have also presented qualitative results for actual EEG datasets. Overall, results on actual EEG datasets confirm that the BSS-REG method is suitable for online removal of different kinds of artifacts (including ocular and muscular artifacts). As expected, its accuracy was on average lower than that of widely used offline ICA method (Jung, Makeig, Humphries, et al. 2000). However, the differences between the two methods were just on the border of significance.

2.4.3 Potential application in the field of BCI

Our validation was conducted on hdEEG recordings, which are not commonly used for BCI applications. Our recent work was focused on the use of hdEEG for accurate source reconstructions and connectivity analyses (Liu et al. 2017). We developed a comprehensive pipeline for offline analysis of hdEEG data, which can contribute to a more widespread utilization of EEG as a brain-mapping tool (Michel and Murray 2012). In future work, our efforts will be devoted to the implementation of computationally-efficient techniques for real-time analysis of hdEEG data, aiming to estimate neural activity in the brain in an online modality. This work will be relevant to all applications that may require estimates of source-based activity rather than EEG recordings. For instance, source-based EEG neurofeedback has been recently introduced (Boe et al. 2014; van Lutterveld et al. 2017). This holds great promise for studies aiming at more specific, and possibly more effective, brain training than with classical EEG neurofeedback. Also, closed-loop neuromodulation techniques combining EEG with transcranial magnetic stimulation or transcranial current stimulation can be developed by controlling the phase of neural signals estimated in specific brain areas (Bergmann et al. 2016; Zrenner et al. 2016). Furthermore, novel BCIs can be optimized for use on activity estimated from different brain regions. This may ultimately lead to increased classification accuracy as compared to classical EEG-based BCIs, and may contribute to bridging the gap between human studies that use scalp EEG and animal studies, for which intracranial recordings are possible (Capogrosso et al. 2016).

2.4.4 Limitations and future work

As many existing online artifact removal approaches, BSS-REG relies on electrical signals recorded simultaneously with EEG, such as EOG and EMG. In our method, the latter are primarily used to identify the components extracted from the calibration dataset, which need to be used for the initialization of the spatial filter. It should be noted that it may be possible to use different criteria for the identification of the artefactual components. For instance, the ocular components are characterized by high kurtosis values (Klados et al. 2010), whereas the muscular components have very low autocorrelation values (De Vos et al. 2010). Future studies are warranted to test the effectiveness of these approaches, and their impact on artifact removal accuracy. The impact of the specific BSS approach used should be also considered. In the present study, we showed that the FastICA algorithm has comparable performance as compared to Infomax, and that ICA-BSS generally outperforms PCA- and CCA-BSS on ocular artifacts. This assessment could be extended to other kinds of artifacts. Furthermore, recent studies are proposing the use of tensor decomposition techniques for artifact removal as a valid alternative to ICA and BSS (Triantafyllopoulos and Megalooikonomou 2014). It may be interesting to verify whether these approaches can effectively yield improved reconstruction of artefactual sources within the BSS-REG framework. Concerning online artifact removal, we opted for the use of a standard linear regression approach based on OLS. This ensures that the removal of artifacts can be implemented using a spatial filter, and therefore that computation time is kept low even for hdEEG recordings. However, alternative regression methods could be implemented and compared to OLS. Finally, it may be worth extending the validation of our approach to other EEG datasets, collected with different systems and different experimental protocols. In particular, it would be important to further validate the efficacy of the BSS-REG method during BCI operation, as for example during ERP-based BCI control. Considering the growing interest of the neuroscientific community on closed-loop neuromodulation approaches (Semprini et al. 2018), it would be interesting to extend BSS-REG, such that it can be applied also for the attenuation of electrical noise from transcranial alternating current stimulation.

2.5 Conclusions

We have introduced BSS-REG, a method for the online artifact removal of EEG signals, which is suitable not only for low-density but also high-density systems. The method requires the use of a calibration recording for the initialization of the spatial filter. This ensures a low computation time during the actual EEG experiment. BSS-REG outperforms other methods in terms of artifact removal accuracy and computational time. Furthermore, it can remove different kinds of artifacts with accuracy comparable to achieved by an offline ICA approach (Jung, Makeig, Humphries, et al. 2000). We argue that BSS-REG may enable the development of novel BCI applications requiring high-density recordings, such as source-based neurofeedback and closed-loop neuromodulation.

3 A computationally efficient method for the attenuation of alternating current stimulation artifacts in electroencephalographic recordings

Guarnieri R, Brancucci A, D'Anselmo A, Manippa V, Swinnen SP, Tecchio F, Mantini D. *A computationally efficient method for the attenuation of alternating current stimulation artifacts in electroencephalographic recordings*. J Neural Eng. 2020 Aug 17;17(4):046038. doi: 10.1088/1741-2552/aba99d.

Abstract

Objective. Recent studies suggest that the use of noninvasive closed-loop neuromodulation combining electroencephalography (EEG) and transcranial alternating current stimulation (tACS) may be a promising avenue for the treatment of neurological disorders. However, the attenuation of tACS artifacts in EEG data is particularly challenging, and computationally efficient methods are needed to enable closed-loop neuromodulation experiments. Here we introduce an original method to address this methodological issue.

Approach. Our alternating current regression (AC-REG) method is an adaptive (time-varying) spatial filtering method. It relies on a data buffer of preset size, on which principal component analysis (PCA) is applied. The resulting components are used to build a spatial filter capable of regressing periodic signals in phase with the stimulation. PCA is performed each time that a new sample enters the buffer, such that the spatial filter can be continuously updated and applied to the EEG data.

Main results. The AC-REG accuracy in terms of tACS artifact attenuation was assessed using simulated and real EEG data. Alternative offline processing techniques, such as the superimposition of moving averages (SupMA) and the Helfrich method (HeM), were used as benchmark. Using simulations, we found that AC-REG can yield a more reliable reconstruction of the stimulation signal for any frequency between 1 and 80 Hz. Analysis of real EEG data of 18 healthy volunteers showed that AC-REG was able to better recover hidden neural activity as compared to SupMA and HeM. Also, significantly higher correlations between power spectrum densities in tACS on and off conditions, respectively, were obtained using AC-REG ($r = 0.90$) than using SupMA ($r = 0.80$) and HeM ($r = 0.86$).

Significance. Thanks to its low computational complexity, the AC-REG method can be employed in noninvasive closed-loop neuromodulation experiments, with potential applications both in healthy individuals and in neurological patients.

Keywords: transcranial alternating current stimulation (tACS), closed-loop, low-computational processing, artifact removal, electroencephalography (EEG), principal component analysis (PCA)

3.1 Introduction

During closed-loop neuromodulation experiments, neural activity is continuously recorded, relevant signal signatures are extracted, and the applied magnetic/electrical stimulation is dynamically adapted based on those features (Guggenmos et al. 2013; Rebesco et al. 2010). Notably, closed-loop neuromodulation has been shown to facilitate and/or enhance neural plasticity processes as compared to open-loop neuromodulation, for which a fixed set of stimulation parameters is chosen a-priori by the experimenter (Sun and Morrell 2014). The adaptive nature of closed-loop neuromodulation intrinsically leads to a lower intra- and inter-subject variability (Iturrate et al. 2018), opening the way to its use for the treatment of neurological and psychiatric disorders (Sun and Morrell 2014). Probably, one of the most promising applications of closed-loop neuromodulation is based on deep brain stimulation (DBS) of the basal ganglia for the treatment of movement disorders, including Parkinson's disease, essential tremor and dystonia (Perlmutter and Mink 2006). DBS is however invasive, and not suitable for a wide range of other conditions involving malfunctioning of large-scale brain networks rather than very specific brain regions.

Transcranial alternating current stimulation (tACS) is a non-invasive neuromodulation approach that can be suitable for use in a wider number of neurological and psychiatric conditions (Woods et al. 2016). With tACS, small amounts of current are injected into the scalp via rubber electrodes enclosed in saline soaked sponges (Morales-Quezada et al. 2014). The spatial specificity of the stimulated area is limited, but the use of multi-channel montages (Alekseichuk et al. 2019) and frequency-based interference techniques (Grossman et al. 2017) can mitigate this potential problem. The number of studies employing tACS for addressing basic and clinical neuroscience questions is nowadays very large (Alexander et al. 2019; J Dowsett et al. 2019). There is considerable experimental (Herrmann et al. 2013; Marshall et al. 2011) and computational (Ali et al. 2013; Merlet et al. 2013) evidence that tACS can effectively entrain brain oscillations. It has been successfully used to modulate vision (Vossen et al. 2015), movement (Feurra et al. 2011) and audition (Riecke et al. 2015). Moreover, functional magnetic resonance imaging showed that tACS can induce short-term neuroplastic effects over relatively specific cortical regions (Bächinger et al. 2017; Cabral-Calderin et al. 2016).

When using tACS for closed-loop neuromodulation, neural signals usually need to be acquired in a noninvasive manner, for instance using electroencephalography (EEG). EEG electrodes, which are placed over the scalp of the participant, measure the potentials induced by electrical activity of pyramidal neurons in the cortex (Beres 2017). EEG systems are typically portable and not particularly expensive, especially when the number of recording channels is low. It should be noted, however, that the direct estimate of neural activity in the cortex requires the use of high-density EEG montages, with more than 100 electrodes (Tucker 1993). The combination of EEG and tACS is technically challenging, because of the massive artifact that is mixed in the EEG data, in the form of a quasi-sinusoidal signal with main harmonic at the stimulation frequency. For this reason, most EEG-tACS studies have been so far

conducted using an interleaved stimulation protocol, and in particular analyzing the EEG data collected in the off-stimulation period (Mansouri et al. 2017; Pahor and Jaušovec 2018; Vossen et al. 2015).

To the best of our knowledge, few solutions exist to attenuate the tACS artifact from EEG recordings. A first approach that has been proposed is the subtraction of a constant sine wave fitted to the EEG signal. Due to variations in the EEG signal primarily induced by slow changes in electrode conductance and by movements of the participant's head, this solution often yields unsatisfactory results (Helfrich, Schneider, et al. 2014). Other tACS methods require the whole EEG recording to be available, and are therefore unsuitable for closed-loop neuromodulation studies (Helfrich, Schneider, et al. 2014; Kohli and Casson 2020). For instance, the one proposed by Helfrich and colleagues follows a two-step procedure: an artifact template is first subtracted from the data, and the remaining artifacts are then attenuated using principal component analysis (PCA) (Helfrich, Schneider, et al. 2014). Only one method, the superimposition of moving averages (SupMA) (Kohli and Casson 2015), has been used for real-time removal of tACS artifacts. However, in its current implementation, SupMA can simultaneously process only few EEG signals. Furthermore, it tends to strongly suppress the harmonics associated with the tACS artifact, possibly inducing large distortions in the frequency characteristics of neural signals (Kohli and Casson 2019).

Recent studies suggest that the use of closed-loop neuromodulation based on tACS and EEG maybe a promising avenue for the treatment of neurological disorders (Semprini et al. 2018). Therefore, there is a compelling need of a technological solution with low computational complexity for tACS artifact removal, which could be effectively used with low-density as well as high-density EEG recordings. In this paper we introduce a novel solution to this problem. Our alternating current regression (AC-REG) method can be conceptualized as an adaptive (time-varying) spatial filter method. Specifically, we use a data buffer of preset size, on which we apply PCA; the resulting principal components (PCs) are used to build a spatial filter for the regression of periodic signals in phase with the stimulation. PCA is performed each time that a new sample enters the buffer, such that the spatial filter can be continuously updated and applied to the EEG data. In this study we assess the performance of AC-REG using both simulated and real EEG signals. Simulated data are used to define the main parameters of the method and to assess its performance under controlled conditions. A comparison in terms of accuracy with alternative methods is conducted, using both real and simulated data.

3.2 Methods

3.2.1 Description of the method

The AC-REG method relies on the use of EEG signals that are continuously read and stored in a buffer of n samples. A spatial filter is dynamically updated and applied to the most recent data samples to attenuate the contribution of the tACS artifact mixed in the EEG data. For each given time epoch, PCA is calculated on the data buffer to retrieve the PCs, i.e. underlying signals that are statistically uncorrelated with each other and linearly mixed in the data (Turnip and Junaidi 2014). Notably, the number of

samples n in the data buffer will inherently have an impact on PCA performance, in terms of accuracy and computation time (Guarnieri et al. 2018). The PCA model can be mathematically described as

$$X(\tau) = A \cdot Y(\tau) \quad (3.1)$$

where $X(\tau)$ is a $[k \cdot n]$ -dimensional matrix of k recordings and $Y(\tau)$ is a $[k \cdot n]$ -dimensional matrix of PC time-courses. Furthermore, A is a $[k \cdot k]$ -dimensional matrix that contains the PC weights over the recordings. The matrices A and $Y(\tau)$ can be estimated using a singular value decomposition (SVD), which imposes a constraint of orthogonality among the PCs (Golub and Kahan 1965; Turnip and Junaidi 2014). After PCA decomposition, the PCs with quasi-sinusoidal time-courses in phase with the stimulation signal are selected, by imposing a stringent criterion in terms of temporal correlation ($r > 0.5$). This classification of PCs is used to build the spatial filter capable of attenuating tACS artifacts. To this end, a $[n \cdot n]$ diagonal matrix Z is created, setting each element z_{ii} equal to 0 if the i -th PC is classified as related to tACS artifact, or equal to 1 otherwise. The spatial filter $W(t)$ at any given time τ of the EEG recording, is then obtained as follows:

$$W(t) = A \cdot Z \cdot A^{-1} \quad (3.2)$$

The vector of EEG data corresponding to the last sample in the buffer, indicated as $X(t)$, is combined with the spatial filter $W(t)$ calculated using the buffer data to obtain the vector of artifact-free EEG data $X_c(t)$:

$$X_c(t) = W(t) \cdot X(t) \quad (3.3)$$

In this manner, the artifacts are subtracted from the EEG recordings with appropriate weights for each channel, and the reconstruction of artifact-free EEG signals is accomplished in a continuous manner.

3.2.2 Validation of the method

3.2.2.1 Performance analysis using simulated EEG data

Simulated data used in this study were derived from resting-state EEG recordings collected for 5 min in 12 right-handed healthy participants (four males and eight females, with ages ranging from 21 to 43 years). These recordings were already used in some of our previous studies (Guarnieri et al. 2018; Liu et al. 2017; Samogin et al. 2019). Before undergoing the examination, the participants gave written informed consent to the experimental procedures, which were approved by the Institutional Ethics Committee of ETH Zurich. EEG data were recorded at 1000 Hz using a 256-channel system from Electrical Geodesics (Eugene, US). The electrode at vertex (labeled as Cz in the 10/20 international system) was used as physical reference. EEG data preprocessing was carried out using EEGLAB

(<https://sccn.ucsd.edu/eeglab/index.php>) and built-in MATLAB functions. The preprocessing steps included: bad-channel detection and interpolation, digital filtering in the band 1–80 Hz, resampling to 200 Hz and average re-referencing. In addition, removal of biological artifacts was performed by means of independent component analysis (ICA), as described in Liu et al. (2017). The resulting artifact-cleaned EEG data were then mixed with simulated tACS artifact, generated using the open source toolbox ARtACS (<https://github.com/agricolab/ARtACS>). Temporal changes in artifact amplitude over time were modelled using an Ornstein–Uhlenbeck process. The intensity of the tACS was set as being 100 times larger than background EEG activity, as observed in real data. Simulated tACS artifacts were generated at varying frequencies ranging between 1 and 70 Hz. More detailed analyses were conducted with simulated tACS artifacts at 10, 20 and 70 Hz, as these are frequencies commonly used in tACS studies (Capon et al. 2016; Clayton et al. 2018; Sugata et al. 2018).

Using the simulated EEG data (see figure 3.1), we first performed an optimization of AC-REG settings. Pseudo-online tests were conducted using a moving window approach, to generate a ‘virtual’ buffer of data to be given as input to AC-REG. Specifically, we analyzed how accuracy and computational time vary with different channel numbers, sampling frequencies and data buffer sizes. The number of EEG channels was equal to 16, 32, 64, 128 and 256, respectively, and the sampling frequency was set to 200, 500 and 1000 Hz, respectively; different lengths of the buffer size were tested, in the range between 100 and 2000 ms. Accuracy was quantified by using the correlation between the reconstructed EEG data and those without tACS artifact. Computation time was measured using MATLAB (release 2016b) running under MacOS (with 2.5 GHz Intel Core i7 processor and 16 GB RAM).

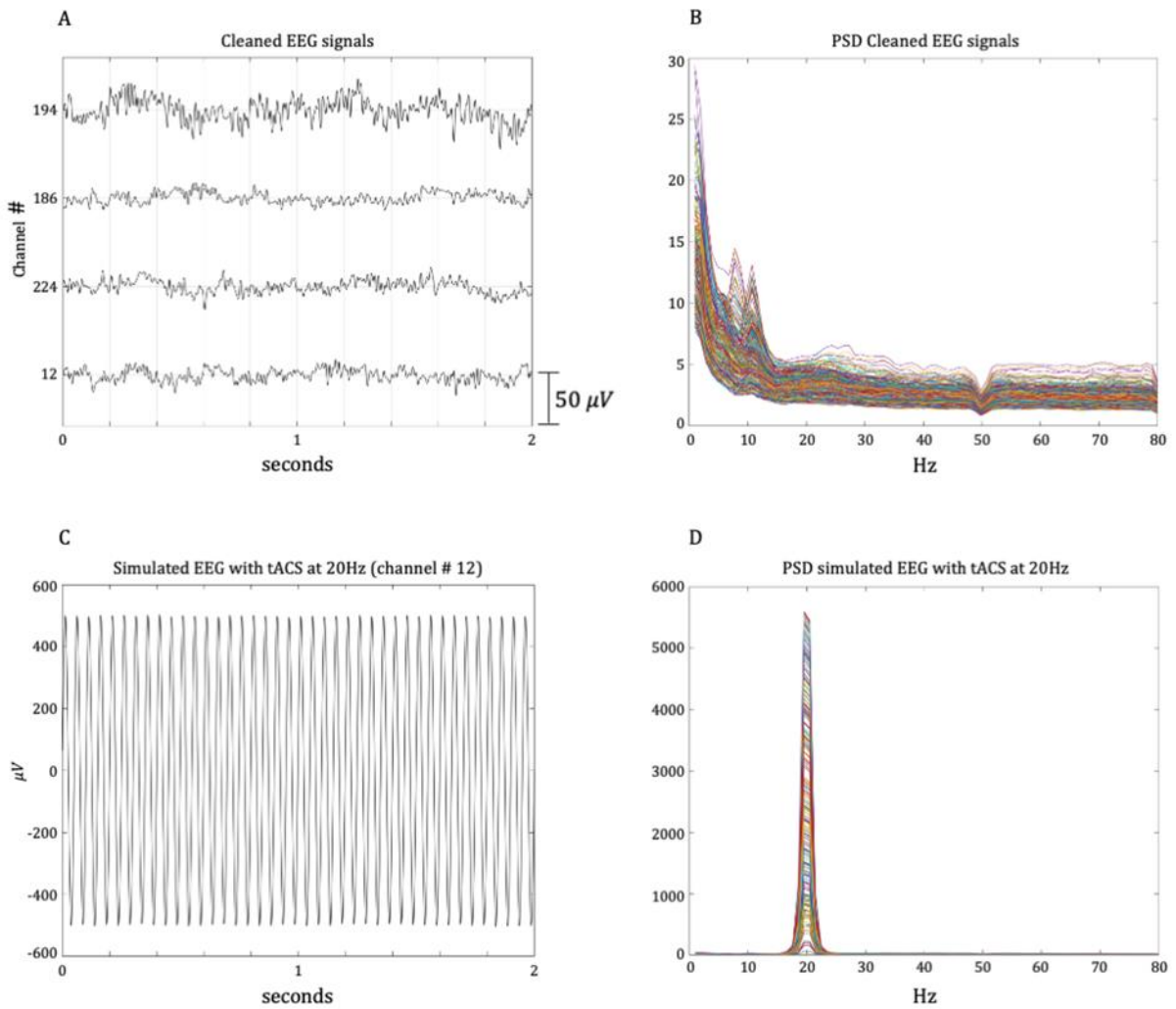


Figure 3.1. Example of simulated EEG data with tACS artifact. (A) 2-second segment of reconstructed artifact-free EEG signals for four representative channels; (B) power spectral density of the reconstructed artifact-free EEG signals (C) 2-second segment of simulated EEG signals, obtained adding the tACS artifact to the artifact-free EEG signals (D) power spectral density of the simulated EEG signals with tACS artifact.

Subsequently, we focused on EEG simulations with 64 channels and with sampling frequency at 500 Hz. The size of the data buffer for AC-REG was set to 500 ms. Hence, we compared the accuracy of AC-REG in tACS artifact attenuation with respect to two alternative approaches: SupMA (Kohli and Casson 2015) and the Helfrich method (HeM) (Helfrich, Schneider, et al. 2014). As for SupMA, we used the implementation included in the ARtACS toolbox. Accordingly, the parameter M was set equal to 10, and the parameter N was equal to the number of stimulation cycles. HeM was implemented in MATLAB, based on the information included in the original study. First, we assessed the sensitivity of AC-REG, SupMA and HeM with respect to the noise level, which was varied between 0% and 20% of the average standard deviation of the clean EEG signal. Furthermore, after selecting a noise level of 5% (Bai and He 2006), we compared the accuracy of the three methods as a function of the stimulation frequency.

3.2.2.2 *Performance analysis using real EEG data*

We used recordings collected in 18 healthy right-handed volunteers (nine males and nine females, age ranging between 20 and 36). Participants gave their written consent before taking part in the experiment. The whole procedure was carried out in accordance with the principles of the Declaration of Helsinki, and the protocol was approved by the Local Ethical Committee of Chieti University. tACS was delivered by a battery-driven, current stimulator (DC-Stimulator, NeuroConn GmbH, Germany) through a pair of conductive rubber electrodes (3 cm × 3 cm, 9 cm²). An electro-conductive gel was applied under the rubber electrodes to reduce contact impedance. We used a stimulation of 90 s duration and fade-in/fade-out times of 5 s. A bilateral montage was used, with patch electrodes placed at the C3 and C4 sites of the 10–20 EEG system. During the tACS stimulation, an alternating current was transmitted with a sinusoidal waveform, the frequency was set at 20 Hz and the relative phase at 0°. Alternating current was applied at 1000 μ A resulting in a mean current density 0.011 mA/cm².

EEG activity was recorded with a Be-plus system manufactured by Eb-Neuro (Florence, Italy) before, during and after tACS, using 57 scalp electrodes positioned according to a standard 10–10 montage. The electrode labeled as AFz was used as physical reference. Impedance of all electrodes was kept lower than 5 k Ω . Signals were sampled at 512 Hz and stored on a computer for offline analysis. The EEG recording started 3 min before the stimulation and ended 3 min after it. The stimulation period lasted 90 s. During the experiment, the participant was seated in a comfortable position and was asked to stay at rest, maintaining a relaxed position, with open eyes and without moving or engaging in any cognitive task. The EEG data were preprocessed offline, using the same analysis workflow used for the generation of the simulated data (see previous section). Specifically, bad-channel detection and interpolation, digital filtering in the band 1–80 Hz and average re-referencing were applied (see figure 3.2 for an illustration of real EEG data).

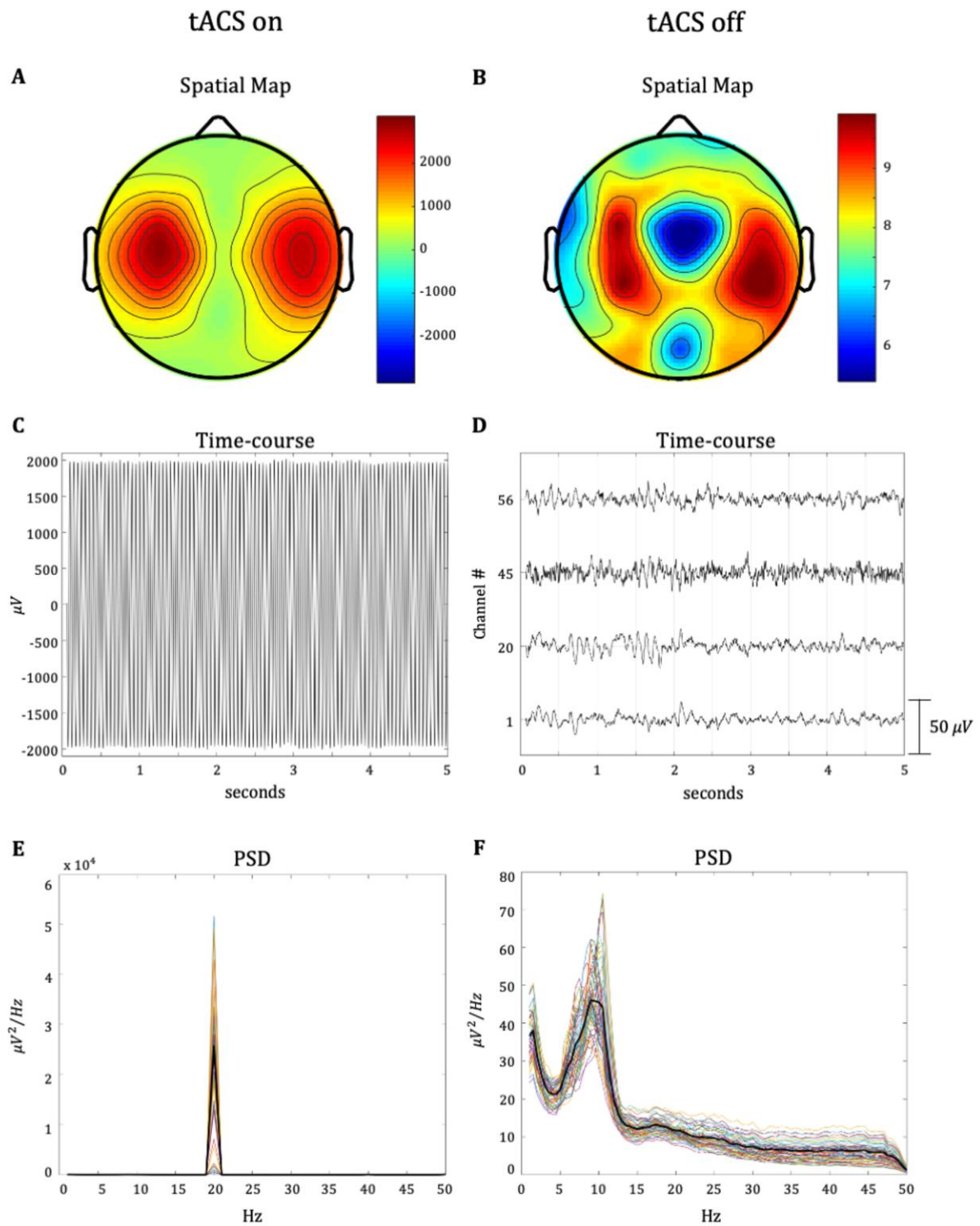


Figure 3.2. Example of real EEG signals in tACS-on and tACS-off conditions. (A-B) topoplots (spatial maps) showing the intensity of EEG data collected with tACS on and off, respectively; (C) 5-second segment of EEG data collected with tACS on (one representative channel); (D) 5-second segment of EEG data collected with tACS off (four representative channels); (E-F) PSDs of EEG data collected with tACS on and off, respectively. The thick black line indicates the grand average of the PSD across channels.

To assess the effectiveness of AC-REG in attenuation the tACS artifact on real EEG data, we conducted three analyses. First, we quantified the correlation between the tACS signal and the artifact-corrected

EEG data, filtered around the stimulation frequency (19–21Hz). This analysis provided an indication concerning the presence of residual artifacts in the EEG data. SupMA and HeM were used as benchmark to evaluate the performance of AC-REG. Second, we performed ICA of the EEG signals using the FastICA algorithm (Hyvärinen 1999), to extract specific components related to eye blinks and the occipital alpha rhythm. The topology of the components extracted from the artifact-free EEG data in the tACS-on period were compared to those from the EEG data in the tACS-off period, by means of their spatial correlation. Third, we investigated the correspondence in the power spectral density (PSD) of the artifact-free EEG data in tACS-on period as compared to the EEG data in the tACS-off period. This correspondence was quantified using the Pearson's correlation, focusing on all frequencies in the band 1–80 Hz except the stimulation frequency and its harmonics (i.e. 20, 40, 60 Hz). A Wilcoxon signed rank test was used to test whether there were significant differences among the correlation values obtained with the three methods. The Bonferroni method was used to correct statistical significance, accounting for multiple comparisons (AC-REG vs. SupMA, AC-REG vs. HeM, SupMA vs. HeM). For all the analyses on real EEG data, AC-REG was used with a buffer size of 500 ms.

3.3 Results

The performance of AC-REG depends on the amount of data that can be used for the definition of the spatial filter. To examine how the number of data channels, sampling frequencies and data buffer sizes impact on accuracy and computational time, we performed pseudo-online tests using the simulated EEG data. Overall, the accuracy in the reconstruction of tACS artifact did not strongly depend on the number of EEG channels and on the sampling frequency, but better performance was nonetheless obtained with higher channel counts and higher sampling frequencies respectively (figure 3.3A). In contrast, the buffer size used for AC-REG processing was an important factor in determining the quality in tACS artifact reconstruction. Specifically, the use of a buffer size of at least 500 ms for AC-REG seemed to be important to ensure an effective artifact attenuation (figure 3.3B).

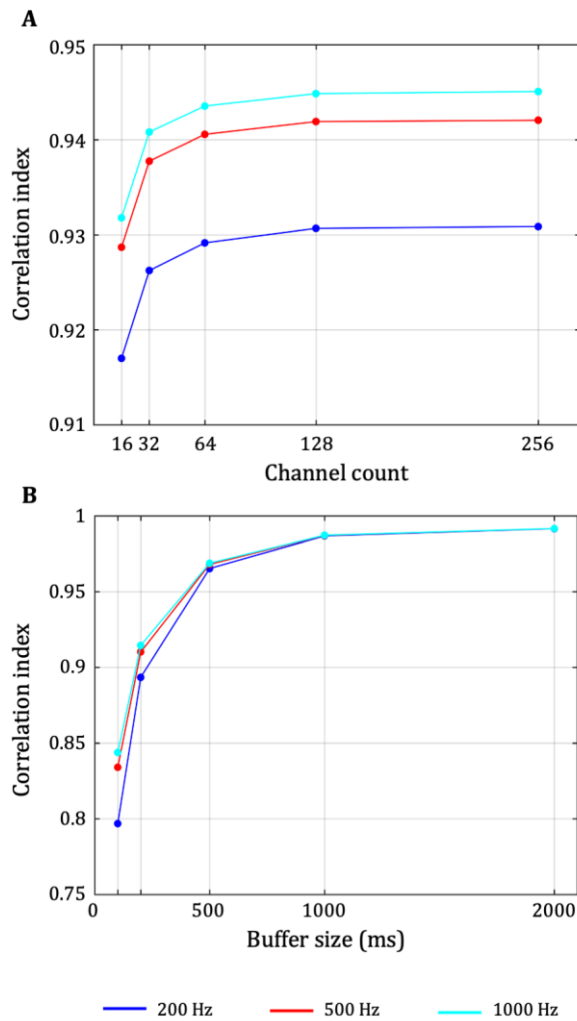


Figure 3.3. Dependence of AC-REG reconstruction accuracy on channel count, sampling frequency and buffer size. We examined how the accuracy in the reconstruction of the tACS artifact, quantified by the correlation index, is influenced by (A) the number of EEG channels given as input to AC-REG and (B) the number of samples in the data buffer used. The accuracy for different sampling frequencies is shown using lines with different colors.

We also found that the computation time had a super-linear relationship with channel count (figure 3.4A), whereas it increased with both sampling frequency and buffer size in a sub-linear manner (figure 3.4B).

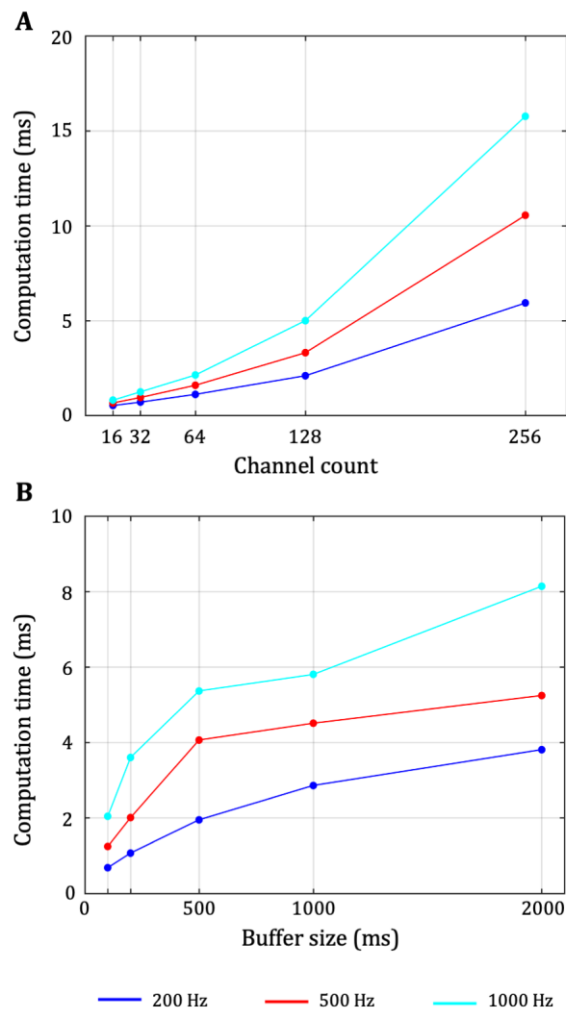


Figure 3.4. Dependence of AC-REG computation time on channel count, sampling frequency and buffer size. We examined how the computation time is influenced by (A) the number of EEG channels given as input to AC-REG and (B) the number of samples in the data buffer used. The computation time for different sampling frequencies is shown using lines with different colors.

By using simulated EEG data, we could also assess the performance of AC-REG with respect to alternative approaches, such as SupMA and HeM. As expected, the correlation between simulated and reconstructed EEG data was only slightly dependent on the noise level for any method under investigation, possibly due to the high intensity of the tACS artifact. Notably, correlations were higher for AC-REG than SupMA and HeM (figure 3.5A). Interestingly, we found that the performance of AC-REG, SupMA and HeM depended on the tACS frequency in a substantial manner (figure 3.5B). All methods had a performance drop below 4 Hz and at around 10 Hz, which are the frequencies with relatively lower ratio between artifact and neural signal amplitudes, respectively. Overall, we observed that SupMA had a clear decrease in reconstruction accuracy with an increase of the stimulation frequency, whereas the performance of AC-REG and HeM was largely stable across frequencies.

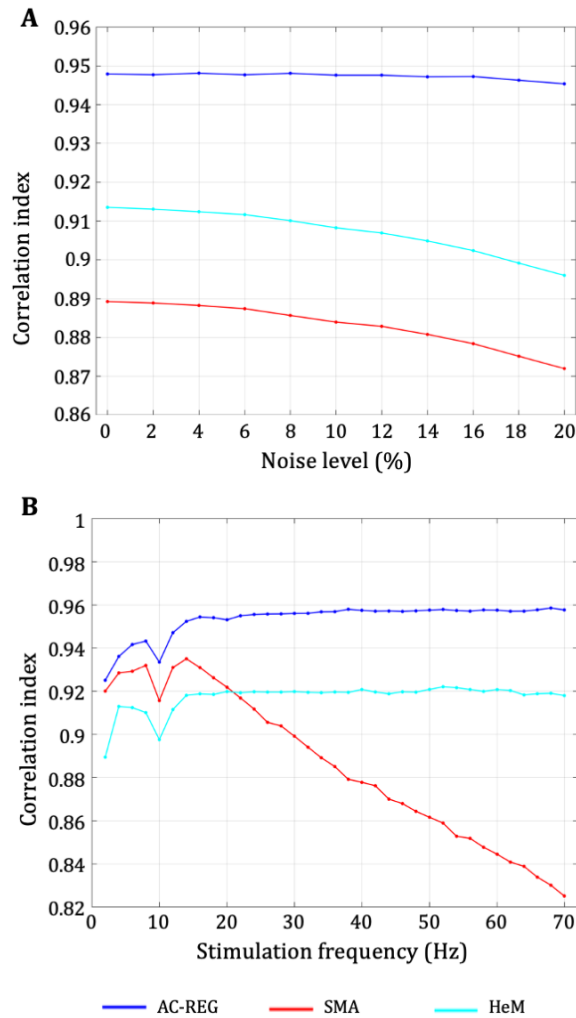


Figure 3.5. Performance of AC-REG, SupMA and HeM for different noise levels and stimulation frequencies. Accuracy in the reconstruction of artifact-free EEG signals, as quantified by the correlation index, was examined (A) for noise levels varying between 0% and 20% of the signal intensity and (B) for stimulation frequency ranging between 1 and 70 Hz.

We finally moved to the assessment of AC-REG using real EEG data. First, we examined whether the EEG data processed by AC-REG, SupMA and HeM possibly included residuals of the tACS signal. We found that the EEG signal at the stimulation frequency was in phase with the tACS artifact for HeM, whereas this was not the case for AC-REG and SupMA (figure 3.6). The correlations between the tACS signal and the EEG signals at the stimulation frequency were significantly lower for AC-REG than SupMA and HeM (both $p < 0.001$, with Bonferroni correction).

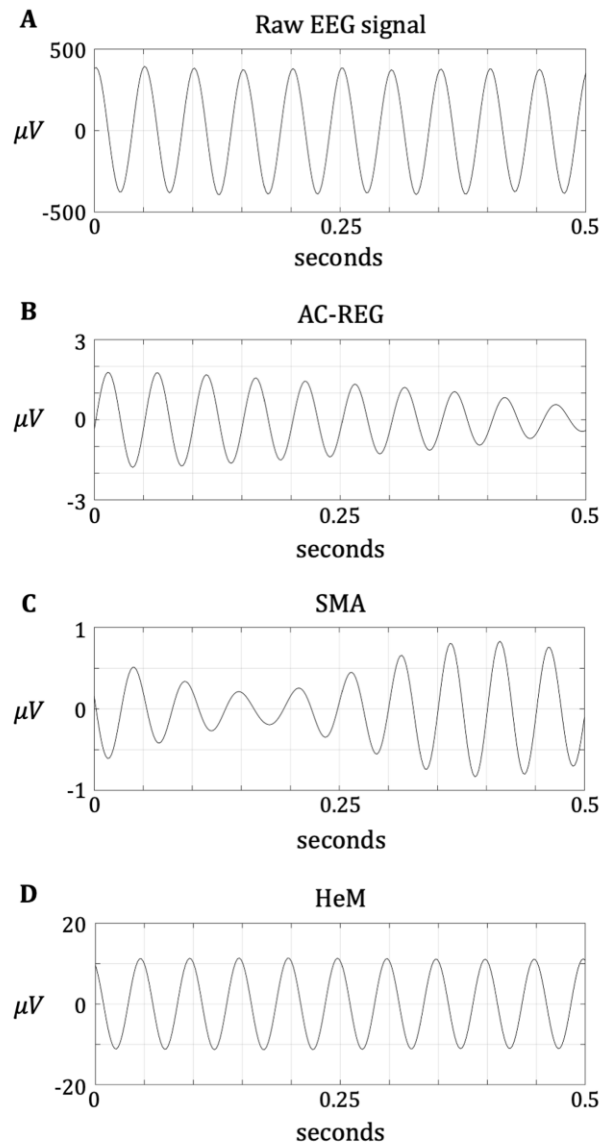


Figure 3.6. Example of a real EEG signal processed using AC-REG, SupMA and HeM. (A) Raw EEG signal from the channel Cz; (B-C-D) The same EEG signal after processing with AC-REG, SupMA and HeM, respectively, and digital filtering in the band 19-21 Hz (i.e., around the stimulation frequency of 20 Hz). The same EEG dataset shown in figure 3.2 has been used for the analysis.

Conversely, the correlation values obtained for SupMA and HeM were not significantly different across participants ($p=0.557$, before Bonferroni correction) (figure 3.7).

Next, we extracted and analyzed the EEG components associated with eye movements and the occipital alpha rhythm, respectively (figure 3.8). AC-REG, SupMA and HeM permitted to reconstruct the ocular component and occipital alpha components.

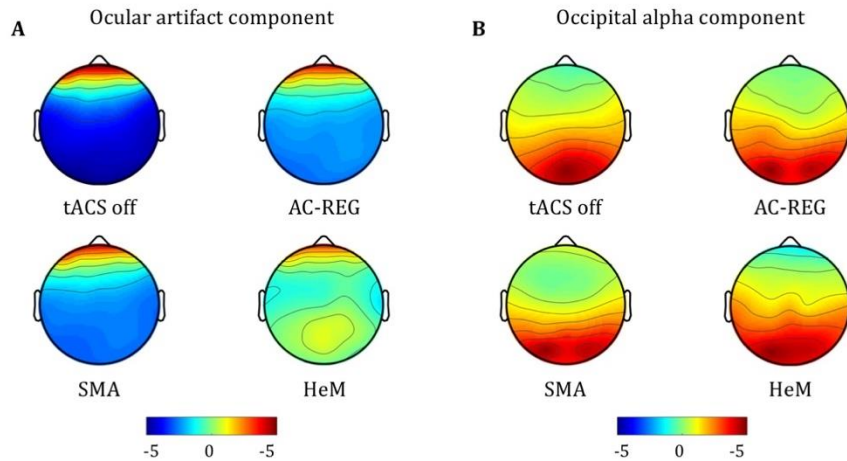


Figure 3.8. Topographies of ocular artifact and occipital alpha components in real EEG data with tACS off and on, respectively. Spatial distribution of (A) the ocular component, and (B) the occipital alpha component in a representative subject, for the tACS-off condition and the tACS-on condition after tACS artifact removal using AC-REG, SupMA and HeM, respectively. The same EEG dataset shown in figure 3.2 has been used for the analysis.

The EEG data processed with SupMA had the highest correlations between the ocular component estimated in the tACS-on and tACS-off periods, respectively (figure 3.9A). These correlations were significantly higher than those obtained with AC-REG and HeM ($p=0.002$ and $p=0.0013$, respectively, with Bonferroni correction). Also, the values of AC-REG were significantly higher than those of HeM ($p=0.018$, with Bonferroni correction). For the occipital alpha component, no significant differences were found between the correlations obtained with AC-REG and SupMA processing, respectively ($p=0.5614$, before Bonferroni correction). In turn, the values of AC-REG and SupMA were significantly higher than those obtained with HeM ($p=0.003$ and $p=0.006$, respectively, with Bonferroni correction).

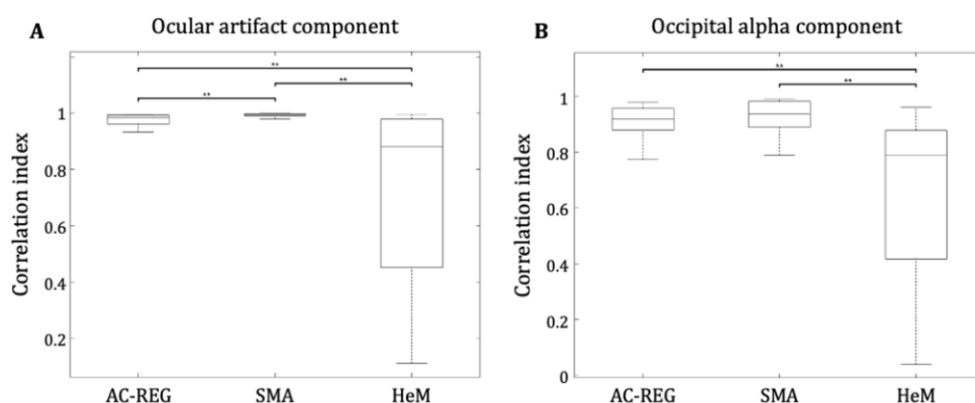


Figure 3.9. Quantification of ocular artifact and occipital alpha reconstruction in real EEG data. We estimated the impact of AC-REG, SupMA and HeM processing, respectively, on the reconstruction of (A) the ocular artifact component and (B) the occipital alpha component. The components obtained from EEG data in the tACS-on condition, were compared with those obtained from EEG data in the tACS-off condition. Correlations were averaged across channels to obtain a single value for each participant, and for each method. These values were displayed in the form of interquartile box plots. Statistical comparisons at the group level were performed using a Wilcoxon signed-rank test. Significance is indicated as follows: * = $p<0.05$, ** = $p<0.01$, *** = $p<0.001$.

The PSD of the EEG signals reconstructed using AC-REG clearly showed a single prominent peak at around 10 Hz and revealed two additional narrow peaks at the main stimulation frequency (20 Hz) and its first harmonic (40 Hz), respectively (figure 3.10). The same two peaks are easily detectable also in the PSD of the EEG signals reconstructed using HeM. With this method, however, the peak at around 10 Hz was much less prominent. In turn, the PSD obtained using SupMA showed a clear peak at around 10 Hz, whereas frequencies around 20 and 40 Hz were completely suppressed.

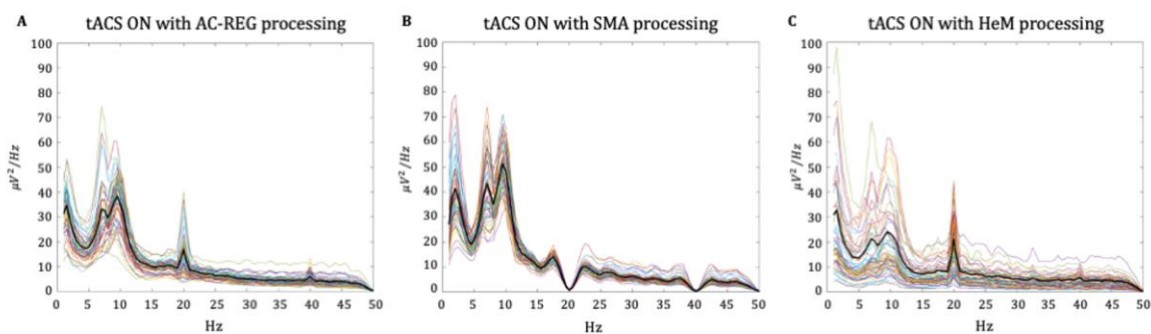


Figure 3.10. Effect of tACS artifact removal methods on spectral properties of EEG data. (A-C) PSDs from EEG data in the tACS-on period, processed using AC-REG, SupMA and HeM, respectively. The same EEG dataset shown in figure 3.2 has been used for the analysis. The thick black line indicates the grand average of the PSD across channels.

In order to perform a more quantitative analysis, we used the PSD of the EEG data in the tACS-off condition as reference, and we quantified its correlation with the PSDs produced by AC-REG, SupMA and HeM, respectively (figure 3.11). A Wilcoxon signed rank test showed that AC-REG had significantly higher values than SupMA and HeM ($p < 0.001$ and $p = 0.0222$, respectively, with Bonferroni correction). Also, the values of SupMA and HeM were not significantly different ($p = 0.075$, with Bonferroni correction).

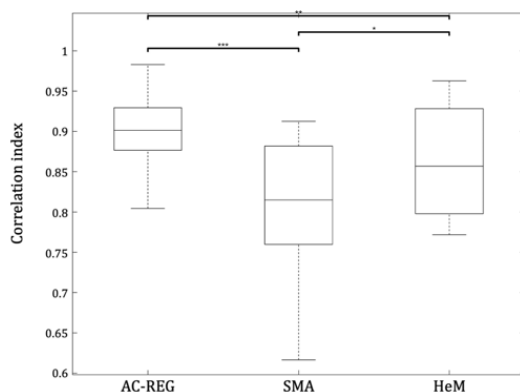


Figure 3.11. Performance of tACS artifact removal methods on real EEG data. We estimated the effectiveness of AC-REG, SupMA and HeM in reconstructing artifact-free EEG signals. To this end, we used as reference the EEG data collected without stimulation. We quantified, channel by channel, the correlation between PSDs, and then we averaged the values across channels to obtain a single correlation value for each of the 18 participants, and for each method. The resulting correlation values were displayed in the form of interquartile box plots. Statistical comparisons at the group level were performed using a Wilcoxon signed-rank test. Significance is indicated as follows: * = $p < 0.05$, ** = $p < 0.01$, *** = $p < 0.001$.

3.4 Discussion

The AC-REG method has been developed for attenuation of tACS artifacts in EEG signals. Due to its low-computational complexity, it may be effectively used in noninvasive closed-loop neuromodulation experiments. AC-REG uses an adaptive spatial filter based on PCA to dynamically estimate and subtract the tACS signal from EEG recordings. It outperforms alternative methods, both on simulated and real data. The low computation time may permit its use in online modality not only with low-density but also high-density EEG recordings. Importantly, the compatibility with high-density EEG may enable the use of AC-REG for source-level closed-loop neuromodulation (Guarnieri, Zhao, et al. 2020).

3.4.1 Primary features of AC-REG

The AC-REG method relies on the use of PCA, a data decomposition technique ensuring low computation times required for noninvasive closed-loop experiments. Specifically, the identification of principal components temporally coherent with tACS signals permits to obtain a spatial filter to be used for artifact removal. By using a data buffer, the spatial filter is dynamically updated such that artifact-free EEG data can be obtained in an online manner. A possible caveat of our approach is that the data buffer should contain enough samples for an effective PCA decomposition, hence for an accurate definition of the spatial filter. On the other hand, it should be considered that computation times need to be kept as low as possible to enable the use of AC-REG in closed-loop neuromodulation experiments. Our results suggest that AC-REG can be used for the simultaneous processing of up to 256 EEG recordings, with low computation time. This is essential for the development of source-level closed-loop neuromodulation systems, in which neural activity in the brain is estimated and used for tuning brain stimulation parameters (Guarnieri, Zhao, et al. 2020).

3.4.2 Analysis of method performance

To assess the performance of the AC-REG, we first relied on a simulated dataset containing a mix of neural signals and tACS artifacts. In this manner, we could define the buffer size of AC-REG yielding a reasonable compromise between accuracy and computation time (figures 3.3–3.4). With known ground truth, we could also examine the effectiveness of AC-REG in tACS artifact removal with alternative approaches, such as SupMA and HeM, under controlled conditions. We found that AC-REG outperformed the other methods for all the noise levels and the stimulation frequencies that were tested (figure 3.5). Notably, AC-REG permitted the simultaneous processing of up to 256 channels (figure 3.4) with relatively low processing time, theoretically compatible with its use in quasi real-time applications. It should be considered that the processing of all EEG channels simultaneously can enable source localization in real-time (Guarnieri, Zhao, et al. 2020).

The analysis conducted using AC-REG, SupMA and HeM on real EEG data largely confirmed the findings from simulated data, and provided further insights in the capability of the methods for preserving true neural oscillations. The analysis of the artifact-corrected EEG data suggested that AC-

REG successfully removes the sinusoidal signal that completely synchronized with the stimulation, possibly preserving neural signals entrained by the stimulation itself (figures 3.6–3.7). Notably, other sources of EEG activity were also preserved by AC-REG. For instance, we were able to reconstruct components associated with eye blinks and the occipital alpha rhythm (figure 3.8). In this regard, SupMA seemed to be more accurate than AC-REG in preserving eyeblinks, whereas no significant differences in reconstruction performance were found between AC-REG and SupMA for the occipital alpha rhythm (figure 3.9). To evaluate the performance of AC-REG, SupMA and HeM on real data, we also compared the spectral properties of EEG signals in tACS-on and tACS-off conditions. It should be noted that modulations of neural activity and connectivity during and following tACS have been reported (Bächinger et al. 2017; Neuling et al. 2013; Voskuhl et al. 2016). Considering the relatively short duration of the stimulation and the strength of the injected current, any assessment of stimulation-induced neural changes needs to be conducted with caution (Vöröslakos et al. 2018). On the other hand in this study, we focused on gross alterations in power spectrum density introduced by artifact removal methods. Our results suggested that AC-REG could largely preserve EEG signals for frequencies below the one of the stimulation itself (figures 3.10–3.11). We also found that, unlike AC-REG and HeM, SupMA strongly suppressed all the harmonics associated with the tACS artifact, inducing distortions in the frequency content of neural signals. The differences between AC-REG and HeM were less marked, although still significant. Notably, the use of HeM yielded an overall reduction of power at all frequencies compared to AC-REG and SupMA, in particular at around 10 Hz.

3.4.3 Limitations and future work

In this study, we introduced AC-REG and validated it using both simulated and real EEG data. Simulated EEG data were created by adding sinusoidal signals generated using the ARtACS toolbox to artifact-cleaned EEG signals. Temporal distortions introduced by changes in electrode impedance occurring during data acquisition were modelled using an Ornstein–Uhlenbeck process. However, the possible impact of time-sample jitters (Barban et al. 2019) and biological artifacts (Noury and Siegel 2017) was not taken into account. The validation on real data was conducted by testing the correspondence between the PSDs with tACS on and off, respectively, in resting state condition. This approach can be justified by the fact that the stimulation induces entrainment primarily of brain oscillations at the frequency of the tACS and its harmonics (Adaikkan and Tsai 2020; Antal and Herrmann 2016). To ensure the generalizability of our results, it would be important to extend the validation of AC-REG on real EEG data collected with other experimental protocols. In particular, event-related protocols may be used to test whether the reconstruction of neural activity at the single-trial level is unaffected by residual noise (Giroladini et al. 2016; Helfrich, Schneider, et al. 2014; Mantini et al. 2007). Another important aspect to consider is that real EEG data were collected during tACS at 20 Hz. It is therefore worth investigating how our findings might generalize to other stimulation frequencies,

also considering that non-linear distortions can be more easily observed at higher stimulation frequencies (Noury et al. 2016).

AC-REG was introduced and validated using methods typically used for offline analyses, such as SupMA and HeM. The comparison may be extended in future studies to other methods that have been proposed to attenuate high-voltage simulation artifacts mixed in EEG recordings, as for instance quadrature-regression independent vector analysis (q-IVA) (S. Lee et al. 2019). This method has been so far validated only on EEG data collected during galvanic vestibular stimulation, but it could be readily used to attenuate artifacts generated by tACS. AC-REG may be particularly valuable for applications in which EEG recordings need to be processed simultaneously and in real-time, as for instance in source-based closed-loop experiments (Bergmann et al. 2016). It should be noted, however, that the specific multi-channel implementation of AC-REG make the method potentially sensitive to the presence of bad channels. In this regard, specific solutions for enabling the effective use of AC-REG in online modality will need to be addressed in future studies. It would be important to test the effectiveness and validity of AC-REG in a noninvasive closed-loop neuromodulation experiment. As such, EEG data will have to be processed in real-time for the attenuation of the tACS artifact (Kohli et al. 2017; Schlegelmilch et al. 2013), as well as biological signals (Guarnieri et al. 2018). The readout of EEG activity will then be used to adjust phase and intensity of the stimulation (Bergmann et al. 2016).

3.5 Conclusions

We have introduced AC-REG, a method for the attenuation of tACS artifacts removal that is suitable not only for low-density but also high-density EEG recordings. The method requires the use of PCA on short time windows for the dynamic update of a spatial filter. This ensures low computation times, potentially enabling its use in real-time during EEG experiments. Just as importantly, AC-REG outperforms other methods for tACS artifact removal, which normally operate in an offline modality. We argue that AC-REG may enable further development of closed-loop neuromodulation techniques, with potential applications both in healthy individuals and in neurological patients.

4 RT-NET: real-time source reconstruction of neural activity using high-density EEG

Guarnieri R, Zhao M, Taberna GA, Ganzetti M, Swinnen SP, Mantini D. *RT-NET: real-time reconstruction of neural activity using high-density electroencephalography*. Neuroinformatics. 2020 Jul 28. doi: 10.1007/s12021-020-09479-3. Epub ahead of print.

Abstract

High-density electroencephalography (hdEEG) has been successfully used for large-scale investigations of neural activity in the healthy and diseased human brain. Because of their high computational demand, analyses of source-projected hdEEG data are typically performed offline. Here, we present a real-time noninvasive electrophysiology toolbox, RT-NET, which has been specifically developed for online reconstruction of neural activity using hdEEG. RT-NET relies on the Lab Streaming Layer for acquiring raw data from a large number of EEG amplifiers and for streaming the processed data to external applications. RT-NET estimates a spatial filter for artifact removal and source activity reconstruction using a calibration dataset. This spatial filter is then applied to the hdEEG data as they are acquired, thereby ensuring low latencies and computation times. Overall, our analyses show that RT-NET can estimate real-time neural activity with performance comparable to offline analysis methods. It may therefore enable the development of novel brain-computer interface applications such as source-based neurofeedback.

4.1 Introduction

Functional magnetic resonance imaging (fMRI) is currently the primary research tool for investigating human brain function (Fox and Raichle 2007; Ganzetti and Mantini 2013). However, fMRI only provides an indirect measure of neural activity mediated by a slow hemodynamic response. Electroencephalography (EEG) is a brain imaging technique alternative to fMRI. EEG measures changes in electric potentials over the scalp, which are generated by neuronal currents flowing through the head (Speckmann et al. 2012). Notably, source activity reconstruction using EEG requires realistic biophysical models that incorporate the exact positions of EEG electrodes as well as the anatomical properties of an individual's head (Brett et al. 2002). Estimation of brain sources from EEG recordings (Ganzetti and Mantini 2013; Pfurtscheller and Lopes Da Silva 1999) is typically referred to as the *inverse problem*. On the other hand, the assessment of EEG recordings from brain sources is referred to as the *forward problem* (Hallez et al. 2007).

To date, several software solutions have been made available to the neuroscientific community for offline analysis of EEG recordings, including EEGLab (Arnaud Delorme and Makeig 2004), Fieldtrip (Oostenveld et al. 2011), Brainstorm (Tadel et al. 2011), SPM (Litvak et al. 2011) and MNE (Gramfort et

al. 2014). Recently, our research group proposed an offline analysis workflow specifically suited for high-density (hdEEG) data, which integrates several tools from existing software with original solutions for data preprocessing, realistic head model generation and source localization. So far, our analysis workflow for hdEEG has been used to reconstruct large-scale brain networks (Liu et al. 2017, 2018) and to examine functional connectivity between network nodes (Samogin et al. 2019). Such an application does not require online data processing, which is instead needed for brain-computer interface (BCI) studies. Real-time reconstructions of source-space EEG activity could enhance the effectiveness of BCI applications, such as neurofeedback (Boe et al. 2014; van Lutterveld et al. 2017). MNE Scan (<https://www.mne-cpp.org/index.php/category/development/mne-scan>) and NeuroPype (<https://www.neuropype.io>) have been recently introduced as new software packages for online analysis of EEG data. They offer several tools for real-time EEG data processing and feature extraction, and also incorporate source localization tools. They are not optimized for hdEEG systems as they rely on a template head model that does not consider electrode positions collected during the same experimental session (Van Hoey et al. 2000).

To address the limitation described above, we introduce a novel software package for Real-Time Noninvasive Electrophysiology (RT-NET), which is distributed under a GNU General Public License (GPL). RT-NET permits online neural activity reconstruction from hdEEG recordings. The user can access the different analysis steps through a graphical user interface (GUI). Unlike MNE Scan and NeuroPype, RT-NET permits the generation and use of a realistic head model based on electrode positions collected just before EEG recordings, leading to an enhanced precision in neural activity reconstruction. To ensure very short processing times, it relies on an adaptive spatial filter for artifact attenuation as well as for source localization. In the present study, we assessed the effectiveness and validity of RT-NET on hdEEG data collected during hand movements. Specifically, we compared the neural activity reconstructed online with that estimated by an offline analysis workflow.

4.2 Methods

RT-NET was written using the MATLAB (The Mathworks, Natick, MA, US) programming environment. Therefore, existing libraries and functions for EEG data analysis such as EEGLab, Fieldtrip, Brainstorm, SPM and Lab Streaming Layer (LSL) can be easily integrated. The source code and the software manual can be downloaded using the following links: <https://www.nitrc.org/projects/rtnet> or <https://github.com/robertoguarnieri/rtnet>. Being the source code available, software customization or extension is possible. The documentation specifies the software requirements and guides the user through the whole processing pipeline. RT-NET has been specifically developed for optimal integration with the stages of a classical hdEEG experiment (Liu et al. 2017; Michel and Brunet 2019), such as the collection of a magnetic resonance (MR) image, of electrode positions, as well as of hdEEG data (figure 4.1).

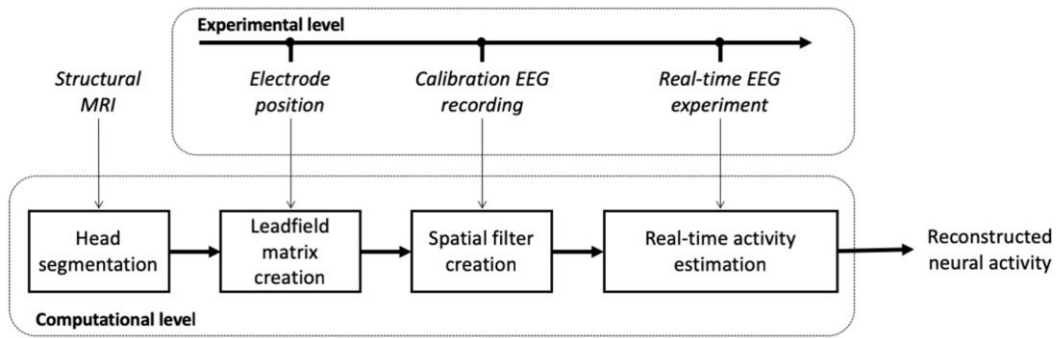


Figure 4.1. RT-NET modules and their execution during a typical hdEEG experimental session. Prior to the hdEEG session, the anatomical MR image is segmented into three tissue classes. During hdEEG, the participant wears the hdEEG cap and the electrode positions over the scalp are recorded. After the co-registration of the complete set of electrode positions over the MR image, the leadfield matrix is generated. A calibration recording is acquired in the participant. This recording is used to estimate an *artifact attenuation filter*, F_0 , which reduces noise and non-neuronal signals, and a *source localization filter*, K , for reconstructing neural activity in the source-space. Finally, during the real-time EEG experiment, the spatial filter is applied to the hdEEG data, generating the reconstruction of active brain sources in an online modality.

4.2.1 Toolbox description

As already mentioned, the GUI of RT-NET gives access to all the functions required for online brain activity reconstruction. Therefore, there is no need for the user to have programming experience. The GUI offers indeed a simplified, structured and user-friendly tool (figure 4.2).

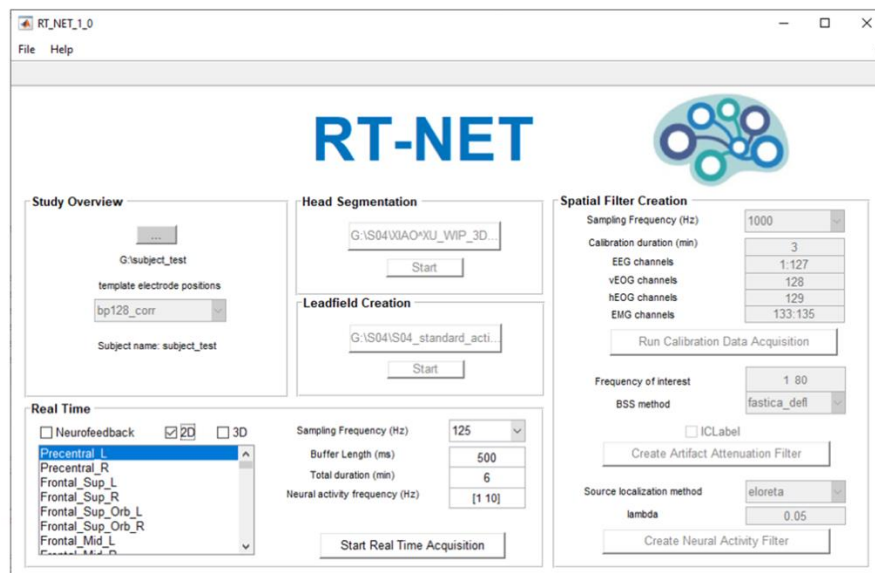


Figure 4.2. RT-NET graphical user interface. *Study Overview* is the first panel of the toolbox, in which it is possible to load the output folder of the study and visualize the information. After that, the user can load the structural image of the subject's head, previously acquired, and start the *Head Segmentation*. The *Leadfield creation* step starts when the file containing the electrode positions over the subject's scalp are loaded. For the *Spatial Filter Creation* step, the user needs to acquire a hdEEG calibration recording. A filter for real-time neural reconstruction is initialized using this recording. Finally, the user can enable and customize the online reconstruction of neural activity by using the *Real-Time* panel.

The GUI is organized in five different modules: *Study overview*, *Head segmentation*, *Leadfield matrix creation*, *Spatial filter creation* and *Real-time activity estimation*. Each time an analysis step is completed through a module of RT-NET, a new panel is activated. First, in the *Study Overview window*, the user, after the initialization of a new project, can choose the output folder and the type of EEG system that will be used. Before the EEG session, an anatomical image of the participant's head needs to be acquired using MR imaging, or alternatively, a template included in the software's directory can be used. Through the *Head segmentation* module, the structural MR image is segmented into different tissue classes. Next, the EEG cap is positioned over the participant's scalp and the electrode positions are recorded. After the co-registration of the complete set of electrode positions over the MR image and the generation of a realistic volume conductor model, the *Leadfield matrix creation* tool calculates the linear relationships between neural currents in the brain (sources) and electric potentials measured at the electrode level. The *Spatial filter creation* module can be initialized through the acquisition of an EEG calibration recording. By using this recording, a spatial filter is produced, which is capable of attenuating artifactual signals in the hdEEG data and estimating neural activity in the brain. With the *Real-time activity estimation* module, the spatial filter is applied to the EEG data, supporting the online reconstruction of brain sources. A detailed description of RT-NET modules is provided here below.

4.2.1.1 Initialization and Study Overview

When the GUI is launched, the user is required to initialize anew project through the *Study Overview* module. This permits the user to choose the output folder for saving the data and the EEG system that will be used for the experiment. The EEG systems that are recognized by RT-NET are those compatible with LSL (<https://github.com/sccn/labstreaminglayer>), an open-source software solution for communicating with external devices in real-time and with millisecond accuracy. It should be noted that, although LSL is platform-independent, it is more easily accessible in its Windows implementation. This may also result in an easier use of RT-NET with the Windows operating system. After defining the input required by the *Study Overview* module, it is possible to start the *Head Segmentation* module.

4.2.1.2 Head segmentation

The second module of RT-NET, *Head Segmentation*, is designed to automatically perform the segmentation of the MR image of the subject's head. The estimation of EEG signals from the brain sources (also known as the *forward solution*) requires a realistic head-volume conductor model to be generated from an individual's MR image, and the correct electrode locations to be defined with respect to the conductor model. Therefore, the first processing stage of our workflow involves the segmentation of the MR image into three different tissue classes: brain, skull and skin (Gramfort et al. 2010). This is done using the unified segmentation algorithm implemented in SPM12 (Ashburner and Friston 2005) (<https://www.fil.ion.ucl.ac.uk/spm/software/spm12/>). The choice of segmenting the brain in three

tissue classes is due to the need of balancing realistic modelling and computational efficiency (Fuchs et al. 2002).

The tissue probability maps produced by SPM12 are then binarized using a winner-takes-all approach (Ashburner and Friston 2005). Finally, the three tissue compartments in the volume space are processed with Fieldtrip (<http://www.fieldtriptoolbox.org>) to build hexahedral meshes.

4.2.1.3 Leadfield matrix creation

Once the head segmentation is performed, the *Leadfield matrix creation* window is activated. First, the electrode positions file, previously acquired, needs to be loaded and then the computations can start. This preprocessing module allows the generation of the leadfield matrix, L , containing the scalp potentials putatively measured for each possible configuration of neural source position and orientation. Specifically, the scalp potential θ , can be expressed as follows (Pascual-Marqui et al. 2011):

$$\theta(t) = L \cdot J(t) \quad (4.1)$$

where, if n_E is the number of electrodes and n_V the number of voxels, then the leadfield matrix, L , has dimension $[n_E \cdot n_V]$; the current density $J(t)$ has dimension $[3n_V \cdot 1]$; and $\theta(t)$ has dimension $[n_E \cdot 1]$.

The first step for leadfield matrix creation is the co-registration of the electrode positions in the same space, defined by the MR image. To this end, a rigid-body transformation matching the landmarks in the electrode space to the corresponding ones in the MR space is computed and applied to the electrode positions. These are then aligned to the head surface extracted from the individual MR image using the iterative closest point algorithm (Besl and McKay 1992) implemented in SPM12. Finally, each electrode is orthogonally projected onto the head surface.

The second step is the creation of the volume conductor model. The meshes derived from MR images for the brain, skull and skin compartments are used, along with the conductivity values defined for each of them. These are set by default to 0.33, 0.01 and 0.43, respectively, in line with the relevant literature (Haueisen et al. 1997; Holdefer et al. 2006), but can also be modified by the user if needed.

The electrode positions and the volume conduction model are combined to create the leadfield matrix by numerical simulations, which are conducted using the symmetric boundary element method (sBEM) implemented in OpenMEEG (Gramfort et al. 2010, 2011). The leadfield matrix, initially computed for each mesh element spanning the gray matter, is then resampled in the volume space, defined as a regular volumetric grid with 6-mm resolution.

4.2.1.4 Spatial filter creation

The *Spatial filter creation* module permits the generation, from a hdEEG calibration recording, of a spatial filter that will subsequently be used for online artifact reduction and source localization. First, the user needs to choose the length of the calibration recording (in minutes), the sampling frequency

(in Hz), the frequency band of interest (in Hz), the EEG channels, the data decomposition technique, the auxiliary electrical channels (i.e. electrooculogram or electromyogram) to be used for artifact detection, the source localization method and its parameters. Next, the calibration recording can be acquired by pressing the corresponding button.

First of all, we detect channels with low signal quality and label them as ‘bad channels’. To this end, we use an automated procedure that combines information from two different parameters. The first parameter is the minimum Pearson correlation of the signal in the frequency band of interest selected by the user, against all the signals from the other channels. The second parameter is the noise variance in the band 200-250 Hz, where the contribution of the EEG signal can be considered negligible. We define the list of bad channels b , including those channels for which at least one of the two channel-specific parameters are outliers as compared to the total distribution of values. To ensure robustness of the detection, the threshold to define an outlier is set to $m + 4s$, where m is the average value and s is the standard deviation. Subsequently, the list of neighboring channels is defined using the FieldTrip toolbox (<http://www.fieldtriptoolbox.org>). A *channel adjacency matrix* D with dimension $[n_E \cdot n_E]$, is created, with each element d_{ij} equal to 1 if channels i and j are adjacent (and not labelled as ‘bad channels’), and equal to 0 otherwise. A *bad-channel correction matrix* C , with dimension $[n_E \cdot n_E]$, is then created:

$$c_{ij} = \begin{cases} d_{ij}/\sum_j d_{ij} & \text{if } i \in b \\ 1 & \text{if } i \notin b \text{ and } i = j. \\ 0 & \text{if } i \notin b \text{ and } i \neq j \end{cases} \quad (4.2)$$

Next, we generate a data re-referencing matrix R to perform average re-referencing (Liu et al. 2015). The matrix R , with dimension $[n_E \cdot n_E]$, is defined as follows:

$$r_{ij} = \begin{cases} (n_E - 1)/n_E & \text{if } i = j \\ -\frac{1}{n_E} & \text{if } i \neq j \end{cases} \quad (4.3)$$

We apply the spatial filters described by matrices C and R to the raw EEG data $X(t)$, so to obtain a new EEG dataset $X_q(t)$, in which all signals are in average reference and those from bad channels are repaired:

$$X_q(t) = C \cdot R \cdot X(t). \quad (4.4)$$

Using EEGLab (<https://sccn.ucsd.edu/eeglab>), we band-pass filter the resulting EEG data in the frequency range selected by the user, so to obtain the new EEG dataset $\tilde{X}_q(t)$. Then, we apply independent component analysis (ICA) (Mantini et al. 2008) using a fast fixed-point ICA (FastICA) algorithm (<http://research.ics.aalto.fi/ica/fastica>) in deflation approach and with hyperbolic tangent as

contrast function (Hyvärinen 1999). Other ICA algorithms are implemented in RT-NET, and can be alternatively used: FastICA in symmetric approach, Infomax (T.-W. Lee et al. 1999) and JADE (Cardoso 1999). The ICA model can be described as:

$$\tilde{X}_q(t) = A \cdot S(t) \quad (4.5)$$

where $\tilde{X}_q = [X_1(t), \dots, X_{n_E}(t)]$ is the matrix of n_E observed signals; $S(t) = [S_1(t), \dots, S_{n_S}(t)]$ is the matrix of n_S underlying signals, or independent components (ICs); A , with dimension $[n_E \cdot n_S]$, denotes the mixing matrix (Stone 2004). The ICs can be retrieved by determining the unmixing matrix W , with dimension $[n_S \cdot n_E]$, such that:

$$S(t) = W \cdot \tilde{X}_q(t). \quad (4.6)$$

After that FastICA has been run on the EEG calibration dataset $\tilde{X}_q(t)$, the ICs associated with the artifacts (or artifactual ICs) are automatically identified. This can be done either using ICLabel (<https://sccn.ucsd.edu/wiki/ICLabel>) (Pion-Tonachini et al. 2019), or the IC artifact detection solution implemented in Liu et al. (2017). The latter, which is the default solution in RT-NET, relies on the following parameters: 1) correlation between the power of the IC with vertical electrooculogram (vEOG), horizontal electrooculogram (hEOG) and electromyogram (EMG); 2) the coefficient of determination obtained by fitting the IC power spectrum with a $1/f$ function; 3) the kurtosis of the IC. An IC is classified as artifactual if at least one of the above parameters is above its specific threshold, set in accordance with previous studies (De Pasquale et al. 2010; Liu et al. 2017; Mantini et al. 2009). The unmixing matrix W_A for the artifactual components $S_A(t)$ is obtained by selecting the corresponding rows of the matrix W , such that:

$$S_A(t) = W_A \cdot X(t). \quad (4.7)$$

An *artifact attenuation filter* F_0 , with dimension $[n_E \cdot n_E]$, is initialized as:

$$F_0 = I - X \cdot S_A^T \cdot (S_A \cdot S_A^T)^{-1} \cdot W_A \quad (4.8)$$

where I is an identity matrix with dimension $[n_E \cdot n_E]$.

The artifact-free calibration dataset $\tilde{X}_p(t)$ is generated by applying the initial artifact attenuation filter F_0 to $\tilde{X}_q(t)$, as follows:

$$\tilde{X}_p(t) = F_0 \cdot \tilde{X}_q(t). \quad (4.9)$$

It should be noted that the *artifact attenuation filter* $F(t)$ is dynamically defined during the acquisition of real hdEEG data, following the approach described in Guarnieri et al. (2018). This approach is explained in detail in the next section, dedicated to online data analysis.

Using the artifact-free calibration dataset $\tilde{X}_p(t)$, a *source localization filter* K , with dimension $[3n_V \cdot n_E]$, is also created. This specific filter depends on the selected source localization algorithm. RT-NET integrates the exact low-resolution brain electromagnetic tomography (eLORETA) algorithm (Pascual-Marqui et al. 2011) as default solution. In this case, the source localization filter K is calculated using the following formula:

$$K = G^{-1} \cdot L^T \cdot (L \cdot G^{-1} \cdot L^T + \alpha H)^+ \quad (4.10)$$

where L is the leadfield matrix, G is a symmetric positive definite weight matrix with dimension $[3n_V \cdot 3n_V]$, H is the noise covariance matrix estimated from $\tilde{X}_p(t)$, $\alpha > 0$ is the Tikhonov regularization parameter and $+$ denotes the Moore–Penrose pseudoinverse. The regularization parameter α is set by default to 0.05 and can be changed by the user if needed. Other source localization algorithms implemented in RT-NET are the standardized low resolution brain electromagnetic tomography (sLORETA) algorithm (Pascual-Marqui 2002), the minimum norm estimates (MNE) (Hämäläinen and Ilmoniemi 1994), its weighted version wMNE (Lin et al. 2006) and the linearly constrained minimum variance beamformer (LCMV) (Van Veen et al. 1997). All the source localization methods above are implemented in volumetric space. In particular, eLORETA, LORETA, MNE and LCMV are those integrated in FieldTrip (<http://www.fieldtriptoolbox.org>), whereas sLORETA and wMNE are those in Brainstorm (<https://neuroimage.usc.edu/brainstorm>).

4.2.1.5 Real-time activity estimation

The *Real-time activity estimation* module allows the reconstruction of ongoing neural activity for all the voxels in the gray matter or, alternatively for selected regions of interest (ROIs), by using the spatial filters created using the calibration recording. The parameters that need to be defined before real-time activity estimation are: buffer length (in ms), total duration of the experiment (in minutes), sampling frequency and the frequency band of interest for neural activity estimation (both in Hz). Furthermore, it is necessary either to select the ROIs for which neural activity needs to be extracted, or to enable reconstruction in each voxel of the gray matter for real-time mapping of neural activity.

Within the real-time activity estimation module, EEG data are stored in a buffer with n_T samples, determined based on the sampling frequency and the buffer length set by the user. The EEG data in the buffer $X(\tau)$ is filtered in the frequency band of interest, thereby obtaining $\tilde{X}(\tau)$. Next, the *bad-channel correction matrix* C and the *re-referencing matrix* R are applied

$$\tilde{X}_q(\tau) = C \cdot R \cdot \tilde{X}(\tau). \quad (4.11)$$

Starting from the resulting dataset $\tilde{X}_q(\tau)$, we estimate artifactual signals that are present in the buffer, using the matrix W_A obtained from the calibration dataset:

$$S_A(\tau) = W_A \cdot \tilde{X}_q(\tau). \quad (4.12)$$

At this point, linear regression analysis is used to estimate the weight matrix B_A associated with the artifactual signals in the buffer. In particular, the following equation is considered to account for the non-stationarity of the artifactual contribution in the EEG signals:

$$\tilde{X}_q(\tau) = B_A \cdot S_A(\tau) + \varepsilon(\tau) \quad (4.13)$$

where $\varepsilon(\tau)$ is the residual of $X(\tau)$ that cannot be explained by a linear combination of $S_A(\tau)$. Using the method proposed in Guarnieri et al. (2018), an adaptive spatial filter $F(\tau)$ is built to dynamically obtain artifact-free signals $\tilde{X}_p(\tau)$, such that:

$$\tilde{X}_p(\tau) = F(\tau) \cdot \tilde{X}_q(\tau) \quad (4.14)$$

where $F(\tau)$ is defined as follows:

$$F(\tau) = I - X(\tau) \cdot S_A^T(\tau) \cdot \left(S_A(\tau) \cdot S_A^T(\tau) \right)^{-1} \cdot W_A. \quad (4.15)$$

Considering that the buffer is dynamically updated at the same frequency as the sampling rate, the latest sample in the artifact-cleaned EEG dataset $\tilde{X}_p(\tau)$ is continuously extracted to estimate real-time neural activity in the sensor space $Y(t)$.

When the reconstruction of neural activity from ROIs is selected, the primary voxel indices corresponding to the ROIs are identified and the source localization matrix K is downsampled accordingly. In this case, the dimension of matrix K becomes $[3n_R \cdot n_E]$, where n_R is the number of ROIs, and the neural signals are separately reconstructed for the three directions. The source localization filter K is then applied to $Y(t)$, such that real-time neural activity in the sourcespace $B(t)$ is also obtained:

$$B(t) = K \cdot Y(t) \quad (4.16)$$

By default, the artifact-free signals in the sensor space $Y(t)$, and in the source space $B(t)$, are forwarded to LSL for real-time visualization or control of other devices, such as a brain stimulation system for closed-loop applications (Boe et al. 2014; Semprini et al. 2018). These reconstructed neural signals are also saved in the *output folder*, to be analyzed offline.

4.2.2 Validation of RT-NET

We assessed the performance of the RT-NET toolbox using real hdEEG data. We compared the signals processed with RT-NET against those obtained with our offline analysis workflow (Liu et al. 2017). Specifically, we focused on the modulations of neural activity induced by movements of the right hand (Weiss et al. 2013).

4.2.2.1 Data collection

Data used in this study were obtained from hdEEG recordings collected in 10 healthy right-handed participants (five men and five women, age range 23–39 years). All participants reported normal or corrected-to-normal vision and had no psychiatric or neurological history. They gave written informed consent to the experimental procedures, which were approved by the Institutional Ethics Committee of KU Leuven.

In a first experimental session, a structural T1-weighted MR image of the participant's head was collected with a 3 T Philips Achieva MR scanner (Philips Medical Systems, Best, Netherlands) using a magnetization-prepared rapid-acquisition gradient-echo (MP-RAGE) sequence (Mugler and Brookeman 1991). The scanning parameters were TR = 9.6 ms, TE = 4.6 ms, 160 coronal slices, 250 × 250 matrix, and voxel size 0.98 × 0.98 × 1.2 mm³. The MR image was used during the EEG experimental session to generate the volume conduction model for source localization.

In a second experimental session, electrode positions were first acquired using the Xensor system (ANT Neuro, Enschede, Netherlands). Subsequently, two hdEEG datasets were collected: the first one, which was used for spatial filter creation using RT-NET, with the participant being at rest for 4 min; the second one with them performing right-hand movements for 6 min. hdEEG signals were sampled at 1 kHz using the 128-channel actiCHamp system (Brain Products GmbH, Gilching, Germany). The electrode at vertex (Cz in the 10/20 international system) was used as the physical reference. In addition, we also recorded horizontal and vertical EOG (hEOG and vEOG) as well as three electromyography (EMG) signals associated with the masseter (right), trapezius (right), splenius capitis (right) and carpi radialis longus (right) muscles. The first three EMG signals were used for artifact removal, whereas the fourth EMG signal was used to detect hand movement onsets. For the resting-state part of the EEG session, participants were asked to fixate on a black cross in the center of a white screen (eyes-open fixation). In the motor-related part of the EEG session, participants were asked to perform right wrist flexions/extensions, alternating 6 s of self-paced uninterrupted movements with 6 s of eyes-open fixation.

4.2.2.2 Analysis of RT-NET performance

A crucial metric to assess the performance of the toolbox is the computational time. This was quantified using a computer with a 2.5-GHz Intel Core i7 processor and 16 GB RAM, running Windows 10. We quantified the time required for the *Head segmentation*, *Leadfield matrix creation* and *Spatial*

filter creation modules of RT-NET. We also evaluated the computational delay during online hdEEG acquisition and processing. This analysis was conducted using a buffer length of 500 ms, as in Guarnieri et al. (2018), band-pass frequency between 1 and 50 Hz, and sampling frequency equal to 100 Hz.

The neural signals reconstructed in real-time using the *Real-time reconstruction* module were used to produce spatial maps reflecting event-related synchronization/desynchronization (ERS/ERD) maps across trials. ERD/ERS can be expressed using the following formula:

$$ERD(f, t) = \frac{P(f, t) - P_b(f)}{P_b(f)} \cdot 100\% \quad (4.17)$$

where $P(f, t)$ is the power in a given frequency band and time interval, and $P_b(f)$ is the average power over time in a baseline period (Pfurtscheller and Lopes Da Silva 1999). ERD maps were calculated for the beta band (13–30 Hz) in the period [0 s, +2 s] with respect to movement onset. The beta band was chosen, as it is typically implicated in motor execution (Pfurtscheller and Lopes Da Silva 1999). The baseline period [−1 s, 0 s] was defined with respect to the same onset. The ERD maps were visualized in real-time using a 3D cortical model with 3500 vertices, which was generated using FieldTrip (Oostenveld et al. 2011). The correlation between ERD maps was calculated offline after the experiment, to quantify the reliability of the results across trials.

After verifying the feasibility of using RT-NET in a real-time hdEEG experiment, we also quantified the accuracy of source localization. To this end, we used an offline analysis as a benchmark. The offline analysis workflow was the same applied to the calibration EEG dataset, and included bad-channel correction, re-referencing, band-pass filtering, ICA-based artifact removal, head modelling using sBEM and source localization using eLORETA (Liu et al. 2017, 2018). The reliability of task-related modulations in neural activity was assessed using the average ERD map across trials, again for the beta band. We also conducted an ERD analysis for selected ROIs, whose MNI coordinates were chosen on the basis of relevant fMRI studies (Debaere et al. 2003, 2004; Gorgolewski et al. 2013; Lv et al. 2013; Rémy et al. 2008; Weiss et al. 2013). The ROIs were the left primary motor cortex (M1; MNI coordinates [−38, −20, 58]), the supplementary motor area (SMA; [0, −4, 56]), the left ventral premotor cortex (VPMC; [−30, −10, 58]), and the left superior temporal gyrus (STG; [−58, −32, 6]). The latter, whose activity is expected to be minimally modulated by motor task performance, was used as the control ROI. For each ROI, the MNI coordinates were converted to individual space. Spherical ROIs with a radius of 6 mm were then created (Marrelec and Fransson 2011). Neural signals from the ROIs were extracted, and first used to assess the presence of residual artifacts in the source-localized data. This was quantified using the absolute temporal correlation between reconstructed neural signals and simultaneously collected EOG and EMG signals. By using temporal correlations, we also compared ERD time-courses obtained using RT-NET and the offline analysis workflow, either in the beta band (13–30 Hz) and in the full band (1–50 Hz). This permitted us to estimate the presence of motor-related activity in the reconstructed neural signals. A Wilcoxon signed rank test was carried out to assess significant differences.

4.3 Results

4.3.1 Computation time for RT-NET analysis

Computational efficiency is a key feature of RT-NET, which was specifically designed to support real-time processing of hdEEG recordings, so we quantified processing times for the different analysis stages. Average processing times for *Head segmentation*, *Leadfield matrix creation* and *Spatial filter creation* were 1938 s, 302 s and 735 s, respectively (figure 4.3). The first of these three modules should be used before the real-time EEG acquisition can start. The time required for the second and third modules should be kept as short as possible. Notably, the processing times we obtained for each of these two modules permit their execution during the EEG experimental session, and before the actual experiment.

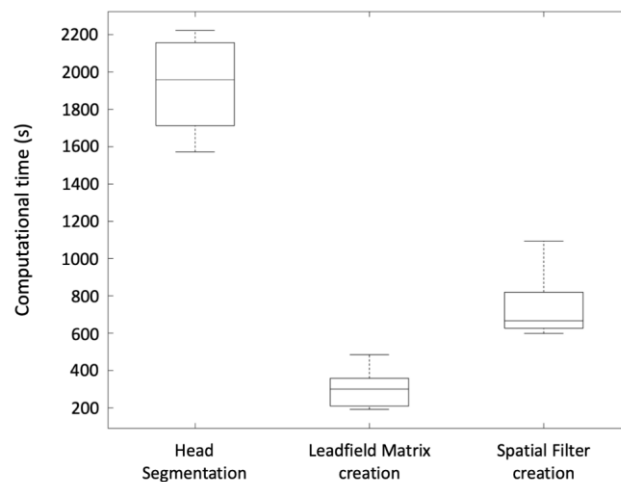


Figure 4.3. Computational time of RT-NET for the *Head segmentation*, *Leadfield matrix creation* and *Spatial filter creation* modules. The boxplots show the processing time calculated for each module, across all participants.

Besides the time required for preparatory steps, it is also important to consider the computational efficiency for real-time acquisition and processing. During our data collection, we measured acquisition time and delay. We divided our 6-minutes recordings, collected at a sampling rate of 1 kHz, into windows of 500 ms. Across all of them, the maximum delay introduced by real-time processing for artifact attenuation and source localization was 4 ms for each data buffer.

4.3.2 Accuracy of RT-NET analysis

First, we examined the ERD maps produced online during the experiment for consecutive trials (figure 4.4). Each of them showed beta-band ERD peak within the primary motor cortex. The average spatial correlation of the ERD maps across trials was equal to 0.78.

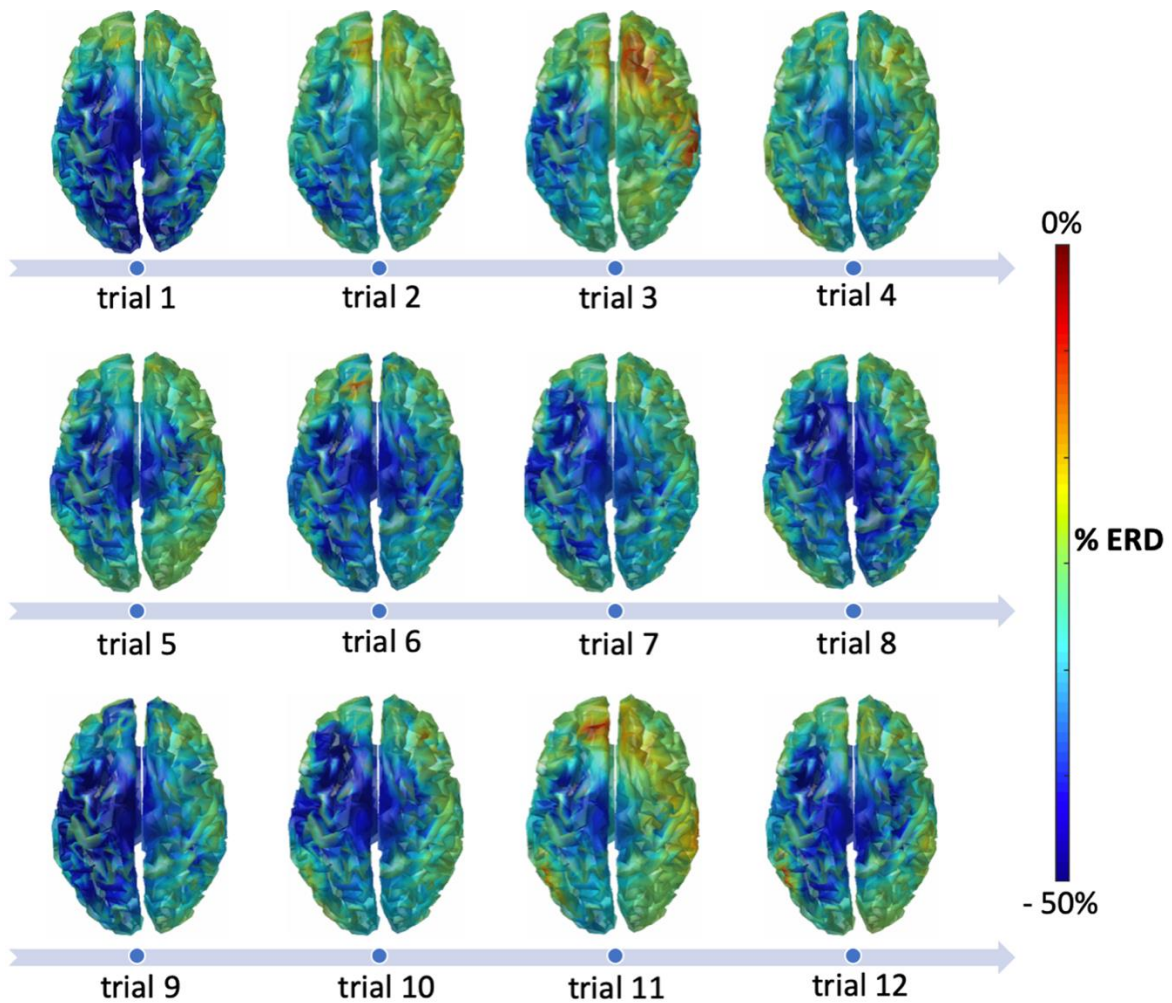


Figure 4.4. ERD maps in the beta band (13–30 Hz) for a single participant, obtained using RT-NET for 12 consecutive trials during right-hand movements. The maps are represented over a 3D cortical model in dorsal view.

The correlation values obtained using EEG data processed with the online analysis workflow were not significantly different (Wilcoxon signed rank test, $p = 0.06$) from those obtained using ERD maps from an offline analysis (figure 4.5).

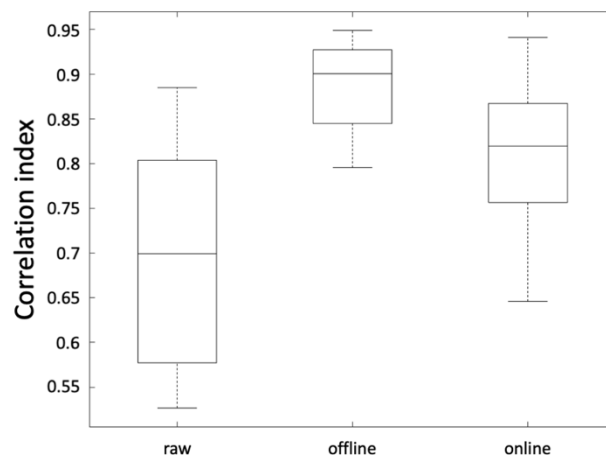


Figure 4.5. Spatial correlation of ERD maps in the beta band (13–30 Hz) calculated without artifact removal, offline and online processing, respectively. The boxplots show the average across-trial correlations across all participants.

Also, the beta-band ERD maps obtained using RT-NET were similar to those obtained using offline processing (figure 4.6). Quantitatively, the correlation of group-level beta ERD maps obtained with RT-NET with the offline processing with and without artifact removal were equal to 0.76 and 0.56, respectively.

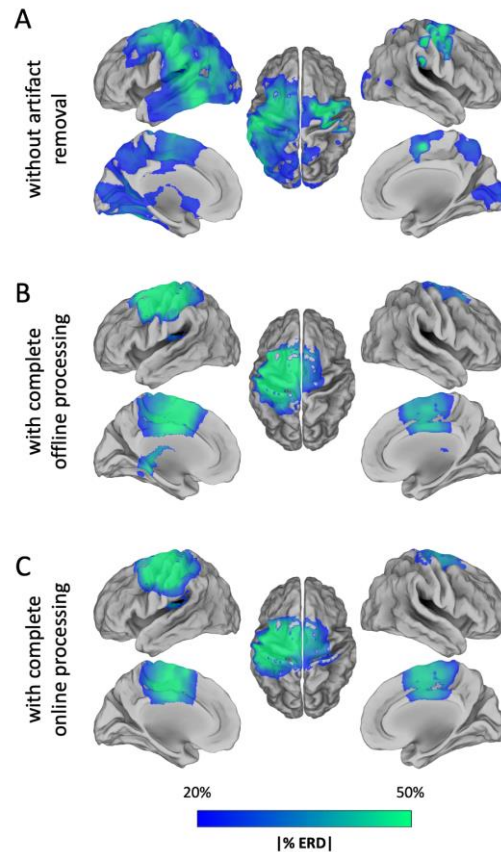


Figure 4.6. Motor-related power modulations in the beta band (13–30 Hz). (A) ERD map obtained without artifact removal (raw); (B) ERD map obtained with a complete offline processing workflow; (C) ERD map obtained by RT-NET. The maps are represented over a cortical surface in lateral, medial and dorsal views.

Similarities between online and offline processing were observed not only in the ERD maps, but also for time-courses reconstructed in three ROIs that are supposedly modulated by right-hand movements (left M1, SMA, left VPMC), and one that is likely not to be involved in task execution (left STG). Notably, there were no evident artifacts in the EEG data, after these were processed using the spatial filter of RT-NET (figure 4.7).

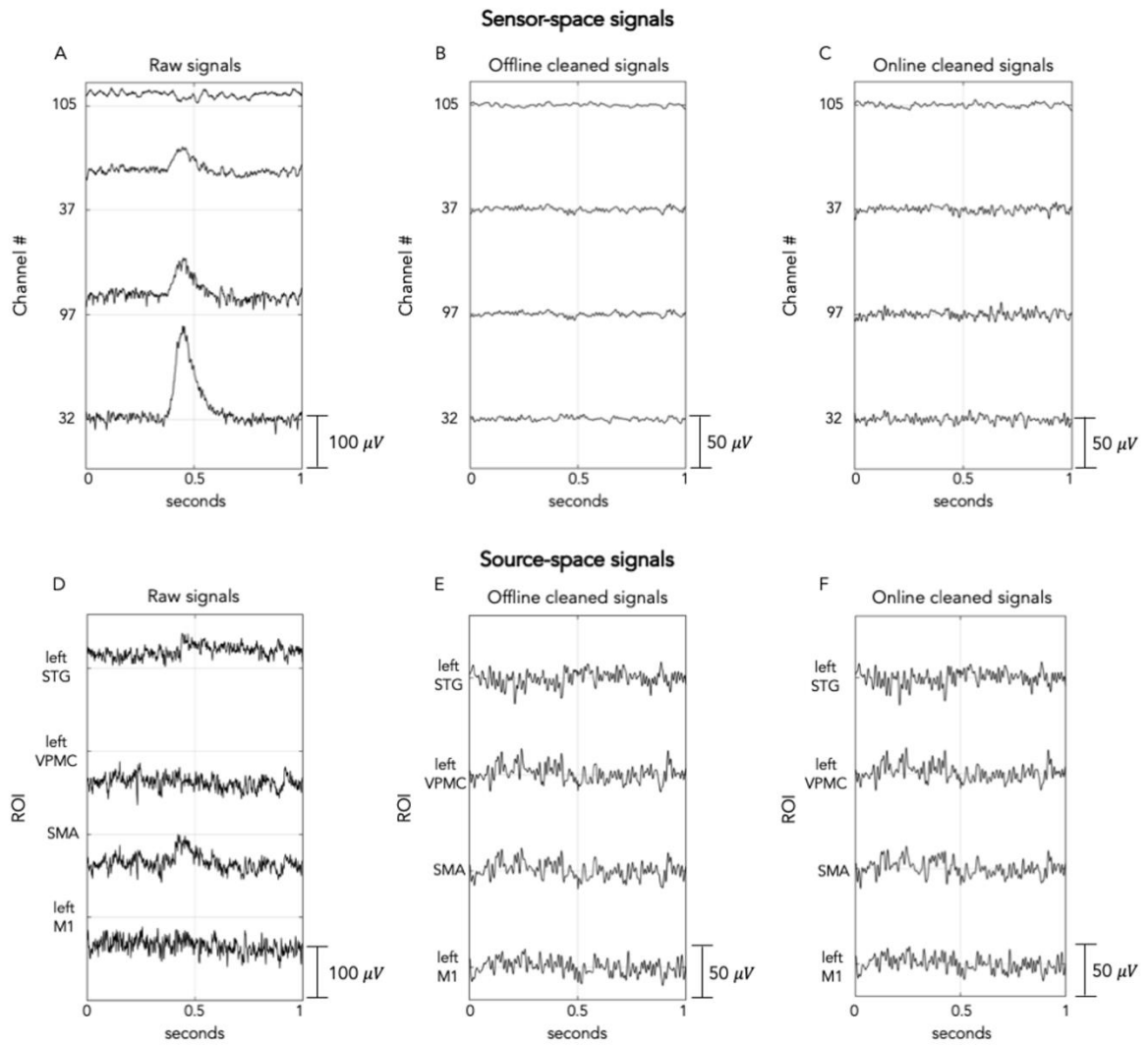


Figure 4.7. Representative examples of sensor-space (A–C) and source-space (D–F) signals from the same participant. Raw (A), offline cleaned (B) and online cleaned (C) EEG recordings in four representative channels; raw (D), offline cleaned (E) and online cleaned (F) voxel time-courses in left M1, SMA, left VPMC and left STG. M1: primary motor cortex; SMA: supplementary motor area; VPMC: ventral premotor cortex; STG: superior temporal gyrus.

The effectiveness of the online artifact removal procedure implemented in RT-NET was quantitatively assessed also by calculating the absolute correlation between reconstructed neural signals and EOG/EMG signals (figure 4.8).

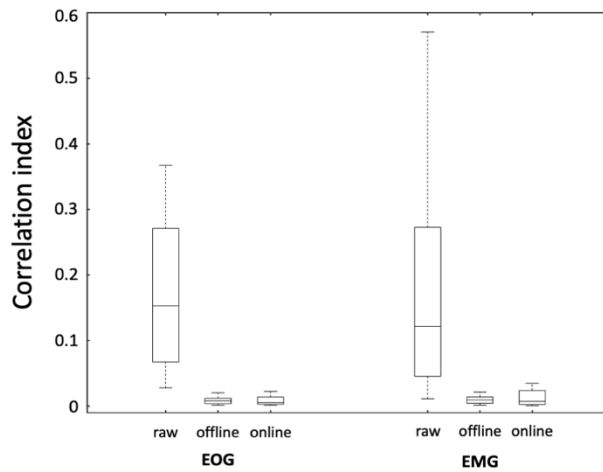


Figure 4.8. Absolute temporal correlation between EMG/EOG signals and neural time-courses. The analysis was conducted for neural signals reconstructed in left M1, SMA, left VPMC and left STG, without artifact removal, with online processing and offline processing, respectively. M1: primary motor cortex; SMA: supplementary motor area; VPMC: ventral premotor cortex; STG: superior temporal gyrus.

Values very close to zero were obtained for both online and offline processing, with no significant difference between them (Wilcoxon signed rank test, $p=0.5542$ and $p=0.1923$ for EOG and EMG, respectively). We then moved to the assessment of ERD after movement onset. Notably, a clear ERD could be detected in left M1, SMA and left VPMC, but not in the control region, left STG (figure 4.9).

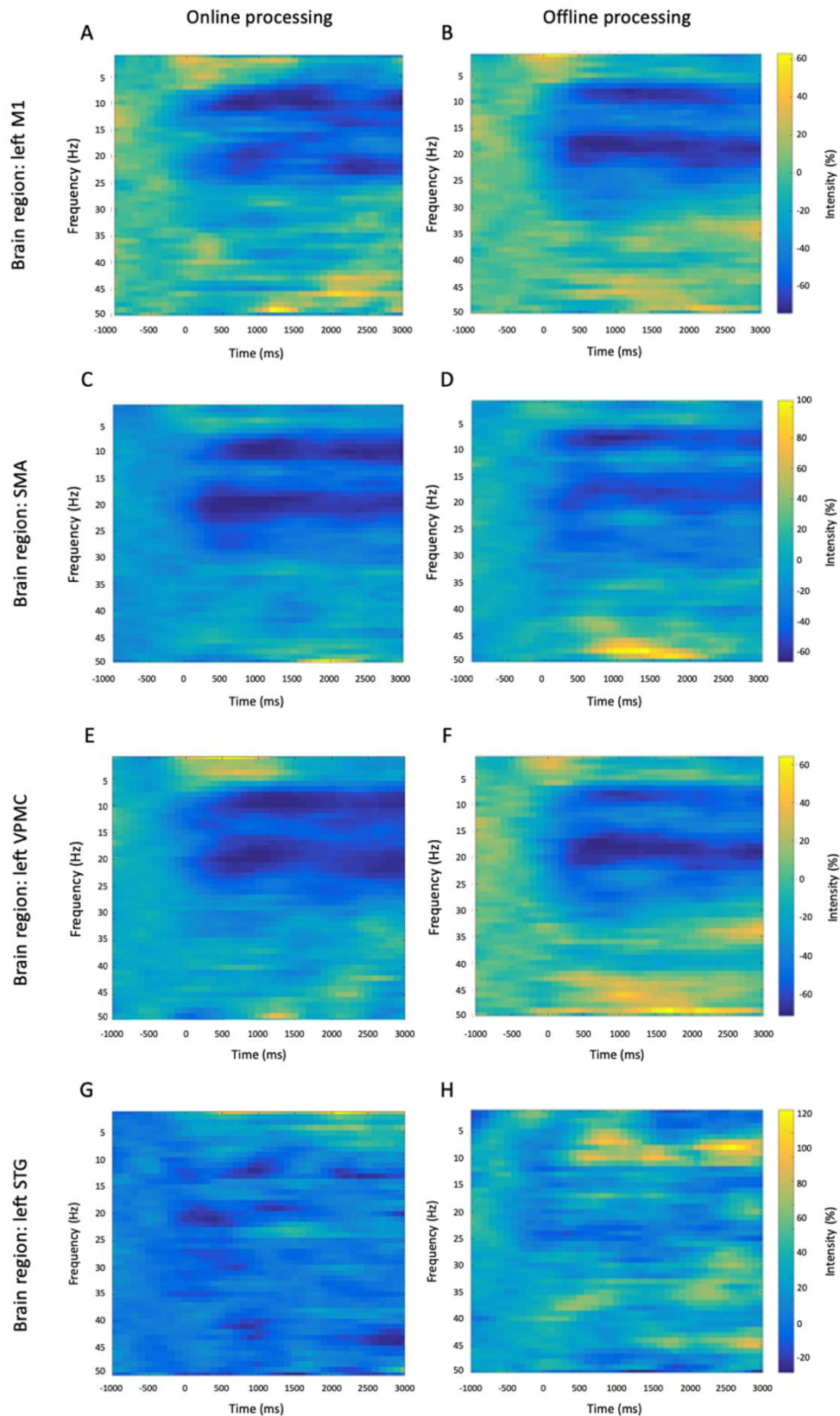


Figure 4.9. Single-subject ERD analysis for online (left column) and offline (right column) neural activity reconstructions. Power modulations are shown for left M1 (A and B), SMA (C and D), left VPMC (E and F) and left STG (G and H). In the left M1, SMA and left VPMC, there is considerable similarity between the online and offline methods in terms of desynchronization in the alpha and beta bands. As expected, the response in the left STG is hardly detectable. M1: primary motor cortex; SMA: supplementary motor area; VPMC: ventral premotor cortex; STG: superior temporal gyrus.

At the quantitative level, we observed that the correlation of power-modulations for the beta band (13–30 Hz), which primarily reflect motor-related neural activity, was significantly higher (Wilcoxon signed rank test, $p < 0.05$) than for the full band (1–50 Hz) in left M1, SMA and left VPMC (figure 4.10).

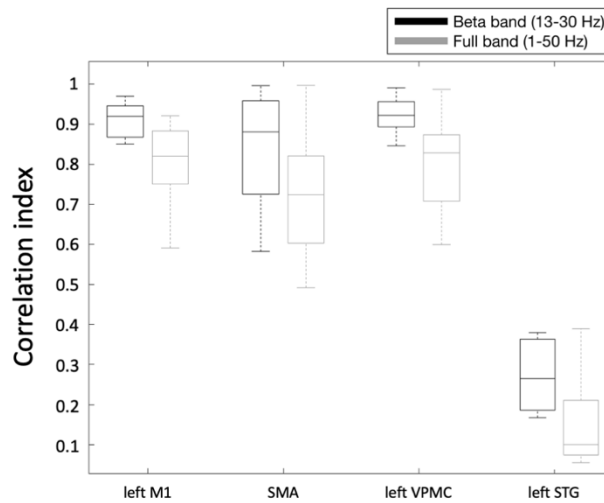


Figure 4.10. Correspondence of band-limited power time-courses between online and offline activity reconstructions in left M1, SMA, left VPMC and left STG. Comparisons were performed by examining the temporal correlation of band-limited power time-courses for the full band (1–50 Hz) and the beta band (13–30 Hz). A Wilcoxon signed rank test revealed higher temporal correlation for the beta compared to the full band for left M1 ($p = 0.0078$), SMA ($p = 0.0156$), left VPMC ($p = 0.0078$), but not for left STG ($p = 0.061$). M1: primary motor cortex; SMA: supplementary motor area; VPMC: ventral premotor cortex; STG: superior temporal gyrus.

4.4 Discussion

We have introduced RT-NET, a novel software package for real-time reconstruction of neural activity, which was specifically developed for the processing of hdEEG recordings. It includes a GUI that guides the user through the analysis steps and streams the processed data externally for real-time visualization or closed-loop applications. Below, we review the strengths and weaknesses of the software in comparison with alternative solutions and discuss the reliability of the results produced in our validation study.

4.4.1 Primary features of RT-NET and comparison with alternative solutions

RT-NET relies on a single-window GUI (figure 4.2) that gives access to four different processing modules. They need to be run sequentially and are compatible with the different stages of a hdEEG experiment (figure 4.1). In previous studies, we have focused on methodological developments supporting the use of hdEEG as a brain imaging tool (Michel et al. 2004). In particular, we showed that combining high-density electrode montages with accurate head models enables more precise source localizations and thereby the reconstruction of brain network activity in the human brain (Liu et al. 2017, 2018). In the present study, we concentrated our efforts on developing novel solutions for the real-time reconstruction of brain activity using hdEEG. RT-NET relies on the online artifact removal

method described in Guarnieri et al. (2018), which is initialized using a calibration dataset collected before the real experiment. This allows the creation of a spatial filter to be applied to the hdEEG data as they are acquired. This solution ensures a low computation time (figure 4.3), which makes RT-NET compatible with neural activity reconstruction.

RT-NET is not the only solution for acquisition and real-time source analysis from electrophysiological data. Indeed, MNE Scan and NeuroPype also provide comprehensive real-time analysis tools for EEG data, including preprocessing and source estimation. Notably, RT-NET has specific features that are not present in MNE Scan and NeuroPype: it permits the creation of a realistic, individualized head model during the EEG experimental session, using the electrode positions and the T1-weighted MR image of the participant's head. In particular, the MR image needs to be segmented to define individual head tissues. This processing step is accomplished in RT-NET using SPM12, which is also written in MATLAB. Another valid tool for MR segmentation is FreeSurfer (<https://surfer.nmr.mgh.harvard.edu>) (Fischl 2012). Both FreeSurfer and SPM12 can provide volumetric measures from T1-weighted images, and a comparison between them has been performed in several studies (Fellhauer et al. 2015; Palumbo et al. 2019; Perdue and Diamond 2014). It has been reported that SPM12 is computationally more efficient than FreeSurfer (Henson et al. 2019; Schwarz et al. 2016), and provides more robust segmentations, except for the white matter (Guo et al. 2019).

Previous studies have already demonstrated that the use individualized head models leads to better source localization results than templated head models (Akalın Acar and Makeig 2013; Brodbeck et al. 2011; Liu et al. 2018). Both MNE Scan and RT-NET calculate the forward model by means of boundary element method (BEM), which provides a realistically shaped volume conductor model without a significant increase in computational demand (Fuchs et al. 2002). Different BEM implementations are available, and in particular, RT-NET and NeuroPype rely on the symmetric BEM (sBEM) implemented in OpenMEEG (Gramfort et al. 2010, 2011). This solution outperforms other BEMs in terms of precision, but has relatively longer computation times (Adde et al. 2003; Clerc et al. 2010; Gramfort et al. 2011).

MNE Scan, NeuroPype and RT-NET implement different solutions for artifact attenuation, i.e. signal-space projection (SSP) (Uusitalo and Ilmoniemi 1997), Artifact Subspace Reconstruction (ASR) (Mullen et al. 2013) and a spatial filter based on ICA (Guarnieri et al. 2018), respectively. It has been shown that, in general, ICA-based artifact correction performs better than SSP (Haumann et al. 2016) and ASR (Kim and Kim 2018). Despite their low computational requirements, both ASR and our ICA-based approach require a calibration recording for reliable filter initialization. Notably, the combination of ASR and our ICA approach could certainly yield superior artifact removal performance than each method separately. However, since ASR and ICA would be to be applied sequentially, their computation times would sum up, and most likely become incompatible with real-time processing requirements.

The estimation of source activity by RT-NET is performed by eLORETA (Pascual-Marqui et al. 2011). However, RT-NET additionally includes MNE (Hämäläinen and Ilmoniemi 1994), sLORETA (Pascual-Marqui 2002), wMNE (Lin et al. 2006) and LCMV (Van Veen et al. 1997). In contrast, eLORETA, sLORETA

and LCMV algorithms are implemented in NeuroPype, whereas MNE Scan can perform source localization with Real-Time Clustered Minimum-Norm Estimates (RTC-MNE) (Dinh et al. 2015) and Real-Time Clustered Multiple Signal Classification (RTC-MUSIC) (Dinh et al. 2017). There is no consensus about which EEG source localization algorithm is best to use, as this may largely depend on the signal-to-noise ratio of the EEG data, the EEG montage density and coverage, and the accuracy of the head model used (Michel et al. 2004). eLORETA has lower localization errors compared to LORETA and sLORETA (Jatoi et al. 2014), but has relatively low spatial resolution (Jatoi and Kamel 2017). Conversely, array signal processing-based algorithms such as MUSIC (Mosher and Leahy 1998) offer high resolution but at the cost of high computational complexity (Jatoi and Kamel 2017), with risk of data loss (Gaho et al. 2018). MNE (Hämäläinen and Ilmoniemi 1994) is less accurate than eLORETA (Im 2018), which is minimally affected by the volume conduction problem under real conditions (Pascual-Marqui et al. 2011). It may also fail in the localization of deep sources (Gaho et al. 2018).

RT-NET can stream data to other applications, as done in the current study (figure 4.4), such that the reconstructed neural activity can also be visualized in real-time. Generally speaking, RT-NET may be beneficial for novel BCI applications, such as source-based neurofeedback (Boe et al. 2014; van Lutterveld et al. 2017) and closed-loop neuromodulation techniques (Semprini et al. 2018).

4.4.2 Validation of real-time neural activity reconstruction by RT-NET

To validate the real-time reconstruction of neural activity using RT-NET, we employed hdEEG recordings collected during right-hand movements. Usually, simple motor tasks are expected to induce prominent contralateral modulation of brain activity. However, depending on task complexity, there may also be ipsilateral modulation. The specific motor task involved in our study is expected to elicit prominent contralateral modulation of brain activity, and in particular an event-related desynchronization in the beta band (Pfurtscheller and Lopes Da Silva 1999), in the hand representation of the left M1, in the SMA and in the left VPMC (Gorgolewski et al. 2013; Grodd et al. 2001; Lotze et al. 2000). The left STG, which was used as a control region, did not show substantial neural activity modulations. We performed an offline analysis of the hdEEG data using the approach we defined in previous studies (Liu et al. 2017). This served as a reference to assess the effectiveness of real-time neural activity reconstruction by RT-NET (figures 4.9 and 4.10).

The ERD map generated for the beta band showed the strongest values in the region covering the left M1, SMA and left VPMC for both online and offline processing (figure 4.6). The peak locations in the map were consistent with those previously reported in transcranial magnetic stimulation and fMRI studies (Gorgolewski et al. 2013; Hlustik 2001; Weiss et al. 2013). Furthermore, the neural signals reconstructed in the selected ROIs not only showed consistent task-related modulations, but also had very small artifactual contamination, as indicated by the absolute temporal correlation with EOG and EMG signals (figures 4.7 and 4.8).

Overall, the results of the present study suggest that the real-time processing of hdEEG data is sufficiently reliable, both in terms of spatial maps and in terms of the reconstructed time-course for specific brain regions. It should be noted, however, that we used hdEEG signals collected during a hand movement task, which is expected to produce robust neural responses. Further methodological work may be necessary to increase the sensitivity and accuracy of hdEEG-based studies in which brain sources produce less intense and more distributed signals. Our results support the idea that hdEEG can be used for solving brain dynamics with high spatial resolution. As such, hdEEG could be used as an alternative to fMRI for functional brain imaging, with the additional benefit of directly measuring brain activity. In addition, hdEEG can provide faster neurofeedback as compared to fMRI (Thibault et al. 2016).

4.4.3 Limitations and possible caveats

A possible caveat of RT-NET may be the use of a relatively simple head modelling strategy, to keep the processing time compatible with that of a typical EEG experiment. Notably, whereas the MR image segmentation can be performed before the experiment, electrode positions need to be obtained from the participant before the leadfield matrix can be created. In this study we used a standard digitizing technique for extracting electrode positions, but it is worth noting that 3D scanning has been recently proposed to yield rapid and reliable electrode positioning (Taberna, Guarnieri, et al. 2019; Taberna, Marino, et al. 2019). 3D scanning technology may be particularly useful for hdEEG systems, approximately halving the acquisition time. For the head modelling step, a three-layer sBEM model is currently used in RT-NET because of its relatively low computational demand. Whereas most BEM implementations rely on 3 layers (brain, skull, skin), the use of 4-layer BEMs that includes the cerebrospinal fluid (CSF) around the brain has been proposed to improve source localization (Akalin Acar and Makeig 2013). BEM solutions using 4 layers (Stenroos and Nummenmaa 2016) may be integrated in future versions of RT-NET, if their computation time will become as low as few minutes, such that they can be used in real-time EEG experiments. It should also be noted that head modelling approaches other than BEMs are also used by the neuroimaging community: finite element methods (FEMs) and finite difference methods (FDMs) (Hallez et al. 2007). FEMs and FDMs can take advantage of a more refined head segmentation than BEMs, and typically yield more precise estimates of the leadfield matrix. However, due to their computational requirements, they are not compatible with the creation of a head model in the course of an EEG experiment. Future methodological developments for parallelized FEM and/or FDM computations (Cuartas Morales et al. 2019) are warranted to reduce processing times and make them compatible with the requirements of real-time EEG experiments using RT-NET. Furthermore, RT-NET performs online artifact attenuation as well as source localization. To optimize artifact attenuation, we recently proposed a method relying on a calibration dataset (Guarnieri et al. 2018). This calibration dataset should contain a sufficient number of artifactual occurrences for an effective setup of the spatial filter. Although it remains difficult to determine how long the calibration dataset should be, it may be helpful to ask the participant to intentionally generate such artifacts (Zhang

et al. 2015). Finally, we would like to point out that a more extensive validation of RT-NET using different tasks and experimental conditions, would be very important. In this study, we have tested RT-NET using hdEEG data obtained during motor task performance. Further work should extend the validation to hdEEG data during auditory stimulation, such that it would be possible to examine the performance of RT-NET when bilateral sources are active.

4.5 Conclusions

RT-NET is a toolbox for the online reconstruction of neural activity from hdEEG signals. It has been specifically conceived and designed to support real-time analyses in the source space. This makes it unlike most software that, given the high computational demand of hdEEG processing, can only support offline source-space analyses. Notably, the accuracy of online neural activity reconstruction by RT-NET is comparable to that achieved with offline processing. We hope that our software package will contribute to the development of novel BCI applications based on hdEEG, such as source-based neurofeedback (Boe et al. 2014; van Lutterveld et al. 2017). Our future research endeavor will be directed towards an extensive validation of RT-NET in a wide range of real-time hdEEG experiments.

5 General discussion

In the field of human neuroscience, an increasing attention is given to the study of neural dynamics at high temporal resolution. In this thesis, we focused on the development of a complete analysis workflow for real-time estimation of source-level hdEEG data. Importantly, we addressed some important technical issues related to real-time hdEEG analysis, such as the estimation of a realistic head model and source localization filter in the course of an hdEEG experiment. In addition, we also focused on the use of spatial filtering for online biological artifact attenuation, an important EEG analysis step. Then, we developed an online stimulating artifact removal to be used also during closed-loop neuromodulation experiments. Finally, we created a software with graphical user interface, which estimates brain activity in real-time.

We believe that the analysis tools we developed can find several applications in the field of human neuroscience. For instance, they can help participants to learn how to actively increase or decrease neural activity in selected cortical regions, thereby having potential impact in the context of neurorehabilitation and neuroenhancement.

5.1 Summary of main findings

In this thesis, the general goal is to develop the necessary technological solutions to obtain a real-time hdEEG system to be used in the context of neurofeedback and closed-loop neuromodulation experiments. To reach this goal, three more specific findings have been attained.

First, the performance of neurofeedback application based on EEG data strongly depends on the effective attenuation of artifacts that are mixed in the recordings. To address this problem, we have developed a novel online EEG artifact removal method, that can be used in neurofeedback and closed-loop neuromodulation experiments

It should also be mentioned that artifacts induced by simultaneous tACS are very large, and this has so far been a strong limitation for the study of neural dynamics during stimulation. Indeed, most EEG-tACS studies have been so far conducted analyzing the EEG data collected in the off-stimulation period. To enable closed-loop neuromodulation applications, we developed a novel online tACS artifact removal technique with low computational complexity. This was necessary to enable attenuation of the stimulation artifact in real-time.

Finally, high-density montages are required to perform source localizations using EEG data. Dedicated tools to perform real-time reconstruction of neural activity are currently lacking. We filled this gap by developing a real-time noninvasive electrophysiology toolbox, which -through a dedicated graphical user interface- enables online artifact removal and source localization of hdEEG data.

5.1.1 Real-time biological artifact removal

We have introduced BSS-REG, a novel method for the online artifact removal for hdEEG systems. We adapted the offline processing tools for hdEEG (bad channel correction, artifact removal, data re-referencing) (Liu et al. 2017) and re-implemented them for real-time applications, in form of spatial filters (Guarnieri et al. 2018). Importantly, our method requires the use of a calibration recording for the initialization of the spatial filter. The latter has been exploited in order to have minimum computational cost and be appropriate for real-time processing. Thanks to its low computational requirements, BSS-REG can be effectively applied to low-density as well as hdEEG data in real-time applications. As a general approach, we used simulated data to test the method under controlled condition (with known ground truth), and hdEEG datasets collected during oddball tasks in healthy volunteers to confirm the findings from the simulation. We generated simulated data by defining brain sources, back projecting them to the sensors and adding different types of artifact and noise. The performance of the real-time artifact removal method has been assessed against alternative online (Haykin 1996; P. He et al. 2004; Puthusserypady and Ratnarajah 2005) and offline methods (Jung, Makeig, Humphries, et al. 2000). Our technique outperformed alternative methods in terms of artifact removal accuracy and computational efficiency. Furthermore, it could remove different kinds of artifacts with accuracy comparable to the one achieved by an offline ICA approach while preserving true neural activity. We therefore argue that BSS-REG may enable the development of novel BCI applications requiring high-density recordings, such as source-based neurofeedback and closed-loop neuromodulation.

5.1.2 Real-time stimulation artifact removal

When combined with tACS, the novel system AC-REG can be used in noninvasive closed-loop neuromodulation experiments. Importantly, the attenuation of tACS artifacts in an online manner is ideal not only for low-density but also for high-density EEG recordings, thanks to AC-REG's quick computation times. We validated our method using both simulated and real EEG signals. We generated simulated data containing a mix of neural signals and tACS artifact. Simulated data were used to define the main parameters and to assess the method efficacy under controlled conditions. Notably, we analyzed the variation of the performance and the computational time with different channel counts, sampling frequencies and data buffer sizes. In addition, the latter is a meaningful component in determining the quality of tACS artifact reconstruction. Importantly, the computation time showed a super-linear relationship with channels number. On the other hand, it increased with both sampling frequency and buffer size in a sub-linear manner. Then, simulated data have been employed also for comparison with alternative online (Kohli and Casson 2019) and offline methods (Helfrich, Schneider, et al. 2014), together with real signals acquired during resting-state in healthy participants. Interestingly, we found that the performance of all the techniques substantially depended on the tACS

frequency. Moreover, AC-REG outperforms other methods in terms of artifact removal accuracy and computational time, while preserving true neural activity. Finally, we argue that AC-REG may enable further development of closed-loop neuromodulation techniques, with potential applications both in healthy individuals and in neurological patients.

5.1.3 Real-time source localization

Given the need of performing real-time analysis of hdEEG data for estimating neural activity in the brain, we developed a real-time noninvasive electrophysiology toolbox, RT-NET. We assessed the effectiveness and validity of RT-NET on real hdEEG data collected during hand movements in healthy volunteers (Weiss et al. 2013). Specifically, we compared the neural activity reconstructed online with that estimated by our offline analysis workflow (Liu et al. 2017). Importantly, there were no evident artifacts in the EEG data, after these were processed using the spatial filter of RT-NET. Overall, our analysis showed that RT-NET can estimate real-time neural activity with performance comparable to offline methods (Liu et al. 2017). Importantly, we created a GUI for allowing real-time visualization of sensor and source data in 2D and 3D. EEG systems likewise play an important role in BCI applications, allowing data collection in a vast range of environments. The GUI will make RT-NET accessible to a wide community of researchers who are not familiar with complex analysis workflows and software.

5.2 Clinical impact

Just a few decades ago, it was widely assumed that the brain remained relatively unchanged after childhood. And it was presumed that if parts of the brain were destroyed, the functions governed by those areas would be lost forever (Pickersgill et al. 2015). The fact that people with stroke or brain damage recover spontaneously from injury, for example, contradicts this theory. Every part of the brain is continually evolving and adapting in reaction to what we think, see, and do. If the brain is asked to do so, it may form new neuronal connections at any time during its existence (Kolb and Gibb 2011). Since the brain controls emotional health, psychological health, and all of the body's systems, teaching it to work better can have substantial effects at the behavioral level. There are several potential uses of these technologies, both in the context of rehabilitation and of performance enhancement. We may use source-based neurofeedback to teach individuals with ADHD and autism how to relax and focus by modulating prefrontal cortex activity, and in stroke patients to enhance attention output by rebalancing activity in the left and right parietal cortex as an illustration of rehabilitation application. In the context of performance enhancement, source-based neurofeedback can be very important for high-level sportsmen, and in particular for professional football players and Olympic athletes. In this case, neurofeedback offers the possibility of a targeted training of motor, perceptual and cognitive functions that are crucial for sport performance, which can be very hardly achieved by physical training only. Closed-loop neuromodulation, on the other hand, attempts to treat disease by electrically stimulating the peripheral nervous system in response to physiological changes. There is considerable experimental

(Herrmann et al. 2013; Marshall et al. 2011) and computational (Ali et al. 2013; Merlet et al. 2013) evidence that tACS can effectively entrain brain oscillations. It has been successfully used to modulate vision (Vossen et al. 2015), movement, (Feurra et al. 2011) and audition (Riecke et al. 2015). Moreover, fMRI showed that tACS can induce short-term neuroplastic effects over relatively specific cortical regions. Notably, closed-loop neuromodulation is used for a variety of clinical purposes, including pharmaco-resistant epilepsy, movement disorders, and possibly psychiatric disorders including depression and drug addiction. The enhancement of sleep quality and performance is one of the most significant applications of tACS combined in a closed-loop experiment.

5.3 Future directions

The novel techniques presented in this PhD thesis may allow the use of source-based neurofeedback and closed-loop neuromodulation using hdEEG. In this section, we will suggest potential research avenues.

5.3.1 Source-based neurofeedback

In future studies, it will be important to show that source-based neurofeedback based on brain activity reconstructed in real-time from hdEEG data can ensure a superior effectiveness as compared to the classical sensor-based neurofeedback. Extensive testing should be first performed in healthy volunteers who will be asked to perform neuromodulation training sessions. Indeed, a first goal would be to demonstrate that healthy individuals can learn to increase specific components of brain oscillations, and that such increased activity may facilitate sensory, motor and/or cognitive performance. This proof-of-concept study is expected to open the way to further source-based neurofeedback experiments aimed at restoring a normal functioning in the brain of neurological and psychiatric patients, or at optimizing functioning of the healthy brain. In the future, it will also be interesting to develop and incorporate connectivity measures that can work on short time windows, as to enable connectivity-based neurofeedback. Importantly, a real-time estimator based on high-density EEG can be used to train subjects to actively increase or decrease connectivity activity between selected cortical regions. We believe that connectivity-based neurofeedback based on high-density EEG may strongly contribute to the advancement of the current brain rehabilitation technology, as it will be easily applicable for the training of patients showing deficits in brain connectivity.

5.3.2 Closed-loop neuromodulation

In Chapter 3 we introduced a novel approach for tACS artifact removal in real-time. We validated our technique by using both simulated and real EEG data. To ensure the generalizability of our results, it would be important to extend the validation of our novel approach on real EEG data collected with several experimental protocols and by using different stimulation frequencies.

Furthermore, it would be interesting to test the effectiveness and validity of our tACS artifact removal approach not only in open-loop brain stimulation experiments, but also closed-loop ones. In this case, EEG data will have to be necessarily processed in real-time for the attenuation of the tACS artifact, such that the readout of EEG activity can be effectively used to adjust phase and/or intensity of the stimulation (Bergmann et al. 2016). Notably, closed-loop systems are expected to increase the precision and effectiveness of non-invasive brain stimulation for neuroscientific research and to boost its potential for the treatment of brain disorders.

References

- Adaikkan, C., & Tsai, L.-H. (2020). Gamma Entrainment: Impact on Neurocircuits, Glia, and Therapeutic Opportunities. *Trends in Neurosciences*, 43(1), 24–41. <https://doi.org/10.1016/j.tins.2019.11.001>
- Adde, G., Clerc, M., Faugeras, O., Keriven, R., Kybic, J., & Papadopoulos, T. (2003). Symmetric BEM Formulation for the M/EEG Forward Problem. In *Taylor C., Noble J.A. (eds) Information Processing in Medical Imaging. IPMI 2003. Lecture Notes in Computer Science, vol 2732. Springer, Berlin, Heidelberg*. https://doi.org/10.1007/978-3-540-45087-0_44
- Akalin Acar, Z., & Makeig, S. (2013). Effects of forward model errors on EEG source localization. *Brain Topography*, 26(3), 378–96. <https://doi.org/10.1007/s10548-012-0274-6>
- Al-Ezzi, A., Kamel, N., Faye, I., & Gunaseli, E. (2020). Review of EEG, ERP, and Brain Connectivity Estimators as Predictive Biomarkers of Social Anxiety Disorder. *Frontiers in psychology*, 11, 730. <https://doi.org/10.3389/fpsyg.2020.00730>
- Alekseichuk, I., Falchier, A. Y., Linn, G., Xu, T., Milham, M. P., Schroeder, C. E., & Opitz, A. (2019). Electric field dynamics in the brain during multi-electrode transcranial electric stimulation. *Nature communications*, 10(1), 2573. <https://doi.org/10.1038/s41467-019-10581-7>
- Alexander, M. L., Alagapan, S., Lugo, C. E., Mellin, J. M., Lustenberger, C., Rubinow, D. R., & Fröhlich, F. (2019). Double-blind, randomized pilot clinical trial targeting alpha oscillations with transcranial alternating current stimulation (tACS) for the treatment of major depressive disorder (MDD). *Translational Psychiatry*, 9(1), 106. <https://doi.org/10.1038/s41398-019-0439-0>
- Ali, M. M., Sellers, K. K., & Fröhlich, F. (2013). Transcranial Alternating Current Stimulation Modulates Large-Scale Cortical Network Activity by Network Resonance. *The Journal of Neuroscience*, 33(27), 11262–11275. <https://doi.org/10.1523/JNEUROSCI.5867-12.2013>
- Andrade-Talavera, Y., Duque-Feria, P., Paulsen, O., & Rodríguez-Moreno, A. (2016). Presynaptic Spike Timing-Dependent Long-Term Depression in the Mouse Hippocampus. *Cerebral Cortex*, 26(8), 3637–3654. <https://doi.org/10.1093/cercor/bhw172>
- Antal, A., Boros, K., Poreisz, C., Chaieb, L., Terney, D., & Paulus, W. (2008). Comparatively weak after-effects of transcranial alternating current stimulation (tACS) on cortical excitability in humans. *Brain Stimulation: Basic, Translational, and Clinical Research in Neuromodulation*, 1(2), 97–105. <https://doi.org/10.1016/j.brs.2007.10.001>
- Antal, A., & Herrmann, C. S. (2016). Transcranial Alternating Current and Random Noise Stimulation: Possible Mechanisms. *Neural Plasticity*, 2016, 3616807. <https://doi.org/10.1155/2016/3616807>
- Ashburner, J., & Friston, K. J. (2005). Unified segmentation. *NeuroImage*, 26(3), 839–851. <https://doi.org/10.1016/j.neuroimage.2005.02.018>
- Azevedo, F. A. C., Carvalho, L. R. B., Grinberg, L. T., Farfel, J. M., Ferretti, R. E. L., Leite, R. E. P., et al. (2009). Equal numbers of neuronal and nonneuronal cells make the human brain an isometrically scaled-up primate brain. *Journal of Comparative Neurology*, 513(5), 532–541. <https://doi.org/10.1002/cne.21974>

- Bächinger, M., Zerbi, V., Moisa, M., Polania, R., Liu, Q., Mantini, D., et al. (2017). Concurrent tACS-fMRI Reveals Causal Influence of Power Synchronized Neural Activity on Resting State fMRI Connectivity. *The Journal of neuroscience : the official journal of the Society for Neuroscience*, 37(18), 4766–4777. <https://doi.org/10.1523/JNEUROSCI.1756-16.2017>
- Bai, X., & He, B. (2006). Estimation of number of independent brain electric sources from the scalp EEGs. *IEEE Transactions on Biomedical Engineering*, 53(10), 1883–1892. <https://doi.org/10.1109/TBME.2006.876620>
- Baillet, S. (2013). Forward and Inverse Problems of MEG/EEG BT - Encyclopedia of Computational Neuroscience. In D. Jaeger & R. Jung (Eds.), (pp. 1–8). New York, NY: Springer New York. https://doi.org/10.1007/978-1-4614-7320-6_529-1
- Barban, F., Buccelli, S., Mantini, D., Chiappalone, M., & Semprini, M. (2019). Removal of tACS artefact: A simulation study for algorithm comparison. In *9th International IEEE/EMBS Conference on Neural Engineering (NER)* (pp. 393–396). <https://doi.org/10.1109/NER.2019.8717102>
- Bell, A. J., & Sejnowski, T. J. (1995). An Information-Maximization Approach to Blind Separation and Blind Deconvolution. *Neural Computation*, 7(6), 1129–1159. <https://doi.org/10.1162/neco.1995.7.6.1129>
- Bennett, C., Voss, L. J., Barnard, J. P. M., & Sleight, J. W. (2009). Practical Use of the Raw Electroencephalogram Waveform During General Anesthesia: The Art and Science. *Anesthesia & Analgesia*, 109(2). https://journals.lww.com/anesthesia-analgesia/Fulltext/2009/08000/Practical_Use_of_the_Raw_Electroencephalogram.40.aspx
- Beres, A. M. (2017). Time is of the Essence: A Review of Electroencephalography (EEG) and Event-Related Brain Potentials (ERPs) in Language Research. *Applied psychophysiology and biofeedback*, 42(4), 247–255. <https://doi.org/10.1007/s10484-017-9371-3>
- Bergmann, T. O., Karabanov, A., Hartwigsen, G., Thielscher, A., & Siebner, H. R. (2016). Combining non-invasive transcranial brain stimulation with neuroimaging and electrophysiology: Current approaches and future perspectives. *Neuroimage*, 140, 4–19. <https://doi.org/10.1016/j.neuroimage.2016.02.012>
- Besl, P., & McKay, N. (1992). A Method for Registration of 3-D Shapes. *IEEE Transactions on Pattern Analysis and Machine Intelligence*, 14(2), 239–256. <https://doi.org/10.1109/34.121791>
- Bhogeshwar, S. S., Soni, M. K., & Bansal, D. (2014). Design of Simulink Model to denoise ECG signal using various IIR & FIR filters. In *2014 International Conference on Reliability Optimization and Information Technology (ICROIT)* (pp. 477–483). <https://doi.org/10.1109/ICROIT.2014.6798370>
- Bi, G., & Poo, M. (1998). Synaptic Modifications in Cultured Hippocampal Neurons: Dependence on Spike Timing, Synaptic Strength, and Postsynaptic Cell Type. *The Journal of Neuroscience*, 18(24), 10464 LP – 10472. <https://doi.org/10.1523/JNEUROSCI.18-24-10464.1998>
- Blaskovits, F., Tyerman, J., & Luctkar-Flude, M. (2017). Effectiveness of neurofeedback therapy for anxiety and stress in adults living with a chronic illness: a systematic review protocol. *JBI*

Evidence Synthesis, 15(7).

https://journals.lww.com/jbisrir/Fulltext/2017/07000/Effectiveness_of_neurofeedback_therapy_for_anxiety.2.aspx

- Boe, S., Gionfriddo, A., Kraeutner, S., Tremblay, A., Little, G., & Bardouille, T. (2014). Laterality of brain activity during motor imagery is modulated by the provision of source level neurofeedback. *Neuroimage*, 101, 159–167. <https://doi.org/10.1016/j.neuroimage.2014.06.066>
- Brett, M., Johnsrude, I. S., & Owen, A. M. (2002). The problem of functional localization in the human brain. *Nature Reviews Neuroscience*, 3, 243–249. <https://doi.org/10.1038/nrn756>
- Brittain, J. S., Probert-Smith, P., Aziz, T. Z., & Brown, P. (2013). Tremor suppression by rhythmic transcranial current stimulation. *Current Biology*, 23, 436–440. <https://doi.org/10.1016/j.cub.2013.01.068>
- Brodbeck, V., Spinelli, L., Lascano, A. M., Wissmeier, M., Vargas, M. I., Vulliemoz, S., et al. (2011). Electroencephalographic source imaging: A prospective study of 152 operated epileptic patients. *Brain*, 134(10), 2887–2897. <https://doi.org/10.1093/brain/awr243>
- Bronzino, J. (1999). Principles of Electroencephalography. In *The Biomedical Engineering Handbook* (pp. 201–212). <https://doi.org/10.1201/9781420049510.ch15>
- Brown, R. E., Basheer, R., McKenna, J. T., Strecker, R. E., & McCarley, R. W. (2012). Control of sleep and wakefulness. *Physiological reviews*, 92(3), 1087–1187. <https://doi.org/10.1152/physrev.00032.2011>
- Brzosko, Z., Mierau, S. B., & Paulsen, O. (2019). Neuromodulation of Spike-Timing-Dependent Plasticity: Past, Present, and Future. *Neuron*, 103(4), 563–581. <https://doi.org/10.1016/j.neuron.2019.05.041>
- Cabral-Calderin, Y., Williams, K. A., Opitz, A., Dechent, P., & Wilke, M. (2016). Transcranial alternating current stimulation modulates spontaneous low frequency fluctuations as measured with fMRI. *NeuroImage*, 141, 88–107. <https://doi.org/10.1016/j.neuroimage.2016.07.005>
- Cacioppo, J., Tassinary, L., & Berntson, G. (2016). *Handbook of Psychophysiology*. (J. Cacioppo, L. Tassinary, & G. Berntson, Eds.). Cambridge University Press. <https://doi.org/10.1017/9781107415782>
- Capogrosso, M., Milekovic, T., Borton, D., Wagner, F., Moraud, E. M., Mignardot, J.-B., et al. (2016). A brain–spine interface alleviating gait deficits after spinal cord injury in primates. *Nature*, 539, 284. <https://doi.org/10.1038/nature20118><https://www.nature.com/articles/nature20118#supplementary-information>
- Capon, D., D’Ostilio, K., Garraux, G., Rothwell, J., & Bisiacchi, P. (2016). Effects of 10 Hz and 20 Hz Transcranial Alternating Current Stimulation on Automatic Motor Control. *Brain Stimulation: Basic, Translational, and Clinical Research in Neuromodulation*, 9(4), 518–524. <https://doi.org/10.1016/j.brs.2016.01.001>

- Cardoso, J. (1999). High-Order Contrasts for Independent Component Analysis. *Neural Computation*, 11(1), 157–192. <https://doi.org/10.1162/089976699300016863>
- Choi, S., Cichocki, A., & Park, H. M. (2005). Blind source separation and independent component analysis: A review. *Neural Information Processing - Letters and Reviews*, 6, 1–57.
- Clayton, M. S., Yeung, N., & Cohen Kadosh, R. (2018). The Effects of 10 Hz Transcranial Alternating Current Stimulation on Audiovisual Task Switching. *Frontiers in Neuroscience*, 12, 67. <https://www.frontiersin.org/article/10.3389/fnins.2018.00067>
- Clerc, M., Gramfort, A., Olivi, E., & Papadopoulo, T. (2010). The symmetric BEM: Bringing in more variables for better accuracy. In *Supek S., Sušac A. (eds) 17th International Conference on Biomagnetism Advances in Biomagnetism – Biomag2010. IFMBE Proceedings, vol 28. Springer, Berlin, Heidelberg*. https://doi.org/10.1007/978-3-642-12197-5_21
- Correa, M. A. G. (2011). Noise Removal from EEG Signals in Polisomnographic Records Applying Adaptive Filters in Cascade. In E. L. E.-L. Garcia (Ed.), (p. Ch. 8). Rijeka: IntechOpen. <https://doi.org/10.5772/17219>
- Croft, R. J., & Barry, R. J. (1998). EOG correction: a new aligned-artifact average solution. *Electroencephalogr Clin Neurophysiol*, 107(6), 395–401.
- Croft, R. J., & Barry, R. J. (2000). Removal of ocular artifact from the EEG: a review. *Neurophysiologie Clinique/Clinical Neurophysiology*, 30(1), 5–19. [https://doi.org/https://doi.org/10.1016/S0987-7053\(00\)00055-1](https://doi.org/https://doi.org/10.1016/S0987-7053(00)00055-1)
- Cuartas Morales, E., Acosta-Medina, C. D., Castellanos-Dominguez, G., & Mantini, D. (2019). A Finite-Difference Solution for the EEG Forward Problem in Inhomogeneous Anisotropic Media. *Brain Topography*, 32(2), 229–239. <https://doi.org/10.1007/s10548-018-0683-2>
- Daly, I., Scherer, R., Billinger, M., & Müller-Putz, G. (2015). FORCe: Fully online and automated artifact removal for brain-computer interfacing. *IEEE Transactions on Neural Systems and Rehabilitation Engineering*, 23(5), 725–736. <https://doi.org/10.1109/TNSRE.2014.2346621>
- Datta, A., Elwassif, M., Battaglia, F., & Bikson, M. (2008). Transcranial current stimulation focality using disc and ring electrode configurations: FEM analysis. *Journal of Neural Engineering*, 5(2), 163–174. <https://doi.org/10.1088/1741-2560/5/2/007>
- De Pasquale, F., Della Penna, S., Snyder, A. Z., Lewis, C., Mantini, D., Marzetti, L., et al. (2010). Temporal dynamics of spontaneous MEG activity in brain networks. *Proceedings of the National Academy of Sciences*, 107(13), 6040 LP – 6045. <https://doi.org/10.1073/pnas.0913863107>
- De Vos, M., Ries, S., Vanderperren, K., Vanrumste, B., Alario, F. X., Van Huffel, S., & Burle, B. (2010). Removal of muscle artifacts from EEG recordings of spoken language production. *Neuroinformatics*, 8(2), 135–150. <https://doi.org/10.1007/s12021-010-9071-0>
- Debaere, F., Wenderoth, N., Sunaert, S., Van Hecke, P., & Swinnen, S. P. (2003). Internal vs external generation of movements: Differential neural pathways involved in bimanual coordination performed in the presence or absence of augmented visual feedback. *NeuroImage*, 19(3), 764–

776. [https://doi.org/10.1016/S1053-8119\(03\)00148-4](https://doi.org/10.1016/S1053-8119(03)00148-4)

- Debaere, F., Wenderoth, N., Sunaert, S., Van Hecke, P., & Swinnen, S. P. (2004). Changes in brain activation during the acquisition of a new bimanual coordination task. *Neuropsychologia*, *42*(7), 855–867. <https://doi.org/10.1016/j.neuropsychologia.2003.12.010>
- Delorme, A, Palmer, J., Onton, J., Oostenveld, R., & Makeig, S. (2012). Independent EEG sources are dipolar. *PLoS One*, *7*(2), e30135. <https://doi.org/10.1371/journal.pone.0030135>
- Delorme, Arnaud, & Makeig, S. (2004). EEGLAB: An open source toolbox for analysis of single-trial EEG dynamics including independent component analysis. *Journal of Neuroscience Methods*, *134*(1), 9–21. <https://doi.org/10.1016/j.jneumeth.2003.10.009>
- Dinh, C., Esch, L., Rühle, J., Bollmann, S., Güllmar, D., Baumgarten, D., et al. (2017). Real-Time Clustered Multiple Signal Classification (RTC-MUSIC). *Brain Topography*, *31*(1), 125–128. <https://doi.org/10.1007/s10548-017-0586-7>
- Dinh, C., Strohmeier, D., Luessi, M., Güllmar, D., Baumgarten, D., Haueisen, J., & Hämäläinen, M. S. (2015). Real-Time MEG Source Localization Using Regional Clustering. *Brain Topography*, *28*(6), 771–784. <https://doi.org/10.1007/s10548-015-0431-9>
- Dowsett, J, Herrmann, C., & Taylor, P. (2019). Modulation of SSVEPs using frequency matched tACS. *Brain Stimulation: Basic, Translational, and Clinical Research in Neuromodulation*, *12*(2), 418. <https://doi.org/10.1016/j.brs.2018.12.354>
- Dowsett, James, & Herrmann, C. S. (2016). Transcranial Alternating Current Stimulation with Sawtooth Waves: Simultaneous Stimulation and EEG Recording. *Frontiers in human neuroscience*, *10*, 135. <https://doi.org/10.3389/fnhum.2016.00135>
- Eldeen, A., Seddik, A., & Allah, A. (2017). *A Hybrid Approach for Artifacts Removal from EEG Recordings. International Journal of Computer Applications* (Vol. 168). <https://doi.org/10.5120/ijca2017914301>
- Enriquez-Geppert, S., Smit, D., Pimenta, M. G., & Arns, M. (2019). Neurofeedback as a Treatment Intervention in ADHD: Current Evidence and Practice. *Current psychiatry reports*, *21*(6), 46. <https://doi.org/10.1007/s11920-019-1021-4>
- Ezzyat, Y., Wanda, P. A., Levy, D. F., Kadel, A., Aka, A., Pedisich, I., et al. (2018). Closed-loop stimulation of temporal cortex rescues functional networks and improves memory. *Nature Communications*, *9*(1), 365. <https://doi.org/10.1038/s41467-017-02753-0>
- Faria, P., Leal, A., & Miranda, P. C. (2009). Comparing different electrode configurations using the 10-10 international system in tDCS: A finite element model analysis. In *2009 Annual International Conference of the IEEE Engineering in Medicine and Biology Society* (pp. 1596–1599). <https://doi.org/10.1109/IEMBS.2009.5334121>
- Fatourehchi, M., Bashashati, A., Ward, R. K., & Birch, G. E. (2007). EMG and EOG artifacts in brain computer interface systems: A survey. *Clin Neurophysiol*, *118*(3), 480–494. <https://doi.org/10.1016/j.clinph.2006.10.019>

- Fauth, M., & Tetzlaff, C. (2016). Opposing Effects of Neuronal Activity on Structural Plasticity. *Frontiers in Neuroanatomy*. <https://www.frontiersin.org/article/10.3389/fnana.2016.00075>
- Fellhauer, I., Zöllner, F. G., Schröder, J., Degen, C., Kong, L., Essig, M., et al. (2015). Comparison of automated brain segmentation using a brain phantom and patients with early Alzheimer's dementia or mild cognitive impairment. *Psychiatry Research - Neuroimaging*, *233*(3), 299–305. <https://doi.org/10.1016/j.psychresns.2015.07.011>
- Feurra, M., Bianco, G., Santarnecchi, E., del Testa, M., Rossi, A., & Rossi, S. (2011). Frequency-dependent tuning of the human motor system induced by transcranial oscillatory potentials. *Journal of Neuroscience*, *31*(34), 12165–70. <https://doi.org/10.1523/JNEUROSCI.0978-11.2011>
- Fischl, B. (2012). FreeSurfer. *NeuroImage*, *62*(2), 774–781. <https://doi.org/https://doi.org/10.1016/j.neuroimage.2012.01.021>
- Flanigan, M. J., Morehouse, R. L., & Shapiro, C. M. (1995). Determination of observer-rated alpha activity during sleep. *Sleep*, *18*(8), 702–706. <http://europepmc.org/abstract/MED/8560138>
- Florin, E., Bock, E., & Baillet, S. (2014). Targeted reinforcement of neural oscillatory activity with real-time neuroimaging feedback. *NeuroImage*. <https://doi.org/10.1016/j.neuroimage.2013.10.028>
- Fox, M. D., & Raichle, M. E. (2007). Spontaneous fluctuations in brain activity observed with functional magnetic resonance imaging. *Nature Reviews Neuroscience*, *8*(9), 700–711. <https://doi.org/10.1038/nrn2201>
- Fröhlich, F., Sellers, K. K., & Cordle, A. L. (2015). Targeting the neurophysiology of cognitive systems with transcranial alternating current stimulation (tACS). *Expert Rev Neurother*, *15*(2), 145–167. <https://doi.org/10.1586/14737175.2015.992782>
- Fuchs, M., Kastner, J., Wagner, M., Hawes, S., & Ebersole, J. S. (2002). A standardized boundary element method volume conductor model. *Clinical Neurophysiology*, *113*(5), 702–712. [https://doi.org/10.1016/S1388-2457\(02\)00030-5](https://doi.org/10.1016/S1388-2457(02)00030-5)
- Gaho, A. A., Musavi, S. H. A., Jatoi, M. A., & Shafiq, M. (2018). EEG Signals based Brain Source Localization Approaches. *International Journal of Advanced Computer Science and Applications(ijacs)*, *9*(9), 253–261. <https://doi.org/10.14569/IJACSA.2018.090934>
- Ganzetti, M., & Mantini, D. (2013). Functional connectivity and oscillatory neuronal activity in the resting human brain. *Neuroscience*, *240*, 297–309. <https://doi.org/10.1016/j.neuroscience.2013.02.032>
- Gao, J., Yang, Y., Sun, J., & Yu, G. (2010). Automatic removal of various artifacts from EEG signals using combined methods. *J Clin Neurophysiol*, *27*(5), 312–320. <https://doi.org/10.1097/WNP.0b013e3181f534f4>
- Gao, J., Zheng, C., & Wang, P. (2010). Online Removal of Muscle Artifact from Electroencephalogram Signals Based on Canonical Correlation Analysis. *Clinical EEG and Neuroscience*, *41*(1), 53–59. <https://doi.org/10.1177/155005941004100111>
- Gevensleben, H., Albrecht, B., Lütcke, H., Auer, T., Dewiputri, W. I., Schweizer, R., et al. (2014).

Neurofeedback of slow cortical potentials: neural mechanisms and feasibility of a placebo-controlled design in healthy adults. *Frontiers in human neuroscience*, 8, 990.

<https://doi.org/10.3389/fnhum.2014.00990>

Giroladini, W., Pederzoli, L., Bilucaglia, M., Melloni, S., & Tressoldi, P. (2016). A new method to detect event-related potentials based on Pearson's correlation. *EURASIP journal on bioinformatics & systems biology*, 2016(1), 11. <https://doi.org/10.1186/s13637-016-0043-z>

Golub, G., & Kahan, W. (1965). Calculating the Singular Values and Pseudo-Inverse of a Matrix. *Journal of the Society for Industrial and Applied Mathematics Series B Numerical Analysis*, 2, 205–24.

<https://doi.org/10.1137/0702016>

Gomez-Herrero, G., Clercq, W. D., Anwar, H., Kara, O., Egiazarian, K., Huffel, S. V., & Paesschen, W. V. (2006). Automatic Removal of Ocular Artifacts in the EEG without an EOG Reference Channel. In *Proceedings of the 7th Nordic Signal Processing Symposium - NORSIG 2006* (pp. 130–133).

<https://doi.org/10.1109/NORSIG.2006.275210>

Gorgolewski, K. J., Storkey, A. J., Bastin, M. E., Whittle, I., & Pernet, C. (2013). Single subject fMRI test-retest reliability metrics and confounding factors. *NeuroImage*, 69, 231–243.

<https://doi.org/10.1016/j.neuroimage.2012.10.085>

Gramfort, A., Luessi, M., Larson, E., Engemann, D. A., Strohmeier, D., Brodbeck, C., et al. (2014). MNE software for processing MEG and EEG data. *NeuroImage*, 86, 446–460.

<https://doi.org/10.1016/j.neuroimage.2013.10.027>

Gramfort, A., Papadopoulos, T., Olivi, E., & Clerc, M. (2010). OpenMEEG: Opensource software for quasistatic bioelectromagnetics. *BioMedical Engineering Online*, 9, 45.

<https://doi.org/10.1186/1475-925X-9-45>

Gramfort, A., Papadopoulos, T., Olivi, E., & Clerc, M. (2011). Forward field computation with OpenMEEG. *Computational Intelligence and Neuroscience*, 2011:13. <https://doi.org/10.1155/2011/923703>

Grodd, W., Hülsmann, E., Lotze, M., Wildgruber, D., & Erb, M. (2001). Sensorimotor mapping of the human cerebellum: fMRI evidence of somatotopic organization. *Human Brain Mapping*, 13(2), 55–73. <https://doi.org/10.1002/hbm.1025>

Grossman, N., Bono, D., Dedic, N., Kodandaramaiah, S. B., Rudenko, A., Suk, H.-J., et al. (2017).

Noninvasive Deep Brain Stimulation via Temporally Interfering Electric Fields. *Cell*, 169(6), 1029–1041.e16. <https://doi.org/10.1016/j.cell.2017.05.024>

Guarnieri, R., Brancucci, A., D'Anselmo, A., Manippa, V., Swinnen, S. P., Tecchio, F., & Mantini, D. (2020).

A computationally efficient method for the attenuation of alternating current stimulation artifacts in electroencephalographic recordings. *Journal of Neural Engineering*, 17, 046038.

Guarnieri, R., Marino, M., Barban, F., Ganzetti, M., & Mantini, D. (2018). Online EEG artifact removal for BCI applications by adaptive spatial filtering. *Journal of Neural Engineering*, 15(5), 056009.

<https://doi.org/10.1088/1741-2552/aacfd>

Guarnieri, R., Zhao, M., Taberna, G. A., Ganzetti, M., Swinnen, S. P., & Mantini, D. (2020). RT-NET: real-

time reconstruction of neural activity using high-density electroencephalography.

Neuroinformatics. <https://doi.org/10.1007/s12021-020-09479-3>

Guggenmos, D. J., Azin, M., Barbay, S., Mahnken, J. D., Dunham, C., Mohseni, P., & Nudo, R. J. (2013).

Restoration of function after brain damage using a neural prosthesis. *Proceedings of the National Academy of Sciences of the United States of America*, *110*(52), 21177–21182.

<https://doi.org/10.1073/pnas.1316885110>

Guo, C., Ferreira, D., Fink, K., Westman, E., & Granberg, T. (2019). Repeatability and reproducibility of FreeSurfer, FSL-SIENAX and SPM brain volumetric measurements and the effect of lesion filling in multiple sclerosis. *European Radiology*, *29*, 1355–1364. <https://doi.org/10.1007/s00330-018-5710-x>

Halder, S., Bensch, M., Mellinger, J., Bogdan, M., Kübler, A., Birbaumer, N., & Rosenstiel, W. (2007).

Online Artifact Removal for Brain-Computer Interfaces Using Support Vector Machines and Blind Source Separation. *Computational Intelligence and Neuroscience*, *2007*, 82069.

<https://doi.org/10.1155/2007/82069>

Hallez, H., Vanrumste, B., Grech, R., Muscat, J., De Clercq, W., Vergult, A., et al. (2007). Review on solving the forward problem in EEG source analysis. *Journal of NeuroEngineering and Rehabilitation*, *4*(1), 46. <https://doi.org/10.1186/1743-0003-4-46>

Hämäläinen, M. S., & Ilmoniemi, R. J. (1994). Interpreting magnetic fields of the brain: minimum norm estimates. *Medical & Biological Engineering & Computing*, *32*(1), 35–42.

<https://doi.org/10.1007/BF02512476>

Hammer, B. U., Colbert, A. P., Brown, K. A., & Ilioi, E. C. (2011). Neurofeedback for Insomnia: A Pilot Study of Z-Score SMR and Individualized Protocols. *Applied Psychophysiology and Biofeedback*, *36*(4), 251–264. <https://doi.org/10.1007/s10484-011-9165-y>

Harvey, V. L., & Dickenson, A. H. (2010). EPSPs and IPSPs. In I. P. Stolerman (Ed.), *Encyclopedia of Psychopharmacology* (p. 489). Berlin, Heidelberg: Springer Berlin Heidelberg.

https://doi.org/10.1007/978-3-540-68706-1_618

Hauelsen, J., Ramon, C., Eiselt, M., Brauer, H., & Nowak, H. (1997). Influence of tissue resistivities on neuromagnetic fields and electric potentials studied with a finite element model of the head. *IEEE Transactions on Biomedical Engineering*, *44*(8), 727–735. <https://doi.org/10.1109/10.605429>

Haumann, N. T., Parkkonen, L., Kliuchko, M., Vuust, P., & Brattico, E. (2016). Comparing the Performance of Popular MEG/EEG Artifact Correction Methods in an Evoked-Response Study. *Computational Intelligence and Neuroscience*, *2016*, 10. <https://doi.org/10.1155/2016/7489108>

Haykin, S. (1996). *Adaptive filter theory (3rd ed.)*. Prentice-Hall, Inc.

He, B., Yang, L., Wilke, C., & Yuan, H. (2011). Electrophysiological Imaging of Brain Activity and Connectivity – Challenges and Opportunities. *IEEE transactions on bio-medical engineering*, *58*(7), 1918–1931. <https://doi.org/10.1109/TBME.2011.2139210>

He, P., Wilson, G., & Russell, C. (2004). Removal of ocular artifacts from electro-encephalogram by

adaptive filtering. *Med Biol Eng Comput*, 42(3), 407–412.

<https://www.ncbi.nlm.nih.gov/pubmed/15191087>

- Heise, K.-F., Kortzorg, N., Saturnino, G. B., Fujiyama, H., Cuypers, K., Thielscher, A., & Swinnen, S. P. (2016). Evaluation of a Modified High-Definition Electrode Montage for Transcranial Alternating Current Stimulation (tACS) of Pre-Central Areas. *Brain Stimulation*, 9(5), 700–704. <https://doi.org/https://doi.org/10.1016/j.brs.2016.04.009>
- Helfrich, R. F., Knepper, H., Nolte, G., Strüber, D., Rach, S., Herrmann, C. S., et al. (2014). Selective Modulation of Interhemispheric Functional Connectivity by HD-tACS Shapes Perception. *PLOS Biology*, 12(12), e1002031. <https://doi.org/10.1371/journal.pbio.1002031>
- Helfrich, R. F., Schneider, T. R., Rach, S., Trautmann-Lengsfeld, S. A., Engel, A. K., & Herrmann, C. S. (2014). Entrainment of brain oscillations by transcranial alternating current stimulation. *Current Biology*, 24(3), 333–339. <https://doi.org/10.1016/j.cub.2013.12.041>
- Henson, R. N., Abdulrahman, H., Flandin, G., & Litvak, V. (2019). Multimodal Integration of M/EEG and f/MRI Data in SPM12. *Frontiers in Neuroscience*, 13, 300. <https://www.frontiersin.org/article/10.3389/fnins.2019.00300>
- Herrmann, C. S., Rach, S., Neuling, T., & Strüber, D. (2013). Transcranial alternating current stimulation: A review of the underlying mechanisms and modulation of cognitive processes. *Frontiers in Human Neuroscience*, 7, 279. <https://doi.org/10.3389/fnhum.2013.00279>
- Hlustik, P. (2001). Somatotopy in Human Primary Motor and Somatosensory Hand Representations Revisited. *Cerebral Cortex*, 11(4), 312–321. <https://doi.org/10.1093/cercor/11.4.312>
- Holdefer, R. N., Sadleir, R., & Russell, M. J. (2006). Predicted current densities in the brain during transcranial electrical stimulation. *Clinical Neurophysiology*, 117(6), 1388–1397. <https://doi.org/10.1016/j.clinph.2006.02.020>
- Holmes, G. L., & Khazipov, R. (2007). Basic Neurophysiology and the Cortical Basis of EEG BT - The Clinical Neurophysiology Primer. In A. S. Blum & S. B. Rutkove (Eds.), (pp. 19–33). Totowa, NJ: Humana Press. https://doi.org/10.1007/978-1-59745-271-7_2
- Hopfinger, J. B., Parsons, J., & Fröhlich, F. (2017). Differential effects of 10-Hz and 40-Hz transcranial alternating current stimulation (tACS) on endogenous versus exogenous attention. *Cognitive Neuroscience*, 8(2), 102–111. <https://doi.org/10.1080/17588928.2016.1194261>
- Hotelling, H. (1936). Relations Between Two Sets of Variates. *Biometrika*, 28(3/4), 321–377. <https://doi.org/10.2307/2333955>
- Hsueh, J. J., Chen, T. S., Chen, J. J., & Shaw, F. Z. (2016). Neurofeedback training of EEG alpha rhythm enhances episodic and working memory. *Human Brain Mapping*, 37(7), 2662–2675. <https://doi.org/10.1002/hbm.23201>
- Huster, R. J., Mokom, Z. N., Enriquez-Geppert, S., & Herrmann, C. S. (2014). Brain–computer interfaces for EEG neurofeedback: Peculiarities and solutions. *International Journal of Psychophysiology*, 91(1), 36–45. <https://doi.org/https://doi.org/10.1016/j.ijpsycho.2013.08.011>

- Hyvärinen, A. (1999). Fast and robust fixed-point algorithms for independent component analysis. *IEEE Transactions on Neural Networks*, 10(3), 626–634. <https://doi.org/10.1109/72.761722>
- Hyvärinen, A., Karhunen, J., & Oja, E. (2004). *Independent component analysis* (Vol. 46). John Wiley & Sons.
- Im, C.-H. (2018). Computational EEG analysis : methods and applications. <http://public.ebib.com/choice/publicfullrecord.aspx?p=5494653>
- Iturrate, I., Chavarriaga, R., Montesano, L., Minguetz, J., & Millán, J. del R. (2015). Teaching brain-machine interfaces as an alternative paradigm to neuroprosthetics control. *Scientific Reports*, 5(1), 13893. <https://doi.org/10.1038/srep13893>
- Iturrate, I., Pereira, M., & Millán, J. del R. (2018). Closed-loop electrical neurostimulation: Challenges and opportunities. *Current Opinion in Biomedical Engineering*, 8, 28–37. <https://doi.org/10.1016/j.cobme.2018.09.007>
- Jatoui, M. A., & Kamel, N. (2017). *Brain source localization using EEG signal analysis*. Boca Raton: CRC Press. <https://doi.org/https://doi.org/10.1201/9781315156415>
- Jatoui, M. A., Kamel, N., Malik, A. S., & Faye, I. (2014). EEG based brain source localization comparison of sLORETA and eLORETA. *Australasian Physical and Engineering Sciences in Medicine*, 37(4), 713–721. <https://doi.org/10.1007/s13246-014-0308-3>
- Jervis, B. W., Ifeachor, E. C., & Allen, E. M. (1988). The removal of ocular artefacts from the electroencephalogram: a review. *Med Biol Eng Comput*, 26(1), 2–12. <https://www.ncbi.nlm.nih.gov/pubmed/3059085>
- Jung, T. P., Makeig, S., Humphries, C., Lee, T. W., McKeown, M. J., Iragui, V., & Sejnowski, T. J. (2000). Removing electroencephalographic artifacts by blind source separation. *Psychophysiology*, 37(2), 163–178.
- Jung, T. P., Makeig, S., Westerfield, M., Townsend, J., Courchesne, E., & Sejnowski, T. J. (2000). Removal of eye activity artifacts from visual event-related potentials in normal and clinical subjects. *Clin Neurophysiol*, 111(10), 1745–1758.
- Kanoga, S. (2017). Review of Artifact Rejection Methods for Electroencephalographic Systems. In Y. M. E.-P. Sittiprapaporn (Ed.), (p. Ch. 6). Rijeka: IntechOpen. <https://doi.org/10.5772/68023>
- Kasten, F. H., & Herrmann, C. S. (2017). Transcranial Alternating Current Stimulation (tACS) Enhances Mental Rotation Performance during and after Stimulation. *Frontiers in human neuroscience*, 11, 2. <https://doi.org/10.3389/fnhum.2017.00002>
- Kayser, J., & Tenke, C. E. (2010). In search of the Rosetta Stone for scalp EEG: Converging on reference-free techniques. *Clinical Neurophysiology*, 121(12), 1973–1975. <https://doi.org/https://doi.org/10.1016/j.clinph.2010.04.030>
- Keifer Jr, O. P., Riley, J. P., & Boulis, N. M. (2014). Deep brain stimulation for chronic pain: intracranial targets, clinical outcomes, and trial design considerations. *Neurosurgery clinics of North America*, 25(4), 671–692. <https://doi.org/10.1016/j.nec.2014.07.009>

- Kim, M., & Kim, S. (2018). A comparison of artifact rejection methods for a BCI using event related potentials. In *2018 6th International Conference on Brain-Computer Interface (BCI)* (pp. 1–4). <https://doi.org/10.1109/IWW-BCI.2018.8311530>
- Kirschstein, T., & Köhling, R. (2009). What is the Source of the EEG? *Clinical EEG and Neuroscience*, *40*(3), 146–149. <https://doi.org/10.1177/155005940904000305>
- Klados, M. A., Bratsas, C., Frantzidis, C., Papadelis, C. L., & Bamidis, P. D. (2010). A Kurtosis-Based Automatic System Using Naïve Bayesian Classifier to Identify ICA Components Contaminated by EOG or ECG Artifacts. In P. D. Bamidis & N. Pallikarakis (Eds.), *XII Mediterranean Conference on Medical and Biological Engineering and Computing 2010: May 27 – 30, 2010 Chalkidiki, Greece* (pp. 49–52). Berlin, Heidelberg: Springer Berlin Heidelberg. https://doi.org/10.1007/978-3-642-13039-7_13
- Klados, M. A., Papadelis, C., Braun, C., & Bamidis, P. D. (2011). REG-ICA: A hybrid methodology combining Blind Source Separation and regression techniques for the rejection of ocular artifacts. *Biomedical Signal Processing and Control*, *6*(3), 291–300. <https://doi.org/https://doi.org/10.1016/j.bspc.2011.02.001>
- Klem, G. H., Lüders, H. O., Jasper, H. H., & Elger, C. (1999). The ten-twenty electrode system of the International Federation. The International Federation of Clinical Neurophysiology. *Electroencephalography and clinical neurophysiology. Supplement*, *52*, 3–6. <http://europepmc.org/abstract/MED/10590970>
- Kohli, S., & Casson, A. J. (2015). Removal of Transcranial a.c. Current Stimulation artifact from simultaneous EEG recordings by superposition of moving averages. In *Proceedings of the Annual International Conference of the IEEE Engineering in Medicine and Biology Society, EMBS* (pp. 3436–3439). Milano. <https://doi.org/10.1109/EMBC.2015.7319131>
- Kohli, S., & Casson, A. J. (2019). Removal of Gross Artifacts of Transcranial Alternating Current Stimulation in Simultaneous EEG Monitoring. *Sensors (Basel, Switzerland)*, *19*(1), 190. <https://doi.org/10.3390/s19010190>
- Kohli, S., & Casson, A. J. (2020). Machine learning validation of EEG+tACS artefact removal. *Journal of Neural Engineering*, *17*(1), 16034. <https://doi.org/10.1088/1741-2552/ab58a3>
- Kohli, S., Krachunov, S., & Casson, A. J. (2017). Towards closed-loop transcranial electrical stimulation: a comparison of methods for real time tES-EEG artefact removal using a phantom head model. *Brain Stimulation*, *10*, 467–468. <https://doi.org/10.1016/j.brs.2017.01.370>
- Kolb, B., & Gibb, R. (2011). Brain plasticity and behaviour in the developing brain. *Journal of the Canadian Academy of Child and Adolescent Psychiatry = Journal de l'Academie canadienne de psychiatrie de l'enfant et de l'adolescent*, *20*(4), 265–276. <https://pubmed.ncbi.nlm.nih.gov/22114608>
- Kolb, B., & Whishaw, I. Q. (1998). Brain plasticity and behavior. *Annual Review of Psychology*, *49*(1), 43–64. <https://doi.org/10.1146/annurev.psych.49.1.43>

- Kondraske, G. V. (1986). Neurophysiological measurements. *Biomedical Engineering and Instrumentation*, 138–179.
- Kong, W., Zhou, Z., Hu, S., Zhang, J., Babiloni, F., & Dai, G. (2013). Automatic and direct identification of blink components from scalp EEG. *Sensors (Basel)*, 13(8), 10783–10801.
<https://doi.org/10.3390/s130810783>
- Krause, C. M., Boman, P.-A., Sillanmäki, L., Varho, T., & Holopainen, I. E. (2008). Brain oscillatory EEG event-related desynchronization (ERD) and -synchronization (ERS) responses during an auditory memory task are altered in children with epilepsy. *Seizure*, 17(1), 1–10.
<https://doi.org/https://doi.org/10.1016/j.seizure.2007.05.015>
- Krucoff, M. O., Rahimpour, S., Slutzky, M. W., Edgerton, V. R., & Turner, D. A. (2016). Enhancing Nervous System Recovery through Neurobiologics, Neural Interface Training, and Neurorehabilitation. *Frontiers in Neuroscience*, 10(584). <https://doi.org/10.3389/fnins.2016.00584>
- Lagerlund, T. D., Sharbrough, F. W., & Busacker, N. E. (1997). Spatial filtering of multichannel electroencephalographic recordings through principal component analysis by singular value decomposition. *Journal of Clinical Neurophysiology*. <https://doi.org/10.1097/00004691-199701000-00007>
- Lee, S., McKeown, M. J., Wang, Z. J., & Chen, X. (2019). Removal of High-Voltage Brain Stimulation Artifacts From Simultaneous EEG Recordings. *IEEE Transactions on Biomedical Engineering*, 66(1), 50–60. <https://doi.org/10.1109/TBME.2018.2828808>
- Lee, T.-W., Girolami, M., & Sejnowski, T. J. (1999). Independent Component Analysis Using an Extended Infomax Algorithm for Mixed Subgaussian and Supergaussian Sources. *Neural Computation*, 11(2), 417–441. <https://doi.org/10.1162/089976699300016719>
- Li, Y., Ma, Z., Lu, W., & Li, Y. (2006). Automatic removal of the eye blink artifact from EEG using an ICA-based template matching approach. *Physiological Measurement*, 27(4), 425–436.
<https://doi.org/10.1088/0967-3334/27/4/008>
- Liew, S.-L., Rana, M., Cornelsen, S., Fortunato de Barros Filho, M., Birbaumer, N., Sitaram, R., et al. (2016). Improving Motor Corticothalamic Communication After Stroke Using Real-Time fMRI Connectivity-Based Neurofeedback. *Neurorehabilitation and neural repair*, 30(7), 671–675.
<https://doi.org/10.1177/1545968315619699>
- Lin, F. H., Witzel, T., Ahlfors, S. P., Stufflebeam, S. M., Belliveau, J. W., & Hämäläinen, M. S. (2006). Assessing and improving the spatial accuracy in MEG source localization by depth-weighted minimum-norm estimates. *NeuroImage*, 31(1), 160–171.
<https://doi.org/10.1016/j.neuroimage.2005.11.054>
- Little, S., Pogosyan, A., Neal, S., Zavala, B., Zrinzo, L., Hariz, M., et al. (2013). Adaptive deep brain stimulation in advanced Parkinson disease. *Annals of Neurology*, 74(3), 449–457.
<https://doi.org/10.1002/ana.23951>
- Little, S., Tripoliti, E., Beudel, M., Pogosyan, A., Cagnan, H., Herz, D., et al. (2016). Adaptive deep brain

- stimulation for Parkinson's disease demonstrates reduced speech side effects compared to conventional stimulation in the acute setting. *Journal of Neurology, Neurosurgery & Psychiatry*, 87(12), 1388 LP – 1389. <https://doi.org/10.1136/jnnp-2016-313518>
- Litvak, V., Mattout, J., Kiebel, S., Phillips, C., Henson, R., Kilner, J., et al. (2011). EEG and MEG data analysis in SPM8. *Computational Intelligence and Neuroscience*, 2011, 32. <https://doi.org/10.1155/2011/852961>
- Liu, Q., Balsters, J. H., Baechinger, M., van der Groen, O., Wenderoth, N., & Mantini, D. (2015). Estimating a neutral reference for electroencephalographic recordings: the importance of using a high-density montage and a realistic head model. *Journal of Neural Engineering*, 12(5), 056012. <https://doi.org/10.1088/1741-2560/12/5/056012>
- Liu, Q., Farahibozorg, S., Porcaro, C., Wenderoth, N., & Mantini, D. (2017). Detecting large-scale networks in the human brain using high-density electroencephalography. *Human Brain Mapping*, 38(9), 4631–4643. <https://doi.org/10.1002/hbm.23688>
- Liu, Q., Ganzetti, M., Wenderoth, N., & Mantini, D. (2018). Detecting Large-Scale Brain Networks Using EEG: Impact of Electrode Density, Head Modeling and Source Localization. *Frontiers in Neuroinformatics*, 12, 4. <https://doi.org/10.3389/fninf.2018.00004>
- Lodish, H. F., Berk, A., Zipursky, S., Matsudaira, P., Matsudaira, P., Baltimore, D., & Darnell, J. (2000). *Molecular Cell Biology* (4th editio.). W. H. Freeman and Company. <https://books.google.be/books?id=WYcMqgAACAAJ>
- Lotze, M., Erb, M., Flor, H., Huelsmann, E., Godde, B., & Grodd, W. (2000). fMRI evaluation of somatotopic representation in human primary motor cortex. *NeuroImage*, 11(5), 473–481. <https://doi.org/10.1006/nimg.2000.0556>
- Lv, Y., Margulies, D. S., Villringer, A., & Zang, Y. F. (2013). Effects of Finger Tapping Frequency on Regional Homogeneity of Sensorimotor Cortex. *PLoS ONE*, 8(5), e64115. <https://doi.org/10.1371/journal.pone.0064115>
- Mahajan, R., & Morshed, B. I. (2015). Unsupervised eye blink artifact denoising of EEG data with modified multiscale sample entropy, Kurtosis, and wavelet-ICA. *IEEE J Biomed Health Inform*, 19(1), 158–165. <https://doi.org/10.1109/JBHI.2014.2333010>
- Makeig, S., Bell, A. J., Jung, T. P., & Sejnowski, T. J. (1996). Independent Component Analysis of Electroencephalographic Data. In *Advances in Neural Information Processing Systems 8* (pp. 145–151).
- Mannan, M. M., Jeong, M. Y., & Kamran, M. A. (2016). Hybrid ICA-Regression: Automatic Identification and Removal of Ocular Artifacts from Electroencephalographic Signals. *Front Hum Neurosci*, 10, 193. <https://doi.org/10.3389/fnhum.2016.00193>
- Mansouri, F., Dunlop, K., Giacobbe, P., Downar, J., & Zariffa, J. (2017). A fast EEG forecasting algorithm for phase-locked transcranial electrical stimulation of the human brain. *Frontiers in Neuroscience*, 11, 1–14. <https://doi.org/10.3389/fnins.2017.00401>

- Mantini, D., Corbetta, M., Perrucci, M. G., Romani, G. L., & Del Gratta, C. (2009). Large-scale brain networks account for sustained and transient activity during target detection. *NeuroImage*, *44*(1), 265–274. <https://doi.org/10.1016/j.neuroimage.2008.08.019>
- Mantini, D., Franciotti, R., Romani, G. L., & Pizzella, V. (2008). Improving MEG source localizations: An automated method for complete artifact removal based on independent component analysis. *NeuroImage*, *40*(1), 160–173. <https://doi.org/https://doi.org/10.1016/j.neuroimage.2007.11.022>
- Mantini, D., Perrucci, M. G., Cugini, S., Ferretti, A., Romani, G. L., & Del Gratta, C. (2007). Complete artifact removal for EEG recorded during continuous fMRI using independent component analysis. *NeuroImage*, *34*(2), 598–607. <https://doi.org/10.1016/j.neuroimage.2006.09.037>
- Marino, M., Liu, Q., Del Castello, M., Corsi, C., Wenderoth, N., & Mantini, D. (2018). Heart–Brain Interactions in the MR Environment: Characterization of the Ballistocardiogram in EEG Signals Collected During Simultaneous fMRI. *Brain Topography*. <https://doi.org/10.1007/s10548-018-0631-1>
- Marino, M., Liu, Q., Koudelka, V., Porcaro, C., Hlinka, J., Wenderoth, N., & Mantini, D. (2018). Adaptive optimal basis set for BCG artifact removal in simultaneous EEG-fMRI. *Scientific Reports*, *8*(1), 8902. <https://doi.org/10.1038/s41598-018-27187-6>
- Markram, H., Lübke, J., Frotscher, M., & Sakmann, B. (1997). Regulation of Synaptic Efficacy by Coincidence of Postsynaptic APs and EPSPs. *Science*, *275*(5297), 213 LP – 215. <https://doi.org/10.1126/science.275.5297.213>
- Marrelec, G., & Fransson, P. (2011). Assessing the influence of different ROI Selection Strategies on functional connectivity analyses of fMRI Data acquired during steady-state conditions. *PLoS ONE*, *6*(4), e14788. <https://doi.org/10.1371/journal.pone.0014788>
- Marshall, L., Kirov, R., Brade, J., Mölle, M., & Born, J. (2011). Transcranial electrical currents to probe EEG brain rhythms and memory consolidation during sleep in humans. *PLoS ONE*, *6*(2), e12905. <https://doi.org/10.1371/journal.pone.0016905>
- Marzbani, H., Marateb, H. R., & Mansourian, M. (2016). Neurofeedback: A Comprehensive Review on System Design, Methodology and Clinical Applications. *Basic and clinical neuroscience*, *7*(2), 143–158. <https://doi.org/10.15412/J.BCN.03070208>
- Mateos-Aparicio, P., & Rodríguez-Moreno, A. (2019). The Impact of Studying Brain Plasticity. *Frontiers in Cellular Neuroscience*. <https://www.frontiersin.org/article/10.3389/fncel.2019.00066>
- Merlet, I., Birot, G., Salvador, R., Molaee-Ardekani, B., Mekonnen, A., Soria-Frish, A., et al. (2013). From Oscillatory Transcranial Current Stimulation to Scalp EEG Changes: A Biophysical and Physiological Modeling Study. *PLOS ONE*, *8*(2), e57330. <https://doi.org/10.1371/journal.pone.0057330>
- Michel, C. M., & Brunet, D. (2019). EEG Source Imaging: A Practical Review of the Analysis Steps. *Frontiers in Neurology*. <https://www.frontiersin.org/article/10.3389/fneur.2019.00325>

- Michel, C. M., & Murray, M. M. (2012). Towards the utilization of EEG as a brain imaging tool. *Neuroimage*, *61*(2), 371–385.
<https://doi.org/https://doi.org/10.1016/j.neuroimage.2011.12.039>
- Michel, C. M., Murray, M. M., Lantz, G., Gonzalez, S., Spinelli, L., & Grave De Peralta, R. (2004). EEG source imaging. *Clinical Neurophysiology*, *115*(10), 2195–2222.
<https://doi.org/10.1016/j.clinph.2004.06.001>
- Morales-Quezada, L., Cosmo, C., Carvalho, S., Leite, J., Castillo-Saavedra, L., Rozisky, J. R., & Fregni, F. (2014). Cognitive effects and autonomic responses to transcranial pulsed current stimulation. *Experimental Brain Research*, *233*(3), 701–9. <https://doi.org/10.1007/s00221-014-4147-y>
- Moretti, D. V., Babiloni, F., Carducci, F., Cincotti, F., Remondini, E., Rossini, P. M., et al. (2003). Computerized processing of EEG–EOG–EMG artifacts for multi-centric studies in EEG oscillations and event-related potentials. *International Journal of Psychophysiology*, *47*(3), 199–216.
[https://doi.org/https://doi.org/10.1016/S0167-8760\(02\)00153-8](https://doi.org/https://doi.org/10.1016/S0167-8760(02)00153-8)
- Mosher, J. C., & Leahy, R. M. (1998). Recursive MUSIC: A framework for EEG and MEG source localization. *IEEE Transactions on Biomedical Engineering*, *45*(11), 1342–1354.
<https://doi.org/10.1109/10.725331>
- Mosher, J. C., Lewis, P. S., & Leahy, R. M. (1992). Multiple dipole modeling and localization from spatio-temporal MEG data. *IEEE Transactions on Biomedical Engineering*, *39*(6), 541–557.
<https://doi.org/10.1109/10.141192>
- Mugler, J. P., & Brookeman, J. R. (1991). Rapid three-dimensional T1-weighted MR imaging with the MP-RAGE sequence. *Journal of Magnetic Resonance Imaging*, *1*(5), 561–567.
<https://doi.org/10.1002/jmri.1880010509>
- Mulert, C., Seifert, C., Leicht, G., Kirsch, V., Ertl, M., Karch, S., et al. (2008). Single-trial coupling of EEG and fMRI reveals the involvement of early anterior cingulate cortex activation in effortful decision making. *NeuroImage*, *42*(1), 158–168.
<https://doi.org/https://doi.org/10.1016/j.neuroimage.2008.04.236>
- Mullen, T. R., Kothe, C., Chi, Y. M., Ojeda, A., Kerth, T., Makeig, S., et al. (2013). Real-time modeling and 3D visualization of source dynamics and connectivity using wearable EEG. In *Proceedings of the Annual International Conference of the IEEE Engineering in Medicine and Biology Society, EMBS* (pp. 2184–2187). <https://doi.org/10.1109/EMBC.2013.6609968>
- Müller-Putz, G. R., Scherer, R., Pfurtscheller, G., & Rupp, R. (2005). EEG-based neuroprosthesis control: A step towards clinical practice. *Neuroscience Letters*, *382*(1–2), 169–174.
<https://doi.org/10.1016/j.neulet.2005.03.021>
- Murphy, P. R., O’Connell, R. G., O’Sullivan, M., Robertson, I. H., & Balsters, J. H. (2014). Pupil diameter covaries with BOLD activity in human locus coeruleus. *Human Brain Mapping*, *35*(8), 4140–4154.
<https://doi.org/10.1002/hbm.22466>
- Musall, S., von Pfösl, V., Rauch, A., Logothetis, N. K., & Whittingstall, K. (2012). Effects of Neural

- Synchrony on Surface EEG. *Cerebral Cortex*, 24(4), 1045–1053.
<https://doi.org/10.1093/cercor/bhs389>
- Muthukumaraswamy, S. D. (2013). High-frequency brain activity and muscle artifacts in MEG/EEG: a review and recommendations. *Front Hum Neurosci*, 7, 138.
<https://doi.org/10.3389/fnhum.2013.00138>
- Nandi, D., Aziz, T., Carter, H., & Stein, J. (2003). Thalamic field potentials in chronic central pain treated by periventricular gray stimulation – a series of eight cases. *PAIN*, 101(1).
https://journals.lww.com/pain/Fulltext/2003/01000/Thalamic_field_potentials_in_chronic_central_pain.11.aspx
- Neuling, T., Rach, S., & Herrmann, C. (2013). Orchestrating neuronal networks: sustained after-effects of transcranial alternating current stimulation depend upon brain states. *Frontiers in Human Neuroscience*, 7, 161. <https://doi.org/10.3389/fnhum.2013.00161>
- Niedermeyer, E., & da Silva, F. H. L. (2005). *Electroencephalography: basic principles, clinical applications, and related fields*. Lippincott Williams & Wilkins.
- Niknazar, H., Motie Nasrabadi, A., & Shamsollahi, M. B. (2018). A new similarity index for nonlinear signal analysis based on local extrema patterns. *Physics Letters, Section A: General, Atomic and Solid State Physics*, 382(5), 288–299. <https://doi.org/10.1016/j.physleta.2017.11.022>
- Nitsche, M. A., Doemkes, S., Karaköse, T., Antal, A., Liebetanz, D., Lang, N., et al. (2007). Shaping the Effects of Transcranial Direct Current Stimulation of the Human Motor Cortex. *Journal of Neurophysiology*, 97(4), 3109–3117. <https://doi.org/10.1152/jn.01312.2006>
- Nolan, H., Whelan, R., & Reilly, R. B. (2010). FASTER: Fully Automated Statistical Thresholding for EEG artifact Rejection. *J Neurosci Methods*, 192(1), 152–162.
<https://doi.org/10.1016/j.jneumeth.2010.07.015>
- Noury, N., Hipp, J. F., & Siegel, M. (2016). Physiological processes non-linearly affect electrophysiological recordings during transcranial electric stimulation. *NeuroImage*, 140, 99–109. <https://doi.org/10.1016/j.neuroimage.2016.03.065>
- Noury, N., & Siegel, M. (2017). Phase properties of transcranial electrical stimulation artifacts in electrophysiological recordings. *NeuroImage*, 158, 406–416.
<https://doi.org/10.1016/j.neuroimage.2017.07.010>
- Nunez, P. L., Srinivasan, R., Westdorp, A. F., Wijesinghe, R. S., Tucker, D. M., Silberstein, R. B., & Cadusch, P. J. (1997). EEG coherency: I: statistics, reference electrode, volume conduction, Laplacians, cortical imaging, and interpretation at multiple scales. *Electroencephalography and Clinical Neurophysiology*, 103(5), 499–515. [https://doi.org/https://doi.org/10.1016/S0013-4694\(97\)00066-7](https://doi.org/https://doi.org/10.1016/S0013-4694(97)00066-7)
- O'Connell, R. G., Balsters, J. H., Kilcullen, S. M., Campbell, W., Bokde, A. W., Lai, R., et al. (2012). A simultaneous ERP/fMRI investigation of the P300 aging effect. *Neurobiology of Aging*.
<https://doi.org/10.1016/j.neurobiolaging.2011.12.021>

- Ochs, L. (2013). The Low Energy Neuro Feedback System (LENS): Theory, background, and introduction. *LENS: The Low Energy Neuro Feedback System*, 10(2-3), 5-39.
https://doi.org/10.1300/J184v10n02_02
- Offner, F. F. (1950). The EEG as potential mapping: The value of the average monopolar reference. *Electroencephalography and Clinical Neurophysiology*, 2, 213-4. [https://doi.org/10.1016/0013-4694\(50\)90040-X](https://doi.org/10.1016/0013-4694(50)90040-X)
- Olejniczak, P. (2006). Neurophysiologic Basis of EEG. *Journal of Clinical Neurophysiology*, 23(3).
https://journals.lww.com/clinicalneurophys/Fulltext/2006/06000/Neurophysiologic_Basis_of_EEG.2.aspx
- Oostenveld, R., Fries, P., Maris, E., & Schoffelen, J. M. (2011). FieldTrip: Open source software for advanced analysis of MEG, EEG, and invasive electrophysiological data. *Computational Intelligence and Neuroscience*, 2011, 9. <https://doi.org/10.1155/2011/156869>
- Pahor, A., & Jaušovec, N. (2018). The Effects of Theta and Gamma tACS on Working Memory and Electrophysiology. *Frontiers in human neuroscience*, 11, 651.
<https://doi.org/10.3389/fnhum.2017.00651>
- Palumbo, L., Bosco, P., Fantacci, M. E., Ferrari, E., Oliva, P., Spera, G., & Retico, A. (2019). Evaluation of the intra- and inter-method agreement of brain MRI segmentation software packages: A comparison between SPM12 and FreeSurfer v6.0. *Physica Medica*, 64, 261-272.
<https://doi.org/https://doi.org/10.1016/j.ejmp.2019.07.016>
- Pascual-Marqui, R. D. (1999). Review of Methods for Solving the EEG Inverse Problem. *International Journal of Bioelectromagnetism*, 1, 75-86. <https://doi.org/10.1186/1743-0003-5-25>
- Pascual-Marqui, R. D. (2002). Standardized low-resolution brain electromagnetic tomography (sLORETA): technical details. *Methods and findings in experimental and clinical pharmacology*, 24D, 5-12.
- Pascual-Marqui, R. D., Esslen, M., Kochi, K., & Lehmann, D. (2002). Functional imaging with low resolution electromagnetic tomography (LORETA): review, comparisons, and new validation brain new. *Japanese Journal of Clinical Neurophysiology*. <https://doi.org/841> [pii]
- Pascual-Marqui, R. D., Lehmann, D., Koukkou, M., Kochi, K., Anderer, P., Saletu, B., et al. (2011). Assessing interactions in the brain with exact low-resolution electromagnetic tomography. *Philosophical Transactions of the Royal Society A: Mathematical, Physical and Engineering Sciences*, 369(1952), 3768-3784. <https://doi.org/10.1098/rsta.2011.0081>
- Perdue, K. L., & Diamond, S. G. (2014). T1 magnetic resonance imaging head segmentation for diffuse optical tomography and electroencephalography. *Journal of Biomedical Optics*, 19(2), 026011.
<https://doi.org/10.1117/1.JBO.19.2.026011>
- Pereira, J., Direito, B., Sayal, A., Ferreira, C., & Castelo-Branco, M. (2019). Self-Modulation of Premotor Cortex Interhemispheric Connectivity in a Real-Time Functional Magnetic Resonance Imaging Neurofeedback Study Using an Adaptive Approach. *Brain Connectivity*, 9(9), 662-672.

<https://doi.org/10.1089/brain.2019.0697>

- Perlmutter, J. S., & Mink, J. W. (2006). Deep brain stimulation. *Annual review of neuroscience*, 29, 229–257. <https://doi.org/10.1146/annurev.neuro.29.051605.112824>
- Pfurtscheller, G., & Lopes Da Silva, F. H. (1999). Event-related EEG/MEG synchronization and desynchronization: Basic principles. *Clinical Neurophysiology*, 110(11), 1842–1857. [https://doi.org/10.1016/S1388-2457\(99\)00141-8](https://doi.org/10.1016/S1388-2457(99)00141-8)
- Pickersgill, M., Martin, P., & Cunningham-Burley, S. (2015). The changing brain: Neuroscience and the enduring import of everyday experience. *Public understanding of science (Bristol, England)*, 24(7), 878–892. <https://doi.org/10.1177/0963662514521550>
- Picton, T. W. (1992). The P300 Wave of the Human Event-Related Potential. *Journal of Clinical Neurophysiology*, 9(4), 456–479. <https://doi.org/10.1097/00004691-199210000-00002>
- Pikovsky, A., Kurths, J., Rosenblum, M., & Kurths, J. (2003). *Synchronization: A Universal Concept in Nonlinear Sciences*. Cambridge University Press. <https://books.google.be/books?id=Fulv845q3QUC>
- Pion-Tonachini, L., Hsu, S., Makeig, S., Jung, T. P., & Cauwenberghs, G. (2015). Real-time EEG Source-mapping Toolbox (REST): Online ICA and source localization. In *2015 37th Annual International Conference of the IEEE Engineering in Medicine and Biology Society (EMBC)* (pp. 4114–4117). <https://doi.org/10.1109/EMBC.2015.7319299>
- Pion-Tonachini, L., Kreutz-Delgado, K., & Makeig, S. (2019). ICLabel: An automated electroencephalographic independent component classifier, dataset, and website. *NeuroImage*, 198, 181–197. <https://doi.org/https://doi.org/10.1016/j.neuroimage.2019.05.026>
- Prosperini, L., Piattella, M. C., Gianni, C., & Pantano, P. (2015). Functional and Structural Brain Plasticity Enhanced by Motor and Cognitive Rehabilitation in Multiple Sclerosis. *Neural Plasticity*, 2015, 481574. <https://doi.org/10.1155/2015/481574>
- Puthusserypady, S., & Ratnarajah, T. (2005). H^∞ adaptive filters for eye blink artifact minimization from electroencephalogram. *IEEE Signal Processing Letters*, 12(12), 816–819.
- Pycroft, L., Stein, J., & Aziz, T. (2018). Deep brain stimulation: An overview of history, methods, and future developments. *Brain and Neuroscience Advances*, 2, 2398212818816017. <https://doi.org/10.1177/2398212818816017>
- Radüntz, T., Scouten, J., Hochmuth, O., & Meffert, B. (2015). EEG artifact elimination by extraction of ICA-component features using image processing algorithms. *J Neurosci Methods*, 243(Supplement C), 84–93. <https://doi.org/https://doi.org/10.1016/j.jneumeth.2015.01.030>
- Rebesco, J. M., Stevenson, I. H., Körding, K. P., Solla, S. A., & Miller, L. E. (2010). Rewiring neural interactions by micro-stimulation. *Frontiers in systems neuroscience*, 4, 39. <https://doi.org/10.3389/fnsys.2010.00039>
- Rémy, F., Wenderoth, N., Lipkens, K., & Swinnen, S. P. (2008). Acquisition of a new bimanual coordination pattern modulates the cerebral activations elicited by an intrinsic pattern: An fMRI

- study. *Cortex*, 44(5), 482–493. <https://doi.org/10.1016/j.cortex.2007.07.004>
- Riecke, L. (2016). Studying Effects of Transcranial Alternating Current Stimulation on Hearing and Auditory Scene Analysis BT - Physiology, Psychoacoustics and Cognition in Normal and Impaired Hearing. In P. van Dijk, D. Başkent, E. Gaudrain, E. de Kleine, A. Wagner, & C. Lanting (Eds.), (pp. 371–379). Cham: Springer International Publishing.
- Riecke, L., Formisano, E., Herrmann, C. S., & Sack, A. T. (2015). 4-Hz Transcranial Alternating Current Stimulation Phase Modulates Hearing. *Brain Stimulation*, 8(4), 777–783. <https://doi.org/https://doi.org/10.1016/j.brs.2015.04.004>
- Romero, S., Mañanas, M. A., & Barbanoj, M. J. (2008). A comparative study of automatic techniques for ocular artifact reduction in spontaneous EEG signals based on clinical target variables: A simulation case. *Computers in Biology and Medicine*, 38(3), 348–360. <https://doi.org/https://doi.org/10.1016/j.combiomed.2007.12.001>
- Rousselet, G. A. (2012). Does Filtering Preclude Us from Studying ERP Time-Courses? *Frontiers in psychology*, 3, 131. <https://doi.org/10.3389/fpsyg.2012.00131>
- Rutledge, D. N., & Jouan-Rimbaud Bouveresse, D. (2013). Independent Components Analysis with the JADE algorithm. *TrAC Trends in Analytical Chemistry*, 50(Supplement C), 22–32. <https://doi.org/https://doi.org/10.1016/j.trac.2013.03.013>
- Sadasivan, P. K., & Dutt, D. N. (1996). ANC schemes for the enhancement of EEG signals in the presence of EOG artifacts. *Comput Biomed Res*, 29(1), 27–40. <https://www.ncbi.nlm.nih.gov/pubmed/8689872>
- Samogin, J., Liu, Q., Marino, M., Wenderoth, N., & Mantini, D. (2019). Shared and connection-specific intrinsic interactions in the default mode network. *NeuroImage*, 200, 474–481. <https://doi.org/10.1016/J.NEUROIMAGE.2019.07.007>
- Santaracchi, E., Biasella, A., Tatti, E., Rossi, A., Prattichizzo, D., & Rossi, S. (2017). High-gamma oscillations in the motor cortex during visuo-motor coordination: A tACS interferential study. *Brain Research Bulletin*, 131, 47–54. <https://doi.org/https://doi.org/10.1016/j.brainresbull.2017.03.006>
- Schabus, M., Griessenberger, H., Gnjezda, M.-T., Heib, D. P. J., Wislowska, M., & Hoedlmoser, K. (2017). Better than sham? A double-blind placebo-controlled neurofeedback study in primary insomnia. *Brain : a journal of neurology*, 140(4), 1041–1052. <https://doi.org/10.1093/brain/awx011>
- Schlegelmilch, F., Schellhorn, K., & Stein, P. (2013). A method for online correction of artifacts in EEG signals during transcranial electrical stimulation. *Clinical Neurophysiology*, 124(10), e166–e168. <https://doi.org/10.1016/j.clinph.2013.04.292>
- Schlogl, A., Keinrath, C., Zimmermann, D., Scherer, R., Leeb, R., & Pfurtscheller, G. (2007). A fully automated correction method of EOG artifacts in EEG recordings. *Clin Neurophysiol*, 118(1), 98–104. <https://doi.org/10.1016/j.clinph.2006.09.003>
- Schwarz, C. G., Gunter, J. L., Wiste, H. J., Przybelski, S. A., Weigand, S. D., Ward, C. P., et al. (2016). A

- large-scale comparison of cortical thickness and volume methods for measuring Alzheimer's disease severity. *NeuroImage: Clinical*, 11, 802–812.
<https://doi.org/https://doi.org/10.1016/j.nicl.2016.05.017>
- Semprini, M., Laffranchi, M., Sanguineti, V., Avanzino, L., De Icco, R., De Michieli, L., & Chiappalone, M. (2018). Technological Approaches for Neurorehabilitation: From Robotic Devices to Brain Stimulation and Beyond. *Frontiers in Neurology*, 9, 212.
<https://doi.org/10.3389/fneur.2018.00212>
- Shepherd, G. M. (2004). *The Synaptic Organization of the Brain. The Synaptic Organization of the Brain.*
<https://doi.org/10.1093/acprof:oso/9780195159561.001.1>
- Shih, J. J., Krusienski, D. J., & Wolpaw, J. R. (2012). Brain-computer interfaces in medicine. *Mayo Clin Proc*, 87(3), 268–279. <https://doi.org/10.1016/j.mayocp.2011.12.008>
- Shlens, J. (2014). A Tutorial on Principal Component Analysis. *CoRR*, abs/1404.1, 1–13.
<https://doi.org/10.1.1.115.3503>
- Shouval, H., Wang, S., & Wittenberg, G. (2010). Spike Timing Dependent Plasticity: A Consequence of More Fundamental Learning Rules. *Frontiers in Computational Neuroscience*.
<https://www.frontiersin.org/article/10.3389/fncom.2010.00019>
- Siew Cheok, N., & Raveendran, P. (2008). Removal of EOG Artifacts Using ICA Regression Method. In N. A. Abu Osman, F. Ibrahim, W. A. B. Wan Abas, H. S. Abdul Rahman, & H.-N. Ting (Eds.), *4th Kuala Lumpur International Conference on Biomedical Engineering 2008: BIOMED 2008 25–28 June 2008 Kuala Lumpur, Malaysia* (pp. 226–229). Berlin, Heidelberg: Springer Berlin Heidelberg.
https://doi.org/10.1007/978-3-540-69139-6_59
- Sörnmo, L., & Laguna, P. (2005). *Bioelectrical Signal Processing in Cardiac and Neurological Applications. Bioelectrical Signal Processing in Cardiac and Neurological Applications.*
<https://doi.org/10.1016/B978-0-12-437552-9.X5000-4>
- Speckmann, E.-J., Elger, C. E., & Gorji, A. (2012). Neurophysiologic Basis of EEG and DC Potentials. *Niedermeyer's Electroencephalography*.
- Stenroos, M., & Nummenmaa, A. (2016). Incorporating and Compensating Cerebrospinal Fluid in Surface-Based Forward Models of Magneto- and Electroencephalography. *PloS one*, 11(7), e0159595–e0159595. <https://doi.org/10.1371/journal.pone.0159595>
- Stone, J. V. (2004). *Independent Component Analysis: A Tutorial Introduction*. MIT Press.
- Strüber, D., Rach, S., Trautmann-Lengsfeld, S. A., Engel, A. K., & Herrmann, C. S. (2014). Antiphase 40 Hz Oscillatory Current Stimulation Affects Bistable Motion Perception. *Brain Topography*, 27(1), 158–171. <https://doi.org/10.1007/s10548-013-0294-x>
- Sugata, H., Yagi, K., Yazawa, S., Nagase, Y., Tsuruta, K., Ikeda, T., et al. (2018). Modulation of Motor Learning Capacity by Transcranial Alternating Current Stimulation. *Neuroscience*, 391, 131–139.
<https://doi.org/https://doi.org/10.1016/j.neuroscience.2018.09.013>
- Sun, F. T., & Morrell, M. J. (2014). Closed-loop Neurostimulation: The Clinical Experience.

Neurotherapeutics, 11(3), 553–563. <https://doi.org/10.1007/s13311-014-0280-3>

- Taberna, G. A., Guarnieri, R., & Mantini, D. (2019). SPOT3D: Spatial positioning toolbox for head markers using 3D scans. *Scientific Reports*, 9(1), 12813. <https://doi.org/10.1038/s41598-019-49256-0>
- Taberna, G. A., Marino, M., Ganzetti, M., & Mantini, D. (2019). Spatial localization of EEG electrodes using 3D scanning. *Journal of Neural Engineering*, 16, 02602. <https://doi.org/10.1088/1741-2552/aafdd1>
- Tadel, F., Baillet, S., Mosher, J. C., Pantazis, D., & Leahy, R. M. (2011). Brainstorm: A user-friendly application for MEG/EEG analysis. *Computational Intelligence and Neuroscience*, 2011, 13. <https://doi.org/10.1155/2011/879716>
- Thibault, R. T., Lifshitz, M., & Raz, A. (2016). The self-regulating brain and neurofeedback: Experimental science and clinical promise. *Cortex*, 74, 247–261. <https://doi.org/10.1016/j.cortex.2015.10.024>
- Thut, G., Schyns, P. G., & Gross, J. (2011). Entrainment of perceptually relevant brain oscillations by non-invasive rhythmic stimulation of the human brain. *Frontiers in psychology*, 2, 170. <https://doi.org/10.3389/fpsyg.2011.00170>
- Triantafyllopoulos, D., & Megalooikonomou, V. (2014). Eye Blink Artifact Removal in EEG Using Tensor Decomposition. In L. Iliadis, I. Maglogiannis, H. Papadopoulos, S. Sioutas, & C. Makris (Eds.), *Artificial Intelligence Applications and Innovations: AIAI 2014 Workshops: CoPA, MHDW, IIVC, and MT4BD, Rhodes, Greece, September 19-21, 2014. Proceedings* (pp. 155–164). Berlin, Heidelberg: Springer Berlin Heidelberg. https://doi.org/10.1007/978-3-662-44722-2_17
- Tucker, D. M. (1993). Spatial sampling of head electrical fields: the geodesic sensor net. *Electroencephalography and Clinical Neurophysiology*, 87(3), 154–163. [https://doi.org/https://doi.org/10.1016/0013-4694\(93\)90121-B](https://doi.org/https://doi.org/10.1016/0013-4694(93)90121-B)
- Turnip, A. (2014). JADE-ICA algorithm for EOG artifact removal in EEG recording. In *2014 2nd International Conference on Technology, Informatics, Management, Engineering & Environment* (pp. 270–274). <https://doi.org/10.1109/TIME-E.2014.7011630>
- Turnip, A., & Junaidi, E. (2014). Removal artifacts from EEG signal using independent component analysis and principal component analysis. In *2014 2nd International Conference on Technology, Informatics, Management, Engineering & Environment* (pp. 296–302). <https://doi.org/10.1109/TIME-E.2014.7011635>
- Urigüen, J. A., & Garcia-Zapirain, B. (2015). EEG artifact removal—state-of-the-art and guidelines. *Journal of Neural Engineering*, 12(3), 31001. <https://doi.org/10.1088/1741-2560/12/3/031001>
- Uusitalo, M. A., & Ilmoniemi, R. J. (1997). Signal-space projection method for separating MEG or EEG into components. *Medical and Biological Engineering and Computing*, 35(2), 135–140. <https://doi.org/10.1007/BF02534144>
- Van Hoey, G., Vanrumste, B., D'Havé, M., Van De Walle, R., Lemahieu, I., & Boon, P. (2000). Influence of

- measurement noise and electrode mislocalisation on EEG dipole-source localisation. *Medical and Biological Engineering and Computing*, 38(3), 287–296. <https://doi.org/10.1007/BF02347049>
- van Lutterveld, R., Houlihan, S. D., Pal, P., Sacchet, M. D., McFarlane-Blake, C., Patel, P. R., et al. (2017). Source-space EEG neurofeedback links subjective experience with brain activity during effortless awareness meditation. *Neuroimage*, 151, 117–127. <https://doi.org/10.1016/j.neuroimage.2016.02.047>
- Van Veen, B. D., Van Drongelen, W., Yuchtman, M., & Suzuki, A. (1997). Localization of brain electrical activity via linearly constrained minimum variance spatial filtering. *IEEE Transactions on Biomedical Engineering*, 44(9), 867–880. <https://doi.org/10.1109/10.623056>
- Vanderperren, K., De Vos, M., Ramautar, J. R., Novitskiy, N., Mennes, M., Asseondi, S., et al. (2010). Removal of BCG artifacts from EEG recordings inside the MR scanner: A comparison of methodological and validation-related aspects. *NeuroImage*, 50(3), 920–934. <https://doi.org/10.1016/j.neuroimage.2010.01.010>
- von Bernhardi, R., Bernhardi, L. E., & Eugenín, J. (2017). What Is Neural Plasticity? BT - The Plastic Brain. In R. von Bernhardi, J. Eugenín, & K. J. Muller (Eds.), (pp. 1–15). Cham: Springer International Publishing. https://doi.org/10.1007/978-3-319-62817-2_1
- Vorobyov, S., & Cichocki, A. (2002). Blind noise reduction for multisensory signals using ICA and subspace filtering, with application to EEG analysis. *Biological Cybernetics*, 86(4), 293–303. <https://doi.org/10.1007/s00422-001-0298-6>
- Vöröslakos, M., Takeuchi, Y., Brinyiczki, K., Zombori, T., Oliva, A., Fernández-Ruiz, A., et al. (2018). Direct effects of transcranial electric stimulation on brain circuits in rats and humans. *Nature Communications*, 9(1), 483. <https://doi.org/10.1038/s41467-018-02928-3>
- Vossen, A., Gross, J., & Thut, G. (2015). Alpha power increase after transcranial alternating current stimulation at alpha frequency (a-tACS) reflects plastic changes rather than entrainment. *Brain Stimulation*, 8, 499–508. <https://doi.org/10.1016/j.brs.2014.12.004>
- Voskuhl, J., Huster, R. J., & Herrmann, C. S. (2016). BOLD signal effects of transcranial alternating current stimulation (tACS) in the alpha range: A concurrent tACS-fMRI study. *NeuroImage*, 140, 118–125. <https://doi.org/https://doi.org/10.1016/j.neuroimage.2015.10.003>
- Voskuhl, J., Strüber, D., & Herrmann, C. S. (2018). Non-invasive Brain Stimulation: A Paradigm Shift in Understanding Brain Oscillations. *Frontiers in human neuroscience*, 12, 211. <https://doi.org/10.3389/fnhum.2018.00211>
- Weiss, C., Nettekoven, C., Rehme, A. K., Neuschmelting, V., Eisenbeis, A., Goldbrunner, R., & Grefkes, C. (2013). Mapping the hand, foot and face representations in the primary motor cortex - Retest reliability of neuronavigated TMS versus functional MRI. *NeuroImage*, 66, 531–542. <https://doi.org/10.1016/j.neuroimage.2012.10.046>
- Winkler, I., Brandl, S., Horn, F., Waldburger, E., Allefeld, C., & Tangermann, M. (2014). Robust artifactual independent component classification for BCI practitioners. *J Neural Eng*, 11(3),

35013. <https://doi.org/10.1088/1741-2560/11/3/035013>

- Winkler, I., Haufe, S., & Tangermann, M. (2011). Automatic Classification of Artifactual ICA-Components for Artifact Removal in EEG Signals. *Behavioral and Brain Functions : BBF*, 7, 30. <https://doi.org/10.1186/1744-9081-7-30>
- Wold, S., Esbensen, K., & Geladi, P. (1987). Principal component analysis. *Chemometrics and Intelligent Laboratory Systems*, 2(1), 37–52. [https://doi.org/https://doi.org/10.1016/0169-7439\(87\)80084-9](https://doi.org/https://doi.org/10.1016/0169-7439(87)80084-9)
- Woods, A. J., Antal, A., Bikson, M., Boggio, P. S., Brunoni, A. R., Celnik, P., et al. (2016). A technical guide to tDCS, and related non-invasive brain stimulation tools. *Clinical Neurophysiology*, 127(2), 1031–1048. <https://doi.org/10.1016/j.clinph.2015.11.012>
- Wu, D., King, J.-T., Chuang, C.-H., Lin, C.-T., & Jung, T.-P. (2017). Spatial Filtering for EEG-Based Regression Problems in Brain-Computer Interface (BCI). *IEEE Transactions on Fuzzy Systems*, 1–1. <https://doi.org/10.1109/TFUZZ.2017.2688423>
- Xiaopei, W., & Zhongfu, Y. (2005). Online Infomax Algorithm and its Application to Remove EEG Artifacts. In *2005 IEEE Engineering in Medicine and Biology 27th Annual Conference* (pp. 4203–4207). <https://doi.org/10.1109/IEMBS.2005.1615391>
- Yao, D. (2001). A method to standardize a reference of scalp EEG recordings to a point at infinity. *Physiological Measurement*, 22(4), 693–711. <https://doi.org/10.1088/0967-3334/22/4/305>
- Yavari, F., Nitsche, M. A., & Ekhtiari, H. (2017). Transcranial Electric Stimulation for Precision Medicine: A Spatiomechanistic Framework. *Frontiers in Human Neuroscience*. <https://www.frontiersin.org/article/10.3389/fnhum.2017.00159>
- Zaytsev, A., Cook, G., Liu, W., Paley, M., & Milne, E. (2015). Source Localization for Brain-Computer Interfaces. In *Intelligent Systems Reference Library* (Vol. 74, pp. 125–153). https://doi.org/10.1007/978-3-319-10978-7_5
- Zeng, H., Song, A., Yan, R., & Qin, H. (2013). EOG Artifact Correction from EEG Recording Using Stationary Subspace Analysis and Empirical Mode Decomposition. *Sensors (Basel, Switzerland)*, 13(11), 14839–14859. <https://doi.org/10.3390/s131114839>
- Zhang, C., Tong, L., Zeng, Y., Jiang, J., Bu, H., Yan, B., & Li, J. (2015). Automatic Artifact Removal from Electroencephalogram Data Based on A Priori Artifact Information. *BioMed Research International*, 2015, 720450. <https://doi.org/10.1155/2015/720450>
- Zrenner, C., Belardinelli, P., Muller-Dahlhaus, F., & Ziemann, U. (2016). Closed-Loop Neuroscience and Non-Invasive Brain Stimulation: A Tale of Two Loops. *Front Cell Neurosci*, 10, 92. <https://doi.org/10.3389/fncel.2016.00092>
- Zrenner, C., Desideri, D., Belardinelli, P., & Ziemann, U. (2018). Real-time EEG-defined excitability states determine efficacy of TMS-induced plasticity in human motor cortex. *Brain Stimulation*, 11(2), 374–389. <https://doi.org/https://doi.org/10.1016/j.brs.2017.11.016>

Appositions

1. Nowadays, healthcare systems are required to deliver more and better care with lesser resources, possibly through the development of digital services.
2. Depression is a major contributor to the global disease burden and affects people all over the world.
3. Sport is essential for all people, of all ages, but especially for young people as it engages the body and mind and creates relationships with others.

Acknowledgments

This thesis is the expression of a human and scientific experience enriched by the encounter with many people and special places. I have met many people and professionals on this path; each of them gave me precious time, spent discussing and finding answers to my questions, my beliefs and ideas. I cannot fail to thank them and all the people who have shared these years and this research project with me.

This result would never have seen the light without the availability and patience of its first supervisor, prof. Dante Mantini, whom I sincerely and cordially thank, also for the huge intellectual debt contracted with him beyond the boundaries of this work. Moreover, I will never forget how you 'drastically' changed my life. Life is strange, but thanks to you I was able to get out of my comfort zone, to continuously revolutionize my point of view and to positively change my life. You found me in a strange and difficult moment of my life, and this is something for which I will always personally be grateful to you.

My deepest thanks go to my friends and colleagues in the lab, Gaia, Marco M., Mingqi, Manasa and Jessica. We have shared lots of unforgettable and funny moments together. I want to thank all the colleagues and friends who joined our research group in the past: Camillo, Ernesto, Marco G., Quanying, Ilaria and Mariangela.

Inoltre, vorrei ringraziare la mia famiglia in Italia, che mi ha sempre supportato anche se a distanza. Questa distanza è stata solo un concetto geografico, poiché vi ho sempre sentiti vicini. Un grazie speciale va a Nonna Maria, che dall'alto della sua terza elementare, mi ha spinto a guardare avanti, migliorare, puntando sempre più in alto senza pormi limiti e ad arrivare dove sono ora. Grazie ai miei genitori e a mia sorella, che mi hanno supportato, e spero continuino a farlo, nonostante i miei difetti. Grazie a Nonno Sandro, la stella che mi guida sempre da lassù. Ci hai lasciato tempo fa, ma mi ha sempre guidato nel fare la scelta più giusta, aiutandomi in ogni momento difficile della mia vita.

Un grazie speciale (anche se non sarà mai abbastanza) va ad Erica, la donna della mia vita, che non mi hai mai fatto sentire in colpa di essermi trasferito in Belgio, e che mi ha raggiunto abbandonando tutte le sue sicurezze per seguire le mie ambizioni che sono diventate le NOSTRE. Hai dovuto e dovrai

continuare a soccombere alle mie ansie, paure ed inquietudini, e solo per questo ti sarò eternamente riconoscente. Senza di te, tutto questo non sarebbe stato possibile.

Come non poter menzionare gli amici di Roma, i compagni di mille battaglie, avventure ed errori. Voglio iniziare da Gianluca, il cosiddetto 'fratello non di sangue', che mi sopporta continuamente con le mie lamentele; Toto, l'amico ed il compagno di banco di una vita; Gianma, che nonostante i suoi problemi nel rispondere al telefono ed ai messaggi, so che col pensiero mi è sempre vicino; Monty, sempre pronto per un aperitivo al Chiringuito al mio rientro in patria. E come potrei scordarmi del poker di amici, gli 'alcetti', che nonostante le distanze, sono sempre al mio fianco in ogni momento della mia vita: GRAZIE Ciccio, Natale ed Enrico. Una menzione speciale va ad Andrea, il più folle Amico con la 'A' maiuscola. Una delle persone che sento più vicine nella mia vita quotidiana, nonostante tu viva oltreoceano in un altro fuso orario.

Infine, voglio ringraziare la mia seconda 'famiglia' italiana qui in Belgio. Ho avuto il piacere di incontrare persone speciali, che non condividono con me solo le origini, ma un rapporto solido di profonda stima ed amicizia. Grazie a Francesca, la persona più 'pazza' che conosca, ma fortunatamente più dolce che folle. E grazie per avermi fatto conoscere Luciano, un amico sempre pronto ad aiutarti e a consigliarti saggiamente. Grazie Paolo e Gabriele, senza di voi la mia vita in Belgio sarebbe stata più difficile. Grazie a Maria e Gabriele, due persone amabili e opposte che fortunatamente si compensano. In ordine cronologico siete le persone che ho conosciuto per ultime, ma mi avete rapito il cuore da subito. E per concludere, grazie Fabrizio per tutti i consigli, gli aiuti e le avventure vissute insieme. Sono sicuro che avremo, negli anni a venire, altre avventure altrettanto belle ed indimenticabili.

Finally, I want to thank those who have never been there for me, who were with me only for convenience and who never believed in me! Without you I would never have found an incentive to move forward and overcome the obstacles encountered along my path! And above all, please, do not change your point of view, because you will continue giving me the motivation to improve for my whole life!

Scientific acknowledgments

The studies presented in this thesis involved important scientific collaborations with several scientists. Prof. Dante Mantini performed a key role in designing all three studies and data analysis. The data for the Chapter 2 were recorded by Dr. Quanying Liu, whereas the data used for the study in Chapter 3 were acquired by Mingqi Zhao. The study presented in Chapter 3 was performed in collaboration with researchers of University of Chieti-Pescara and Italian National Research Council, who provided the data needed for the study. Dr. Franca Tecchio and Prof. Alfredo Brancucci provided valuable suggestions and advice during this collaborative research. Prof. Stephan Swinnen gave an important contribution with his expertise in motor control for the studies described in Chapter 3 and 4. The studies were supported also by other scientists, whose name is included in the author list of the manuscripts included in this PhD thesis.

Moreover, those studies counted on the valuable comments of the members of the doctoral committee and the external jury: Prof. Werner Helsen, Prof. Genevieve Albouy, Prof. Marc Van Hulle, Prof. Kaat Alaerts and Prof. Camillo Porcaro.

Finally, the thesis was written by Roberto Guarnieri, the PhD candidate, with the input of his supervisor Prof. Dante Mantini. The summary translation in Dutch was done by Maarten Eerdeken, and the thesis was proofread by Erica Francia.

Personal Contribution

The author of this thesis, Roberto Guarnieri, undertook a major role in the realization of the studies presented in Chapters 2, 3, and 4. Specifically, he had a major role in the analysis of the data, reporting of the results, and in all discussions related to those works.

Conflict of Interests Statement

This thesis was funded by the Research Foundation Flanders (FWO) under the Ph.D. fellowship No. 1104520 N.

About the author

Roberto Guarnieri was born on December 27th, 1991, in Rome, Italy. In 2010 he started his Bachelor in electrical engineering at Roma Tre University. During his master studies, he developed a great interest in EEG signal processing and telemedicine. He graduated with Honors in Biomedical Engineering in March 2016 at Roma Tre University, with a Master thesis on the design and implementation of a smart blister for drugs. In 2016 he moved to Belgium and started his doctoral training in the laboratory of movement Control & Neuroplasticity under the supervision of Prof. Dante Mantini. In October 2017, he was awarded by the FWO PhD scholarship to support his doctoral training.

List of publications

Publications in peer-reviewed journals

Guarnieri R, Marino M, Barban F, Ganzetti M, Mantini D. *Online EEG artifact removal for BCI applications by adaptive spatial filtering*. J Neural Eng. 2018 Oct;15(5):056009. doi: 10.1088/1741-2552/aacfd. Epub 2018 Jun 28.

Taberna GA, **Guarnieri R**, Mantini D. SPOT3D: *Spatial positioning toolbox for head markers using 3D scans*. Sci Rep. 2019 Sep 6;9(1):12813. doi: 10.1038/s41598-019-49256-0.

Guarnieri R, Zhao M, Taberna GA, Ganzetti M, Swinnen SP, Mantini D. *RT-NET: real-time reconstruction of neural activity using high-density electroencephalography*. Neuroinformatics. 2020 Jul 28. doi: 10.1007/s12021-020-09479-3. Epub ahead of print.

Guarnieri R, Brancucci A, D'Anselmo A, Manippa V, Swinnen SP, Tecchio F, Mantini D. *A computationally efficient method for the attenuation of alternating current stimulation artifacts in electroencephalographic recordings*. J Neural Eng. 2020 Aug 17;17(4):046038. doi: 10.1088/1741-2552/aba99d.

Conference Abstracts

Guarnieri, R., Marino, M., Barban, F., Ganzetti, M., & Mantini, D. (2018). *Adaptive spatial filtering for online EEG artifact removal: combining Blind Source Separation and Regression Analysis*. OHBM, Singapore.

Guarnieri, R., Zhao M., Taberna, G. A., Ganzetti, M., Swinnen, S. P., Mantini, D. (2019). *Real-time reconstruction of neural activity using high-density electroencephalography*. Neuro Sense & Sense-ability - Sensing and data processing technology for the brain, Leuven, Belgium.

Guarnieri, R., Marino, M., Barban, F., Ganzetti, M., & Mantini, D. (2019). *Artifact removal in real-time for hdEEG-BCI systems*. IEEE NER, San Francisco, USA.

Guarnieri, R., Zhao M., Taberna, G. A., Ganzetti, M., Swinnen, S. P., Mantini, D. (2019). *Real-time estimation of brain activity from high density EEG*. OHBM, Rome, Italy.

Guarnieri, R., Zhao M., Taberna, G. A., Ganzetti, M., Swinnen, S. P., Mantini, D. (2020). *RT-NET: a software package for neural activity estimation from high-density EEG recordings*. OHBM, Montreal, Canada.